universität wien

MASTERARBEIT / MASTER'S THESIS

Titel der Masterarbeit / Title of the Master's Thesis

„Improving strong coupling determinations from hadronic tau decays"

verfasst von / submitted by

Miguel Angel Benitez-Rathgeb, BSc

angestrebter akademischer Grad / in partial fulfilment of the requirements for the degree of

Master of Science (MSc)

Wien, 2022 / Vienna, 2022

Studienkennzahl lt. Studienblatt / degree programme code as it appears on the student record sheet:	UA 066 876
Studienrichtung lt. Studienblatt / degree programme as it appears on the student record sheet:	Masterstudium Physik UG2002
Betreut von / Supervisor:	Univ.-Prof. Dr. André H. Hoang

Abstract

When extracting the strong coupling from τ hadronic spectral function moments, a discrepancy related to the treatment of logarithms appearing in the theoretical description of the decay process represents one of the dominant contributions to the theoretical uncertainty of this fundamental parameter of Quantum Chromodynamics (QCD). This so-called Contour-Improved Perturbation Theory (CIPT) – Fixed-Order Perturbation Theory (FOPT) discrepancy problem permeated the literature for over a decade. In this work we introduce a scheme for a renormlaon-free gluon condensate (RF GC) matrix element, through which the aforementioned discrepancy problem is resolved. We show how the RF GC scheme impacts the perturbative expansions in full QCD and further study the impact our newly defined scheme has on state-of-the-art strong coupling determinations. Furthermore, we discuss different methods to obtain a value for the norm of the GC, which has to be supplemented to the perturbative series in the RF GC scheme as it is part of the construction.

Zusammenfassung

Im Zusammenhang mit der Bestimmung der Kopplungskonstante der starken Wechselwirkung durch die phänomenologische Analyse hadronsicher τ Zerfälle tritt eine Diskrepanz auf, welche aus der Art und Weise der Resummation der Logarithmen, die in der theoretischen Beschreibung von dem Zerfallsprozess auftreten, resultiert. Der Fehler der aus diesen unterschiedlichen Resummationsansätzen resultiert liefert einen der größten Beiträge zum Gesamtfehler in dieser Art der Bestimmung der Kopplungskonstante. Dieses sogenannte Contour-Improved Perturbation Theory (CIPT) – Fixed-Order Perturbation Theory (FOPT) Problem wird nun seit mehr als 10 Jahren in der Literatur studiert, bisher ohne eine zufriedenstellende Antwort. In dieser Arbeit liefern wir nun die Antwort in Form eines Schemas in dem das Matrix Element des Gluon Kondensates Renormalon frei ist. Wir zeigen den Einfluss unseres neu definierten Schemas auf die perturbativen Reihen. Zudem studieren wir die Bestimmungen der Kopplungskonstante der starken Wechselwirkung durch die phänomenologische Analyse hadronsicher τ Zerfälle in dem Kontext des neuen Renormalon freien Schemas. In dem von uns neu eingeführten Schema ist es nun auch notwendig die Norm des Gluon Kondensates zu bestimmen, da diese Teil der Konstruktion ist. Eine entsprechende Analyse wird in dieser Arbeit durchgeführt.

Table of Contents

List of Figures

Chapter 1

Introduction

Extracting the strong coupling from τ hadronic spectral function moments represents one of the most precise methods to determine this fundamental parameter of Quantum Chromodynamics (QCD) [1]. Since α_s is extracted at relatively low energies, these determinations also represent a stringent test of the concept of asymptotic freedom and the 'running' of the strong coupling. In the past, different treatments of the perturbative contributions that enter the phenomenological analysis led to incompatible outcomes. To be precise, the origin of the problem lies in the different prescriptions for setting the renormalization scale in the QCD corrections of the theoretical description of the hadronic τ decay process. The two most widely used prescriptions are referred to in the literature as contour-improved (CIPT) [2, 3] and fixed-order perturbation theory (FOPT) [4]. When computing the perturbative expansions a clear discrepancy is observed for so-called gluon condensate (GC) suppressed spectral function moments, starting already at lower orders. Due to the fact that the perturbative series yield different outcomes, the corresponding contributions to the phenomenological analysis also differ. As a consequence, assuming the same form of the non-perturbative corrections, the value of the strong coupling has to compensate for this difference and therefore one obtains different outcomes for α_s when using either the FOPT or the CIPT approach in the perturbative contribution.

In Ref. [5] it was pointed out for the first time that the discrepancy related to the different possibilities of resumming the logarithms is of IR origin. In particular, the authors showed that the FOPT-CIPT discrepancy is systematic (and not related to missing higher-orders) and manifests itself in the so-called asymptotic separation. The origin of the asymptotic separation turn out to be the IR renormalons inherent to the perturbative expansions, where the most dominant contribution arises from the gluon condensate renormalon.

In this thesis we take the findings of Ref. [5] as the starting point to introduce a scheme, where the discrepancy between FOPT and CIPT does not arise. What we intend to do is to subtract the gluon condensate renormalon contribution from the perturbative series, through a redefinition of the gluon condensate itself. This should then yield compatible results for the perturbative expansions and subsequently lead to strong coupling determinations which are in much better agreement compared to the results in the literature, where the CIPT-FOPT discrepancy was one of the dominant contributions to the theoretical error of α_s.

The content of this thesis is as follows: In section 2 we review the basic concepts of renormalons and the Operator Product Expansion (OPE). In particular, we discuss how a so-called renormalon divergence in principle arises when considering a perturbative series in QCD and then look at a simple practical example. Then we study the concept of the OPE in detail. In particular, we derive a renormalization-group improved form of the higher-dimensional OPE contributions which will be the starting point of our discussion on re-defining the gluon condensate contribution to the OPE of the Adler function.

In section 3 we provide a rather general introduction to the theory description of hadronic τ decays. We discuss how the experimental and theoretical moments are related, e.g. through the means of Finite-Energy Sum Rules (FESR) and further examine in detail how the CIPT-FOPT discrepancy arises in the higher-order perturbative corrections to the theoretical moments. We also look at some practical examples of the CIPT-FOPT discrepancy problem, first in what is called the *large-β_0 approximation* and then also in full QCD, where we have an additional model dependence. Finally, we review the findings of Ref. [5] and elaborate on their most important results.

In section 4 we introduce our new Renormalon-Free Gluon Condensate (RF GC) scheme, where through a re-definition of the GC we get rid of the GC renormalon contribution in the perturbative series. Our newly defined scheme is then taken to the test in three applications. First we consider a toy model analysis to study the impact our scheme has on a simplistic single-renormalon model containing solely the GC renormalon. Then we again consider the simple case of the large-β_0 approximation and in the end we also study the impact our scheme has on the expansions in full QCD based on a model.

In the last section of this thesis, which is section 5, we investigate how the strong coupling determinations are impacted by switching from the orignal $\overline{\text{MS}}$ GC scheme to the RF GC scheme. First, however, we need to obtain a value for the norm of the GC, which is the content of section 5.1. Then we discuss in a rather compact form some general aspects of strong coupling determinations from τ hadronic spectral function moments. In particular, we elaborate on the fact that there exist two different extraction approaches [6, 7] common in the literature and also explain the situation regarding the experimental data the strong coupling determinations are based on. After this introduction to the phenomenological analysis we study the impact the RF GC scheme has on the two extraction approaches individually. Finally, we conclude.

There are also two appendices. The first appendix contains a brief introduction to the C-scheme for the strong coupling, introduced in Ref. [8]. This choice of scheme for the strong coupling is used throughout sections 4 and 5 since we are able to formulate the RF GC scheme in a closed and compact form within this scheme. Note, however, that we always transform back to the original $\overline{\text{MS}}$ scheme for all numerical studies. The second appendix contains the most important formulae which were not included in the main text of the thesis.

Chapter 2

Basic concepts of renormalons and the Operator Product Expansion

In the past century the question of whether a perturbative series, for instance of a physical matrix element, is convergent or not was heavily investigated. Dyson realized that the number of diagrams contributing to a certain order n in perturbation theory typically grows as $n!$, therefore suggesting that the perturbation series has zero radius of convergence. The question which is of most interest to this thesis, in this context at least, is what one could do if the series turns out not to be convergent. In QCD it is actually very common that the perturbative series of the quantity of interest has an asymptotic behaviour. Therefore, we are interested in a possible cure for this problem or at least some procedure which can be applied in order to improve the asymptotic behaviour of the series of interest. To this extend we will look at a well-known technique for improving the convergence of a power series, the so-called *Borel transformation*.

This chapter intends to give a brief overview of the most important aspects of Borel summation, partly following the lines of Refs. [9, 10]. We discuss how a so-called *renormalon divergence* in principle arises. Furthermore, we establish a relation between infra-red (IR) renormalon singularities and non-perturbative power corrections in the Operator Product Expansion (OPE) of a generic observable $\sigma(Q)$.

2.1 Borel transform

We start the discussion by considering the generic structure of a perturbative series in QCD. In QCD perturbation theory some quantity f can be expressed in terms of a power series in the strong coupling α_s

$$f(\alpha_s) = f(0) + \sum_{n=0}^{\infty} f_n \alpha_s^{n+1}, \tag{2.1}$$

where f_n are some coefficients of the perturbative expansion and $f(0)$ represents the tree-level contribution to the quantity $f(\alpha_s)$. Eq. (2.1) is typically only asymptotically convergent. We can, however, consider the related series

$$B[f](t) = f(0)\delta(t) + \sum_{n=0}^{\infty} \frac{f_n}{n!} t^n, \tag{2.2}$$

which could be regarded as improved with respect to Eq. (2.1), in the sense that for the case of f_n growing no faster than $n!$, $B[f](t)$ generally possesses at least a finite radius of convergence. Eq. (2.2) is the so-called *Borel transform* of $f(\alpha_s)$. If we want to recover the original series from the resummed series given in Eq. (2.2), we can achieve this by defining the so-called *Borel integral* as

$$f(\alpha_s) = \int_0^\infty dt\; e^{-t/\alpha_s} B[f](t). \tag{2.3}$$

In general, one also refers to Eq. (2.3) as the *inverse Borel transform*. Assuming that Eq. (2.3) exists, the perturbation series $f(\alpha_s)$ is *Borel-summable* and unambiguously defined. If, however, $B[f](t)$ has singularities for real positive t, e.g. singularities lying on the path of integration, the inverse Borel transform in Eq. (2.3) becomes ambiguous. In this case the Borel integral can only be defined by deforming the contour of integration away from the singularity, and the inverse Borel transform subsequently becomes dependent on the deformation used. We will elaborate more on this ambiguity at the beginning of section 2.3 and during chapter 3.

In order to get an idea of how a renormalon divergence arises in practice, we consider the following example: Given a general perturbative series in QCD, let us assume that the coefficients of the perturbative expansion are given by

$$f_n = K a^n \Gamma(n+1+b), \tag{2.4}$$

where K, a and b refer to some arbitrary constants. Further we take $b > 0$. This then yields

$$B[f](t) = f(0)\delta(t) + \frac{K\Gamma(1+b)}{(1-at)^{1+b}} \tag{2.5}$$

as the corresponding Borel transform according to Eq. (2.2). At this stage, the choice of Eq. (2.4) might seem completely ad hoc and one could ask why it is particularly suited for the current discussion. The justification of Eq. (2.4) is given by the fact that it reflects all typical characteristics of a QCD perturbation series. The Γ-function contains the expected $n!$ divergent behaviour of the series and the factor of a^n can be considered as a modulation of the singularity. In fact, this alone shows that a pole located close to the origin is more severe than one which is further away from it, since a large value of a corresponds to a smaller value of t at the point of the singularity. Furthermore, we can identify the implications of a attaining negative values. We see, by looking at Eq. (2.4), that this would lead to a sign-alternating $n!$ behaviour of the perturbation series.

After having performed the Borel transformation, the information of the divergent behaviour originally contained in the Γ-function of Eq. (2.4) is now encoded in the singularity at $t = 1/a$ of the Borel transform. These poles in the Borel transform of the perturbative series are precisely what is referred to as *renormalon divergencies*.

Now that we have a basic idea of how renormalon divergencies in principle arise when considering improvements of asymptotically convergent perturbative series, we discuss them in more detail in the following section.

2.2 Renormalons

To get an idea of how a renormalon divergence arises in actual physical computations we consider the example given in section 2.2. of Ref. [9], where we closely follow the presentation therein. Note that in the current discussion we also adopt the notation from Ref. [9] for simplicity and transparency. In the subsequent chapters some of the quantities introduced in the following will reappear, where we then decide to adopt a different notation.

Let the correlation function of two vector currents $j_\mu = \bar{q}\gamma_\mu q$ of massless quarks be [9]

$$(-i)\int d^4x\, e^{-iqx}\langle 0|T\{j_\mu(x)j_\nu(0)\}|0\rangle = \left(q_\mu q_\nu - q^2 g_{\mu\nu}\right)\Pi\left(Q^2\right), \tag{2.6}$$

with $Q^2 = -q^2$. Instead of working with the correlator given in Eq. (2.6), in the context of hadronic tau decays it is customary to define a quantity called the *Adler function* $D(Q^2)$. Since we are interested in contributions to $D(Q^2)$ for the most part of this thesis we will, from the beginning, set up the discussion in such a way that we always talk about the Adler function and not the correlator, if not explicitly mentioned. As opposed to the correlator $\Pi(Q^2)$, $D(Q^2)$ is a physical quantity since the renormalization scale and scheme dependent subtraction constant is removed by taking the derivative w.r.t. Q^2. It is also important to note that the Adler function

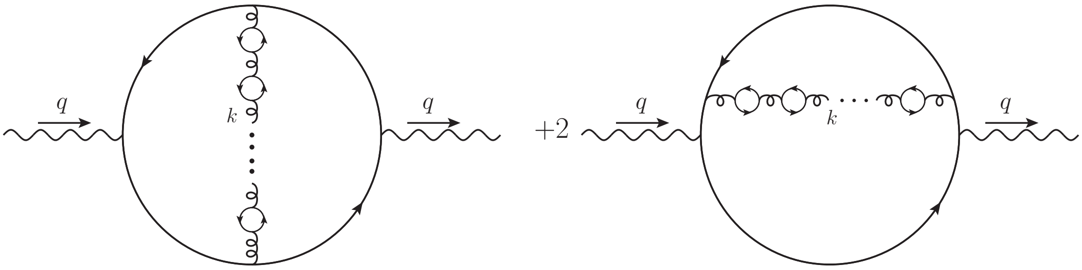

Fig. 2.1: Bubble diagrams of the Adler function. The factor 2 entails the contribution of a bubble chain being attached to the lower quark line of the large fermion loop.

as such is not unique and that there exist different definitions in the literature. For the current discussion we define it to be

$$\frac{1}{4\pi^2}D(Q^2) = \frac{\mathrm{d}\Pi(Q^2)}{\mathrm{d}Q^2}. \tag{2.7}$$

What we want to do in this section is to compute the contribution of the fermion bubble diagrams shown in Fig. 2.1 to $D(Q^2)$. Since the Adler function requires no additional subtractions, except for those already contained in the renormalized QCD Lagrangian, there is no need for regularization. Hence the only ingredient needed for the determination of the contribution of the fermion bubble diagrams to the Adler function is the renormalized fermion loop given by

$$\hat{\pi}(k^2) = -\frac{\alpha_s n_f T}{3\pi}\left[\ln\left(\frac{-k^2}{\mu^2}\right) + c\right], \tag{2.8}$$

with c being a scheme dependent constant attaining the value $c = -5/3$ in the $\overline{\mathrm{MS}}$-scheme. The Adler function corresponding to the diagrams in Fig. 2.1 is obtained by integrating over the loop momentum of the large fermion loop and the angles of the gluon momentum k. Defining the dimensionless integration variable $\hat{k}^2 = -k^2/Q^2$ and taking c in the $\overline{\mathrm{MS}}$-scheme yields [9]

$$D(Q^2) = \sum_{n=0}^{\infty}\alpha_s\int_0^{\infty}\frac{d\hat{k}^2}{\hat{k}^2}F(\hat{k}^2)\left[\frac{\alpha_s n_f T}{3\pi}\ln\left(\hat{k}^2\frac{Q^2 e^{-5/3}}{\mu^2}\right)\right]^n. \tag{2.9}$$

The factor in the brackets taken to the power n arises from multiple insertions of the renormalized fermion loop into the bubble chain of Fig. 2.1. Furthermore the additional α_s in front of the integral appears due to the end points of the gluon propagator being attached to the large fermion loop. The function $F(\hat{k}^2)$ describes the gluon momentum distribution and is given by [11]

$$F(\hat{k}^2) = \frac{2C_F}{\pi^2}\sum_{s=2}^{\infty}(-1)^s\frac{\mathrm{d}}{\mathrm{d}s}\frac{1}{s^2-1}\int_{-\infty}^{\infty}dr\ e^{ir\ln\hat{k}^2}\left(\frac{1+ir}{r^2+s^2} - \frac{1}{1-ir}\right). \tag{2.10}$$

Its exact form shown in Eq. (2.10) is, however, not relevant in the following since the dominant contributions, at large orders, to the integral come from the momentum regions where $k \gg Q$ and $k \ll Q$. This is due to the large logarithmic contributions in these regions. As a consequence it suffices to know the small-$\hat{k}$ and large-$\hat{k}$ behaviour of $F(\hat{k}^2)$, which are found to be of the form [9]

$$\begin{aligned} F(\hat{k}^2) &= \frac{3C_F}{2\pi}\hat{k}^4 + \mathcal{O}(\hat{k}^6\ln\hat{k}^2), \\ F(\hat{k}^2) &= \frac{C_F}{3\pi}\frac{1}{\hat{k}^2}\left(\ln\hat{k}^2 + \frac{5}{6}\right) + \mathcal{O}\left(\frac{\ln\hat{k}^2}{\hat{k}^4}\right). \end{aligned} \tag{2.11}$$

Splitting the integral in Eq. (2.9) at $\hat{k}^2 = \mu^2/(Q^2 e^{-5/3}) \equiv \kappa$ and inserting the expression given in the first line of Eq. (2.11) for the small-$\hat{k}^2$ integral and the expression given in the second line of Eq. (2.11) for the large-$\hat{k}^2$ integral yields

$$\begin{aligned} D(Q^2) &= \sum_{n=0}^{\infty} \alpha_s^{n+1} \left(\frac{n_f T}{3\pi}\right)^n \Bigg\{ \int_0^{\kappa} \frac{d\hat{k}^2}{\hat{k}^2} \left(\frac{3C_F}{2\pi}\hat{k}^4\right) \left[\ln\left(\hat{k}^2\kappa^{-1}\right)\right]^n + \\ &\qquad \int_{\kappa}^{\infty} \frac{d\hat{k}^2}{\hat{k}^2} \left(\frac{C_F}{3\pi}\frac{1}{\hat{k}^2}\left(\ln \hat{k}^2 + \frac{5}{6}\right)\right) \left[\ln\left(\hat{k}^2\kappa^{-1}\right)\right]^n \Bigg\} \\ &= \frac{C_F}{\pi} \sum_{n=0}^{\infty} \alpha_s^{n+1} \Bigg\{ \frac{3}{4}\left(-\frac{n_f T}{6\pi}\right)^n \left(\frac{Q^2}{\mu^2}e^{-5/3}\right)^{-2} \Gamma(n+1) \\ &\qquad + \frac{1}{3}\left(\frac{n_f T}{3\pi}\right)^n \frac{Q^2}{\mu^2} e^{-5/3} \left[\Gamma(n+2) + \Gamma(n+1)\frac{5}{6}\right] \Bigg\} . \end{aligned} \tag{2.12}$$

Note that the second equal sign in Eq. (2.12) is only accurate up to additional non-singular terms from the IR and UV region. Considering the momentum regions from which the divergencies in Eq. (2.12) originate, the factorial divergence exhibited by the two series components are called *infrared (IR) renormalon* and *ultraviolet (UV) renormalon* respectively. The corresponding singularities in the Borel plane lie at $t^{\mathrm{IR}} = -6\pi/(n_f T)$ (IR renormalon) and $t^{\mathrm{UV}} = 3\pi/(n_f T)$ (UV renormalon). Defining $u^{\mathrm{IR/UV}} = -n_f T t^{\mathrm{IR/UV}}/(3\pi)$ one obtains for the Borel transform of Eq. (2.12)

$$B[D](u) = \frac{3C_F}{2\pi}\left(\frac{Q^2}{\mu^2}e^{-5/3}\right)^{-2} \frac{1}{2-u} + \frac{C_F}{3\pi}\frac{Q^2}{\mu^2}e^{-5/3}\left(\frac{1}{(1+u)^2} + \frac{5}{6}\frac{1}{1+u}\right). \tag{2.13}$$

The first term on the RHS of Eq. (2.13) is called the *leading IR renormalon*, whereas the second term is called the *leading UV renormalon* of the regarded Adler function. As one can easily see from Eq. (2.13) the positions of the leading IR and UV renormalon singularities are at

$$u^{\mathrm{IR}} = -\frac{n_f T}{3\pi}\cdot t^{\mathrm{IR}} = -\frac{n_f T}{3\pi}\cdot\frac{-6\pi}{N_f T} = 2$$

and

$$u^{\mathrm{UV}} = -\frac{n_f T}{3\pi}\cdot t^{\mathrm{UV}} = -\frac{n_f T}{3\pi}\cdot\frac{3\pi}{n_f T} = -1$$

on the real axis in the Borel plane. The large-order behaviour is dominated by the UV renormalon, as it is the closest to the origin. The double pole in Eq. (2.13) of the leading UV renormalon can be traced back to the appearance of $\Gamma(n+2)$ in the last term of Eq. (2.12). Originally, this contribution arises from the logarithm of $\hat{k}^2$ contained in the large-$\hat{k}$ expression for $F(\hat{k})$ in Eq. (2.11).

Let us recap the computation we just went through. In order to obtain the leading divergent behaviour of the Adler function, due to the fermion loops it was only necessary to consider the expansion at small or large $\hat{k}$ of the integrand of Fig. 2.1 without fermion loop insertions. In other words: The fermion loop insertions probe the large and small momentum tails of the gluon momentum distribution, which would otherwise give a small contribution to the integral of $F(\hat{k})$.

Although useful for practical applications, one could still ask the question if Fig. 2.1 provides a suitable approximation to renormalon divergences encountered in an actual perturbation series in non-Abelian gauge theories, such as QCD. In QCD, the n_f-terms coming from fermion bubble diagrams shown in Fig. 2.1 only give a small contribution to the complete perturbative coefficients. The problem is of course that other contributions associated with non-Abelian diagrams, like gluon and ghost bubbles, are excluded from the calculation. The absence of gluon self-couplings in the large n_f-limit has severe consequences, since one loses the QCD property of asymptotic freedom [12]. In order to approximately restore this property one needs to estimate the non-Abelian contribution to renormalon divergences. It was suggested, for instance in Refs. [11,13], to apply the substitution

$$n_f \to -\frac{3}{2}\left(\frac{11}{3}C_A - \frac{2}{3}n_f\right) = -\frac{3}{2}\beta_0 \tag{2.14}$$

to calculations involving bubble chains. The replacement rule given in Eq. (2.14) is referred to as *Naive Non-Abelianization* (NNA) [14] and applying it to bubble chain calculations actually gives a major contribution to perturbative coefficients in most of the cases where one can compare with exactly known results. Therefore, Eq. (2.14) is assumed to give a large-order approximation for qualitative (numerical) studies of perturbative series which mimics the large-order behaviour of those series in full QCD [13]. We further note that through the implementation of Eq. (2.14) the QCD property of asymptotic freedom is recovered, since this replacement leads to a sign-flip of the β-function. The bubble chain calculation, together with the replacement rule given in Eq. (2.14), constitutes the so-called *large-β_0 approximation*.

2.3 Operator Product Expansion

We have already eluded to the fact that renormalons, and in particular IR renormalons, arising from applying a Borel transform to a given perturbation series have an impact on the definition of the Borel integral given by Eq. (2.3). UV renormalons, as we saw in the previous section, are located on the negative real axis in the Borel plane and therefore lie outside the integration contour. As a consequence they have no influence on the Borel integral. When it comes to defining the Borel integral there exists an ambiguity generated by the singularities lying on the path of integration, e.g. there exist different possibilities of deforming the integration contour (either above or below the pole). One can estimate the ambiguity caused by an IR renormalon located on the path of integration by a contour integration around the singularity

$$\Delta D(Q^2) \sim \oint\limits_{u=p/2} du\; e^{\frac{-4\pi u}{\beta_0 \alpha_s(Q)}} \frac{1}{p/2-u} \propto \left(e^{-\frac{2\pi}{\beta_0\alpha_s(Q)}}\right)^p \sim \left(\frac{\Lambda_{\mathrm{QCD}}}{Q}\right)^p, \tag{2.15}$$

where Λ_{QCD} is the scale at which perturbation theory is no longer valid in the theory of strong interactions. Note that the Eq. (2.15) is only meaningful if in the singular term

$$\frac{1}{(p/2-u)^\alpha} \tag{2.16}$$

the power α is an integer. For $\alpha \notin \mathbb{Z}$ the singularity becomes a cut along the positive real axis. Hence the approximation in Eq. (2.15) has to be modified and one needs to adopt a prescription on how to deal with this singularity. We will elaborate more on this prescription in section 3.2.1.

Now we are at a crucial point: We know that the physical Adler function beyond perturbation theory, and physical observables in general, must not inhabit renormalon ambiguities. Therefore Eq. (2.15) implies that additional non-perturbative power corrections are needed, such that we obtain an unambiguously defined observable in the end. In this context a formalism can be used which achieves a systematic incorporation of non-perturbative effects in QCD calculations. This formalism is the concept of the Operator Product Expansion (OPE) [15]. In the following we intend to derive the general form of a d-dimensional contribution to the OPE of a generic physical observable (in this case we call it $\sigma(Q)$). The purpose of this derivation is that we understand how the generic structure of such a contribution arises, as this will become important in chapter 4.

It was Wilson who came up with the proposal of replacing a product of local operators evaluated at different space-time points that are close to each other by a linear combination of composite local operators

$$\lim_{x\to y} A(x)B(y) = \sum_i C_i(x-y)O_i(x), \tag{2.17}$$

which is called the OPE of the product on the LHS of Eq. (2.17). The $C_i(x-y)$ on the RHS of Eq. (2.17) are complex-valued coefficient functions, known as Wilson coefficients. Dimensional analysis indicates that those Wilson coefficients behave for $x \to y$ like the power $d_O - d_A - d_B$ of $x-y$, where the d_O refer to the dimensionality of the operator O_i in powers of mass (or momentum). When adding more fields or derivatives to an operator O_i in the OPE of the product $A(x)B(y)$, the mass dimension d_O increases. On a general note we can record the fact that the OPE is an important tool for QCD predictions. It allows to separate short- and long-distance physics into perturbatively computable Wilson coefficients and matrix elements of operators, which can't be accessed through the means of perturbation theory.

Let us now have a closer look at the structure of the OPE of a generic observable $\sigma(Q)$. OPE contributions to the Adler function will only be considered in section 4.1.2, after we have set up the formalism in an adequate way. Neglecting the dimensionality of the generic observable $\sigma(Q)$ for simplicity, the corresponding OPE in the $\overline{\text{MS}}$-scheme, according to Eq. (2.17), is given by

$$\begin{aligned}\sigma(Q) &= \overline{C}_0(Q) + \sum_i C_i(Q,\mu)\frac{\langle O_i(\mu)\rangle}{Q^p} + \ldots \\ &= \overline{C}_0(Q) + \vec{C}^\top(Q,\mu)\frac{\langle \vec{O}(\mu)\rangle}{Q^p} + \ldots \\ &= \overline{C}_0(Q) + \frac{F_O^p}{Q^p} + \ldots,\end{aligned} \tag{2.18}$$

where in the last equality we defined $F_O^p \equiv \vec{C}^\top(Q,\mu)\langle\vec{O}(\mu)\rangle$ as a general d-dimensional contribution to the OPE of $\sigma(Q)$. Starting from Eq. (2.18) we want to achieve the following: In a first step we seek to obtain a so-called Renormalization Group Improved (RGI) scheme of the OPE, where the large and small momentum scales, in the following denoted by Q and Λ_{IR} respectively, are strictly separated. In particular, we want to obtain a representation, where the Wilson coefficients $\vec{C}^\top(Q,\mu)$ only depend on the large momentum scale Q, whereas the matrix elements $\langle\vec{O}(\mu)\rangle$ should only depend on the scale Λ_{IR}. Subsequently we derive an expression for a general dimension d term in the OPE of a generic observable, which consists of the product of a Wilson coefficient that starts with unity at tree level and a non-perturbative matrix element, which one can determine from fits using experimental data. The final expression we are then going to obtain will be the starting point of the discussion in section 4.1.2, where we introduce the only relevant dimension 4 term (in the chiral limit) in the Euclidean Adler functions OPE, called the gluon condensate.

As we know by now, physical observables satisfy a homogeneous RGE. Looking at Eq. (2.18) this implies that the individual contributions to $\sigma(Q)$ have to be RG invariant as well. Hence, we get the relation

$$\frac{\mathrm{d}}{\mathrm{d}\ln\mu}\left(\vec{C}^\top(\mu)\langle\vec{O}(\mu)\rangle\right) = 0, \tag{2.19}$$

which subsequently yields

$$\left[\frac{\mathrm{d}}{\mathrm{d}\ln\mu}\vec{C}^\top(\mu)\right]\langle\vec{O}(\mu)\rangle = -\vec{C}^\top(\mu)\left[\frac{\mathrm{d}}{\mathrm{d}\ln\mu}\langle\vec{O}(\mu)\rangle\right]. \tag{2.20}$$

(In the following we denote $a_s = \alpha_s/\pi$, referring to the strong coupling in the $\overline{\text{MS}}$-scheme. This is not to be confused with the notation introduced in chapter 4 where the barred quantities $\bar{a}_Q$ are introduced for the full QCD studies. Those $\bar{a}_Q$'s denote the strong coupling in the C-scheme, which is discussed in appendix A.) If we now define

$$\frac{\mathrm{d}}{\mathrm{d}\ln\mu}\vec{O}(\mu) = -\gamma_O[a_s(\mu)]\vec{O}(\mu), \tag{2.21}$$

where the anomalous dimension matrix γ_O is of the form

$$\gamma_O[a_s(\mu)] = \gamma_O^{(1)}a_s + \gamma_O^{(2)}a_s^2 + \ldots, \tag{2.22}$$

the RGE for the Wilson coefficient reads

$$\frac{\mathrm{d}}{\mathrm{d}\ln\mu}\vec{C}(\mu) = \gamma_O^\top[a_s(\mu)]\vec{C}(\mu). \tag{2.23}$$

Due to the fact that F_O^p is easier to evaluate in an operator basis where the leading-order anomalous dimension matrix is diagonal, we use our knowledge from linear algebra to write

$$\gamma_D^{(1)} = V^{-1}\gamma_O^{(1)}V. \tag{2.24}$$

Recall that the diagonal elements of $\gamma_D^{(1)}$ in Eq. (2.24) are given by the eigenvalues of the initial leading-order anomalous dimension matrix. Inserting unity in the original definition of F_O^p gives

$$F_O^p = \vec{C}^\top(\mu)\langle\vec{O}(\mu)\rangle = \vec{C}^\top(\mu)VV^{-1}\langle\vec{O}(\mu)\rangle = \vec{C}_D^\top(\mu)\langle\vec{O}_D(\mu)\rangle, \tag{2.25}$$

where

$$\begin{aligned}\langle\vec{O}_D(\mu)\rangle &= V^{-1}\langle\vec{O}(\mu)\rangle,\\ \vec{C}_D(\mu) &= V^\top\vec{C}(\mu),\end{aligned} \tag{2.26}$$

and the leading order RGEs subsequently amount to

$$\begin{aligned}\frac{\mathrm{d}}{\mathrm{d}\ln\mu}\vec{O}_D(\mu) &= -\gamma_D^{(1)}a_s(\mu)\vec{O}(\mu),\\ \frac{\mathrm{d}}{\mathrm{d}\ln\mu}\vec{C}_D(\mu) &= \gamma_D^{(1),\top}a_s(\mu)\vec{C}_D(\mu).\end{aligned} \tag{2.27}$$

Up to this point we basically only reshuffled the expressions into a more convenient form. The next step is the non-trivial part where we separate the long and short distance physics.

The general ansatz for scale separation in this context is the introduction of a so-called renormalization group evolution matrix $U_{\mathrm{LL}}(\mu,\mu')$, which yields, considering at first only leading logarithmic (LL) order, for Eq. (2.25)

$$F_O^p = \vec{C}_D^\top(\mu)U_{\mathrm{LL}}(\mu,\mu')\langle\vec{O}_D(\mu')\rangle. \tag{2.28}$$

The corresponding LL RGE for $U_{\mathrm{LL}}(\mu,\mu')$ reads

$$\frac{\mathrm{d}}{\mathrm{d}\ln\mu}U_{\mathrm{LL}}(\mu,\mu') = -\mathrm{diag}\left[\vec{\gamma}_D^{(1)}\right]a_s(\mu)U_{\mathrm{LL}}(\mu,\mu'), \tag{2.29}$$

giving

$$U_{\mathrm{LL}}(\mu,\mu') = \mathrm{diag}\left[\left(\frac{a_s(\mu)}{a_s(\mu')}\right)^{2\vec{\gamma}_D^{(1)}/\beta_0}\right], \quad U_{\mathrm{LL}}(\mu,\mu) = \mathbb{1}. \tag{2.30}$$

as the solution.

Since we later want to have an expression for a dimension d term in the Euclidean Adler functions OPE series and are in particular interested in the gluon condensate contribution to the Adler functions OPE we also need to consider the next-to-leading order (NLO) contribution and its form in the RGI-scheme. The necessity arises from the fact that the information on the Wilson coefficient of the gluon condensate is known up to $\mathcal{O}(\alpha_s)$. The RGE for $U_{\mathrm{NLL}}(\mu,\mu')$ is given by

$$\frac{\mathrm{d}}{\mathrm{d}\ln\mu}U_{\mathrm{NLL}}(\mu,\mu') = -\left[\mathrm{diag}\left[\vec{\gamma}_D^{(1)}\right]a_s(\mu) + g a_s^2(\mu)\right]U_{\mathrm{NLL}}(\mu,\mu'), \tag{2.31}$$

where we have defined $g := V^{-1}\gamma_O^{(2)}V$. Using the ansatz

$$U_{\mathrm{NLL}}(\mu,\mu') = [\mathbb{1} + a_s(\mu)S]U_{\mathrm{LL}}(\mu,\mu')[\mathbb{1} - a_s(\mu')S] \tag{2.32}$$

one can solve the differential equation given in Eq. (2.31). The matrix S appearing in the ansatz above is (after a short calculation) found to be of the form

$$\begin{aligned} S^{ij} &= \frac{\beta_1}{4\beta_0}\gamma_D^{(1),i}\delta^{ij}\frac{1}{\gamma_D^{(1),i}-\gamma_D^{(1),j}-\beta_0/2} - \frac{g^{ij}}{\gamma_D^{(1),i}-\gamma_D^{(1),j}-\beta_0/2} \\ &= \frac{\beta_1}{2\beta_0^2}\gamma_D^{(1),i}\delta^{ij} + \frac{g^{ij}}{\beta_0/2+\gamma_D^{(1),j}-\gamma_D^{(1),i}}. \end{aligned} \tag{2.33}$$

Having obtained the solution for $U_{\mathrm{NLL}}(\mu,\mu')$, one can write down the general expression for a higher dimensional contribution of the OPE up to NLO in a way where a strict scale separation of the small and large momentum scales Λ_{IR} and Q, with $\Lambda_{\mathrm{IR}} \ll Q$ is implemented. The expression amounts to

$$\begin{aligned} F_O^p &= \vec{C}^\top(Q)U_{\mathrm{NLL}}(Q,\Lambda_{\mathrm{IR}})\langle\vec{O}(\Lambda_{\mathrm{IR}})\rangle \\ &= \vec{C}^\top(Q)[\mathbb{1}+a_s(Q)S]U_{\mathrm{LL}}(Q,\Lambda_{\mathrm{IR}})[\mathbb{1}-a_s(\Lambda_{\mathrm{IR}})S]\langle\vec{O}(\Lambda_{\mathrm{IR}})\rangle \\ &= \vec{C}^\top(Q)\,[\mathbb{1}+a_s(Q)S]\,\mathrm{diag}\left[(a_s(Q))^{\frac{2\vec{\gamma}_D^{(1)}}{\beta_0}}\right]\underbrace{\mathrm{diag}\left[(a_s(\Lambda_{\mathrm{IR}}))^{\frac{-2\vec{\gamma}_D^{(1)}}{\beta_0}}\right][\mathbb{1}-a_s(\Lambda_{\mathrm{IR}})S]\,\langle\vec{O}(\Lambda_{\mathrm{IR}})\rangle}_{\equiv\langle\hat{\vec{O}}(\Lambda_{\mathrm{IR}})\rangle} \\ &= \sum_{i,j} C_i(Q)[\delta_{ij}+a_s(Q)S_{ij}]\,(a_s(Q))^{\frac{2\gamma_{D,j}^{(1)}}{\beta_0}}\,\langle\hat{O}^j(\Lambda_{\mathrm{IR}})\rangle. \end{aligned} \tag{2.34}$$

As it is common in the literature to consider a Wilson coefficient, at least for the case of the gluon condensate, where the leading correction is unity, we take the additional step to rewrite Eq. (2.34) precisely in this way. Decomposing the Wilson coefficient in the form

$$C_i(Q) = a_s^{\delta_i}(Q)\sum_{n=0}^{\infty} c_i^{(n)}a_s^n(Q), \tag{2.35}$$

where δ_i represents the lowest power in the strong coupling contained in the Wilson coefficient C_i, the OPE term F_O^p can further be rewritten as

$$\begin{aligned} F_O^p &= \sum_{i,j} a_s^{\delta_i}(Q)[c_i^{(0)}+a_s(Q)c_i^{(1)}+\dots][\delta_{ij}+a_s(Q)S_{ij}]\,(a_s(Q))^{\frac{2\gamma_{D,j}^{(1)}}{\beta_0}}\,\langle\hat{O}^j(\Lambda_{\mathrm{IR}})\rangle \\ &= \sum_i a_s^{\delta_j}(Q)[c_j^{(0)}+a_s(Q)c_j^{(1)}]\,(a_s(Q))^{\frac{2\gamma_{D,j}^{(1)}}{\beta_0}}\,\langle\hat{O}^j(\Lambda_{\mathrm{IR}})\rangle \\ &\quad + \sum_{i,j} c_i^{(0)}a_s^{\delta_i}(Q)a_s(Q)S_{ij}\,(a_s(Q))^{\frac{2\gamma_{D,j}^{(1)}}{\beta_0}}\,\langle\hat{O}^j(\Lambda_{\mathrm{IR}})\rangle \\ &= \sum_j (a_s(Q))^{\delta_j+\frac{2\gamma_{D,j}^{(1)}}{\beta_0}}\left[c_j^{(0)}+a_s(Q)\left(c_j^{(1)}+\sum_i (a_s(Q))^{\delta_i-\delta_j}\,c_i^{(0)}S_{ij}\right)\right]\langle\hat{O}^j(\Lambda_{\mathrm{IR}})\rangle \\ &= \sum_j c_j^{(0)}\,(a_s(Q))^{\delta_j+\frac{2\gamma_{D,j}^{(1)}}{\beta_0}}\left[1+a_s(Q)(c_j^{(0)})^{-1}\left(c_j^{(1)}+\sum_i a_s(Q)^{\delta_i-\delta_j}c_i^{(0)}S_{ij}\right)\right]\langle\hat{O}^j(\Lambda_{\mathrm{IR}})\rangle. \end{aligned} \tag{2.36}$$

Note that in the above calculation we dropped contributions of $\mathcal{O}(a_s^2)$ in the expansion of the product of the square brackets in the first line, since those are not necessary for the discussion in the following sections. The last step in our derivation of a general dimension d term suited for the discussion in section 4.1.2 is yet another re-definition of the Wilson coefficients C_j and leading powers of the strong coupling δ_j in the following way

$$F_O^p =: \sum_j \hat{c}_j^{(0)} \left(a_s(Q)\right)^{\hat{\delta}_j + \frac{2\gamma_{D,j}^{(1)}}{\beta_0}} \left[1 + a_s(Q)\hat{c}_j^{(1)} + \ldots\right] c^{\hat{\delta}_j} \langle \hat{O}^j(\Lambda_{\mathrm{IR}})\rangle. \tag{2.37}$$

Eq. (2.37) is formulated such that the correction term $a_s(Q)\hat{c}_j^{(1)}$ in the square brackets is $\mathcal{O}(\alpha_s)$-suppressed. Note that the leading powers $\hat{\delta}_j$, which we newly defined, do not need to be identical with δ_j. Eq. (2.37) now concludes our derivation.

In the next chapter we are going to introduce the two resummation approaches for the τ hadronic spectral function moments and discuss the discrepancy related to them. Reconciling those two approaches in the novel framework of the *renormalon-free gluon condensate scheme* will then be the content of section 4 and the main interest of the present thesis.

Chapter 3

Theoretical Overview of Hadronic τ Decays

The determination of the strong coupling α_s from hadronic τ decays represents one of the most precise methods to obtain this fundamental quantity of QCD from experiment. The method of how to extract this parameter in phenomenological analysis using experimental data will be presented in detail in chapter 5. What we want to discuss in the following is the theoretical contribution that enters the analysis. In particular, we are interested in the perturbative part of the theoretical moments as they inhabit one of the dominant contributions to the general uncertainty of the strong coupling. To be concrete, we examine how the discrepancy between Fixed-Order (FOPT) and Contour-Improved (CIPT) perturbation theory arises. Together with a brief introduction to QCD sum rules and a summary of recent publications [5,16] studying the systematic discrepancy between CIPT and FOPT this constitutes the content of the current section.

3.1 Theoretical Introduction

In principle all basic two-point correlation functions (e.g. the vector/axialvector and the scalar /pseudoscalar correlation function) contribute to the theoretical moments of the hadronic τ decay rate. For the current discussion, however, it will be sufficient to concentrate exclusively on the vector correlation function and its corresponding contribution to the theoretical moments. This is, due to the fact that in the chiral limit, considering massless quarks, the scalar contributions vanish, and the vector and axialvector contributions coincide. How the final moments on the theoretical side actually arise in practical fits will be discussed extensively in section 5.2, where further details on the treatment of the remaining correlators will be presented.

3.1.1 The correlation function

In momentum space the vector correlation function $\Pi_{\mu\nu}(p)$ is defined by the following relation

$$\Pi_{\mu\nu}(p) \equiv i \int dx\; e^{ipx} \langle \Omega | T\{ j_\mu(x) j_\nu(0)^\dagger \} | \Omega \rangle, \tag{3.1}$$

where $|\Omega\rangle$ denotes the physical QCD vacuum. For hadronic τ decays (see Fig. 3.1), only two flavour non-diagonal currents contribute. The first current is given by

$$j_\mu = {:}\bar{u}(x)\gamma_\mu d(x){:} \tag{3.2}$$

and the second current has the analogous form except for the replacement of the down quark by a strange quark. One can write down the Lorentz decomposition of the correlator $\Pi_{\mu\nu}(p)$ as

$$\Pi_{\mu\nu}(p) = (p_\mu p_\nu - g_{\mu\nu} p^2)\Pi^{(1+0)}(p^2) + g_{\mu\nu} p^2 \Pi^{(0)}(p^2), \tag{3.3}$$

where the superscripts denote the components corresponding to the transversal, $J = 1$, and longitudinal, $J = 0$, angular momentum in the hadronic rest frame. The longitudinal component

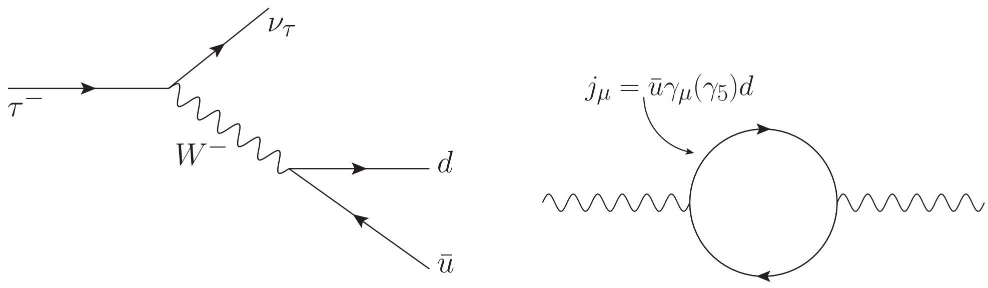

(a) τ lepton decaying hadronically **(b)** Correlator

Fig. 3.1: The process of the τ lepton decaying hadronically (Fig. 3.1a) can be related to the imaginary part of the correlator (Fig. 3.1b) containing the flavor non-diagonal currents j_μ via the optical theorem. Note that the down quark could also be replaced by a strange quark.

$\Pi^{(0)}(s)$, where $s \equiv p^2$, is related to the scalar or pseudoscalar correlators. Therefore it vanishes in the chiral limit. To facilitate the discussion we will further write $\Pi(s) = \Pi^{(1+0)}(s)$.

At this point we have to acknowledge a problem related to the OPE's description of the underlying physics near the positive real axis, which will become relevant in the following: Although the OPE provides a good approximation to the correlator, or the Adler function respectively, in the Euclidean region, when approaching the Minkowskian domain violations of quark hadron duality are expected to occur, due to the presence of bound-state or resonance poles. In other words: In the Euclidean domain, a duality exists between descriptions of the system in terms of the quark and gluon degrees of freedom of QCD, or the physical hadronic degrees of freedom. Upon analytic continuation of correlation functions towards the Minkowskian region, due to the presence of resonances, violations of the quark hadron duality are expected to show up.

This will now become relevant in discussion of QCD sum rules, which play a crucial role in practical calculations of the theoretical moments.

3.1.2 QCD sum rules

When talking about the theoretical correlation function the question of how to conceptually relate it to the experimentally measured spectral function naturally arises. In the context of hadronic τ decays one typically considers so-called *Finite Energy Sum Rules* (FESR), where we seek to exploit the analytic structure of the correlation function. Consider the closed contour in the complex plane depicted in Fig. 3.2. Since the correlation function only has a cut on the positive real s-axis, the integral along the contour in Fig. 3.2 of $w(x)\Pi(s)$, where $w(x)$ is a weight function which does not introduce additional poles or cuts, should vanish due to Cauchy's theorem. Note that the (usually polynomial) weight function is introduced at this point, since it is also part of the hadronic tau decay rate. To relate the spectral function to the correlation function, we recall the well known relation

$$\rho(s) = \frac{1}{\pi}\mathrm{Im}[\Pi(s + i0)] \tag{3.4}$$

derived from analyticity properties of the correlation function, see e.g. [17]. Using further the Schwarz reflection principle, $\Pi(s^*) = \Pi^*(s)$, leading to

$$\Pi(s + i0) - \Pi(s - i0) = \Pi(s + i0) - \Pi^*(s + i0) = 2i\mathrm{Im}\Pi(s + i0) = 2\pi i\rho(s) \tag{3.5}$$

allows us to derive the FESR

$$R(s_0) \equiv \int_0^{s_0} ds\ w(s)\rho(s) = -\frac{1}{2\pi i}\oint_{|s|=s_0} ds\ w(s)\Pi(s). \tag{3.6}$$

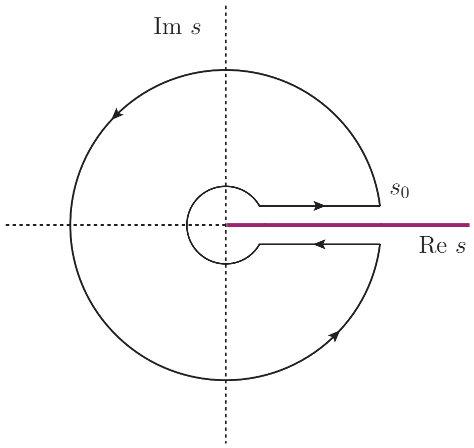

Fig. 3.2: Contour integral in the complex s-plane.

The advantage of the FESR is that the sprectral function is only required up to a finite energy s_0. The downside, however, is that it becomes necessary to evaluate the correlator close to the real axis, where perturbation theory is now longer applicable.

To connect the above discussion to the analysis of the total decay rate of τ-leptons into hadrons, we note that a spectral integral of the type of Eq. (3.6) appears in the process of the τ-lepton decaying hadronically (see Fig. 3.1)

$$R_\tau \equiv 12\pi^2 \int_0^{s_0} \frac{ds}{s_0}\, w(s) \frac{1}{\pi} \mathrm{Im}\Pi(s) = 12\pi^2 \int_0^{s_0} \frac{ds}{s_0}\, w(s)\rho(s) \equiv \frac{\Gamma(\tau \to \text{hadrons } \nu_\tau)}{\Gamma(\tau \to \mu\bar{\nu}_\mu \nu_\tau)}, \tag{3.7}$$

which is the most general definition of spectral-function moments. For the case of the hadronic τ-decay rate (e.g. for the last equality in Eq. (3.7) to be true), the relevant weight function, in Eq. (3.7) denoted by $w(s)$, turns out to be

$$w(s) = \left(1 - \frac{s}{s_0}\right)^2 \left(1 + 2\frac{s}{s_0}\right) \tag{3.8}$$

with $s_0 = m_\tau^2$ in this particular case. Eq. (3.8) merely arises from the kinematics involved in the decay. This is the reason why it is referred to as the kinematic moment. One accidental neat attribute of Eq. (3.8) is that the weight function introduces a double zero at $s = s_0$, such that contributions close to the real axis are suppressed. Nevertheless, contributions arising from duality violations (DV's) remain and can only be estimated by using certain models. We will elaborate more on this in section 5.2.3.

Recalling the vector correlation function and the corresponding Lorentz decomposition given in Eq. (3.3), we write down the theoretical decay rate of the τ-lepton as

$$R_\tau = 12\pi \int_0^{m_\tau^2} \frac{ds}{m_\tau^2} \left(1 - \frac{s}{m_\tau^2}\right)^2 \left(1 + 2\frac{s}{m_\tau^2}\right) \mathrm{Im}\Pi(s). \tag{3.9}$$

Note that in Eq. (3.9) we already took into account the vanishing longitudinal component. Through the FESR, Eq. (3.9) is subsequently expressed as a contour integral

$$R_\tau = 6\pi i \oint_{|s|=m_\tau^2} \frac{ds}{m_\tau^2} \left(1 - \frac{s}{m_\tau^2}\right)^2 \left(1 + 2\frac{s}{m_\tau^2}\right) \Pi(s). \tag{3.10}$$

Using integration by parts, Eq. (3.10) can be rewritten in terms of an expression containing the Adler function $D(s)$. We consider (for the purpose of the current discussion and for the remainder of the thesis) the reduced Adler function $D(s)$ defined as

$$\frac{1}{4\pi^2}(1+D(s)) = -s\frac{\mathrm{d}\Pi(s)}{\mathrm{d}s}. \tag{3.11}$$

Using the dimensionless integration variable $x \equiv s/m_\tau^2$ we obtain

$$R_\tau = \frac{N_c}{2}\left[1 + \frac{1}{2\pi i}\oint\limits_{|x|=1} \frac{dx}{x}(1-x)^3(1+x)D(m_\tau^2 x)\right], \tag{3.12}$$

with $N_c = 3$. In the following the contributions to the Adler function $D(s)$ can be organised through the framework of the OPE in a series of local gauge-invariant operators of increasing dimension times appropriate inverse powers of s. This expansion is expected to be well behaved along the complex contour $|s| = m_\tau^2$, except for the case when one considers to be close to the crossing point with the positive real axis. There, again, the problem related to DV contributions in this region arises. Nevertheless, in the case of Eq. (3.12), the contribution near the physical cut at $s = m_\tau^2$ is strongly suppressed by a zero of order three. Therefore, uncertainties associated to DV effects near the time-like axis are expected to be very small.

If we now take Eq. (3.12), write the Adler function in terms of the sum of perturbative contributions and higher dimensional contributions through the framework of the OPE and further include DV effects, we obtain the general form for the theoretical moments which reads

$$R_{V/A}^{(W)}(s_0) \;=\; \frac{N_c}{2}\, S_{\rm ew}\, |V_{ud}|^2 \Big[\, \delta_W^{\rm tree} + \delta_W^{(0)}(s_0) + \sum_{d\geq 4} \delta_{W,V/A}^{(d)}(s_0) + \delta_{W,V/A}^{(\rm DV)}(s_0) \Big] , \tag{3.13}$$

where the factor $S_{\rm ew}$ represents factorizable electroweak corrections and V_{ud} is a CKM matrix element. Note that s_0 does not have to equal m_τ^2 as it can also attain lower values. This dependence of the moments on s_0 is denoted in Eq. (3.13). The term $\delta_W^{\rm tree}$ is the tree level contribution while $\delta_W^{(0)}(s_0)$ contains the higher-order perturbative QCD corrections in the chiral limit. The power-suppressed non-perturbative corrections from the OPE condensates of dimension d are encoded in $\delta_{W,V/A}^{(d)}(s_0)$ and, finally, $\delta_{W,V/A}^{(\rm DV)}(s_0)$ represents the duality violating contributions. Note that the notation for the weight function $W(x)$ was introduced in Eq. (3.13), denoting the weight function on the level of the Adler function. This is in contrast to $w(x)$, which corresponds to the weight function on the level of the spectral function. The relation between those two polynomials is given by

$$W(x) = 2\int_x^1 dz\; w(z). \tag{3.14}$$

The experimental counterpart to Eq. (3.13) can be obtained from a weighted integral over the spectral functions $\rho_{V/A}(s)$ as

$$R_{V/A}^{(W)}(s_0) \;=\; 12\pi^2\, S_{\rm ew}\, |V_{ud}|^2 \int\limits_0^{s_0} \frac{ds}{s_0} \left[w(\tfrac{s}{s_0})\rho_{V/A}^{(1+0)}(s) - w_L(\tfrac{s}{s_0})\rho_{V/A}^{(0)}(s) \right] , \tag{3.15}$$

where the longitudinal term involving $\rho_{V/A}^{(0)}$ is shown for completeness, but does not play any role in the present analysis as we choose to neglect this contribution.

Now that we have a general idea of how the experimental data is connected to the theoretical description, we will investigate more closely the perturbative contribution of the theoretical moments $\delta_W^{(0)}(s_0)$. This contribution is particularly interesting since it is the origin of a major uncertainty related to α_s extractions in phenomenological analysis of hadronic τ decays.

3.1.3 Perturbative Contribution to Theoretical Moments

We already know that the purely perturbative correction $\delta_W^{(0)}(s_0)$ in Eq. (3.13) only receives contributions from the vector and axialvector in the limit of massless quarks. Since in this limit vector and axialvector contributions coincide, to investigate $\delta_W^{(0)}(s_0)$ we can restrict ourselves to the study of the perturbative expansion of the vector correlator. It exhibits the general structure

$$\Pi(s) = -\frac{N_c}{12\pi^2}\sum_{n=0}^{\infty} a_\mu^n \sum_{k=0}^{n+1} c_{n,k}L^k, \quad L \equiv \ln\left(\frac{-s}{\mu^2}\right), \tag{3.16}$$

with $a_\mu \equiv a(\mu^2) \equiv \alpha_s(\mu^2)/\pi$ and μ being the renormalisation scale. Utilizing Eq. (3.11), we can also write down the Adler function expressed in the form of its general expansion (here and in the following $\hat{D}$ denotes the fact that we consider the perturbative contribution of the Adler function)

$$\hat{D}(s) = \frac{N_c}{3}\sum_{n=1}^{\infty} a_\mu^n \sum_{k=1}^{n+1} k\ c_{n,k}L^{k-1}. \tag{3.17}$$

Since the Adler function satisfies a homogeneous RGE, the logarithms in Eq. (3.17) can be resummed with the choice $\mu^2 = -s$, leading to

$$\hat{D}(s) = \frac{N_c}{3}\sum_{n=1}^{\infty} c_{n,1}a^n(-s). \tag{3.18}$$

The coefficients $c_{n,1}$ in Eq. (3.18) are known analytically up to $\mathcal{O}(\alpha_s^4)$ [18–20]. Considering the $n_f = 3$ flavor scheme, the coefficients $c_{n,1}$ in the $\overline{\mathrm{MS}}$-scheme are given by

$$\begin{aligned}
c_{1,1} &= 1,\\
c_{2,1} &= \frac{299}{24} - 9\zeta_3 = 1.640,\\
c_{3,1} &= \frac{58057}{288} - \frac{779}{4}\zeta_3 + \frac{75}{2}\zeta_5 = 6.371,\\
c_{4,1} &= \frac{78631453}{20736} - \frac{1704247}{432}\zeta_3 + \frac{4185}{8}\zeta_3^2 + \frac{34165}{96}\zeta_5 - \frac{1995}{16}\zeta_7 = 49.076.
\end{aligned} \tag{3.19}$$

In addition to those first four known coefficients, it is common to further consider an estimate for $c_{5,1}$ in order to be able to work at $\mathcal{O}(\alpha_s^5)$. There exist several independent estimates of this 6-loop coefficient. In this thesis we will take $c_{5,1}$ to be [4, 20–23]

$$c_{5,1} \;=\; 280 \pm 140\,. \tag{3.20}$$

In the following section, we will turn our attention to the main point of interest of this thesis, namely the discrepancy which arises when applying different resummation approaches to the perturbative contribution in Eq. (3.13). Getting predictable control of this discrepancy was the main discussion point in recent work by Hoang and Regner [5, 16]. Before we discuss the findings of Hoang and Regner, we first have to introduce the two prescriptions for setting the renormalization scale in the QCD corrections of Eq. (3.13).

3.2 Renormalisation group summation

Let us now discuss the two main different possibilities of performing renormalisation scale settings of the perturbative corrections in Eq. (3.13). The two approaches go under to the names of Fixed-Order (FOPT) and Contour-Improved (CIPT) Perturbation Theory. Starting from Eq. (3.12) and inserting the general expansion of the Adler function given by Eq. (3.17) for $\hat{D}(s)$, the perturbative correction in Eq. (3.13) is found to be

$$\delta_W^{(0)}(s_0) = \sum_{n=1}^{\infty} a_\mu^n \sum_{k=1}^{n} k\ c_{n,k}\frac{1}{2\pi i}\oint\limits_{|x|=1}\frac{dx}{x}(1-x)^3(1+x)\ln^{k-1}\left(\frac{-s_0 x}{\mu^2}\right), \tag{3.21}$$

where the identical contribution from the axialvector correlator has already been taken into account. Note of course that the scalar correlator yields no contribution in the chiral limit we consider. Recalling the fact that the Adler function and therefore also the perturbative corrections $\delta_W^{(0)}(s_0)$ satisfy a homogeneous RGE we are able to implement different conventions for treating the logarithms in Eq. (3.21).

In FOPT the renormalization scale setting $\mu^2 = s_0$ is used, which leads to

$$\delta_{\mathrm{FO}}^{(0)}(s_0) = \sum_{n=1}^{\infty} a^n(s_0) \sum_{k=1}^{n} k \; c_{n,k} J_{k-1}. \tag{3.22}$$

In Eq. (3.22) the J_{k-1} are given by

$$J_k = \frac{1}{2\pi i} \oint\limits_{|x|=1} \frac{dx}{x}(1-x)^3(1+x)\ln^k(-x). \tag{3.23}$$

CIPT, on the other hand, adopts the renormalization scale choice $\mu^2 = -s_0 x$ so that the logarithms vanish, yielding

$$\delta_{\mathrm{CI}}^{(0)}(s_0) = \sum_{n=1}^{\infty} c_{n,1} J_n^a(s_0), \tag{3.24}$$

where the J_n^a are found to be

$$J_n^a(s_0) = \frac{1}{2\pi i} \oint\limits_{|x|=1} \frac{dx}{x}(1-x)^3(1+x)\left(\frac{\alpha_s(-s_0 x)}{\pi}\right)^n. \tag{3.25}$$

In contrast to FOPT, for CIPT each order in n solely depends on the corresponding coefficient $c_{n,1}$. Thus all contributions proportional to the coefficient $c_{n,1}$ which in FOPT appear at all perturbative orders equal or greater than n are resummed into a single term. This is related to the fact that CIPT couples the running of the QCD coupling to the location of the integration contour in the complex s-plane.

An important point worth emphasizing is that while the two expansions are related to a simple change of renormalization scheme for α_s at the level of the underlying Adler function, the resulting CIPT and FOPT moment perturbation series do not have this property (i.e. once the contour integral is carried out). The CIPT method differs from FOPT in that it resums the powers of $\ln(-s/s_0)$ to all orders along the contour integration [2,3]. Furthermore, while the FOPT series for $\delta_W^{(0)}(s_0)$ is an explicit power series in the strong coupling α_s at a fixed renormalization scale, the CIPT series is based on a prescription where a running renormalization scale is considered. This means that it is not possible to obtain the CIPT series from the FOPT series through a change of renormalization scheme after having performed the contour integration.

Before we start with the discussion on how to eliminate the discrepancy arising from the different resummation approaches, we will briefly look at how the numerical results turn out prior to the application of our new method of determining the perturbative series. First, we have a look at the large-β_0 approximation and in the following we will also briefly consider numerical results in full QCD. Furthermore, in the last section of this chapter, we review the key aspects of Refs. [5,16] on how to quantify the discrepancy which arises between CIPT and FOPT.

3.2.1 Fixed-Order and Contour-Improved Perturbation Theory in the large-β_0 approximation

As opposed to full QCD, where one has to rely on models to study the behaviour of the perturbative series at higher orders (see e.g. [4,24]), the full Borel function is actually known to all orders in the large-β_0 approximation. Note that we consider the Adler function along the Euclidean axis. This means, that for $s = -|s|$, we use the definition $Q^2 \equiv -s \equiv |s|$. Furthermore, we define the Borel function w.r.t. the expansion in powers of $\alpha_s(Q^2)$, where for $\hat{D}(-Q^2)$ we obtain $B[\hat{D}(-Q^2)](u)$. To facilitate the discussion we write in the following $B[\hat{D}(-Q^2)](u) = B[\hat{D}](u)$. The Borel function for the Adler function in the large-β_0 approximation is then given by [25]

$$\begin{aligned} B[\hat{D}](u) &= \frac{128}{3\beta_0}\,\frac{e^{5u/3}}{2-u}\sum_{k=2}^{\infty}\frac{(-1)^k\,k}{[k^2-(1-u)^2]^2} \\ &= \tfrac{128}{3\beta_0}\,e^{5u/3}\Big\{\tfrac{3}{16(2-u)}+\sum_{p=3}^{\infty}\Big[\tfrac{d_2(p)}{(p-u)^2}-\tfrac{d_1(p)}{p-u}\Big]-\sum_{p=-1}^{-\infty}\Big[\tfrac{d_2(p)}{(u-p)^2}+\tfrac{d_1(p)}{u-p}\Big]\Big\} \end{aligned} \tag{3.26}$$

with $d_2(p) = \frac{(-1)^p}{4(p-1)(p-2)}$ and $d_1(p) = \frac{(-1)^p(3-2p)}{4(p-1)^2(p-2)^2}$. The perturbative coefficients $c_{n,1}$ of the Adler function (shown in Eq. (3.18)) can be obtained from expanding Eq. (3.26)

$$\Big[B[\hat{D}](u)\Big]_{\text{Taylor}} = \sum_{n=1}^{\infty}\frac{u^{n-1}}{\Gamma(n)}c_{n,1} \tag{3.27}$$

and further integrating the resulting series term-by-term (recall $x = s/s_0$)

$$\hat{D}(s) = \int_0^{\infty}\mathrm{d}u\,\Big[B[\hat{D}](u)\Big]_{\text{Taylor}}\;e^{-\frac{4\pi u}{\alpha_s(-xs_0)\beta_0}}\,. \tag{3.28}$$

To obtain the perturbative coefficients corresponding to a series in $\alpha_s(s_0)$ one can make use of the LL RGE for the strong coupling

$$\alpha_s(-xs_0) = \frac{\alpha_s(s_0)}{1+\frac{\alpha_s(s_0)\beta_0}{4\pi}\ln(-x)}$$

on the perturbative level. In contrast to modifying the perturbative series, it is also a possibility to rewrite Eq. (3.28), using the LL RGE of α_s, into the following form

$$\hat{D}(s) = \int_0^{\infty}\mathrm{d}u\,\Big[B[\hat{D}](u)\,e^{-u\ln(-x)}\Big]_{\text{Taylor}}\;e^{-\frac{4\pi u}{\alpha_s(s_0)\beta_0}} \tag{3.29}$$

and then carry out the expansion consistently.

Another important aspect related to the Borel calculus is the presence of an all order value of the perturbative series, called the *Borel sum*. This Borel sum is in principle not unique, due to the presence of poles (or cuts in full QCD) on (along) the positive real axis in the Borel plane. We therefore adopt in the following for the definition of the Borel sum the common principal value (PV) prescription, where the average of deforming the integration contour above and below the pole (or cut) on the real u-axis is taken. The expression for the Borel sum then reads

$$\hat{D}(s) = \text{PV}\int_0^{\infty}\mathrm{d}u\,\Big[B[\hat{D}](u)\Big]\,e^{-\frac{4\pi u}{\alpha_s(-xs_0)\beta_0}}\,. \tag{3.30}$$

The PV definition of the Borel sum integral is, however, ambiguous and the size of this ambiguity is, for the purpose of this thesis, defined by taking the size of the imaginary part of the u-contour integral either above or below the real axis multiplied by the standard normalization of $1/\pi$. Both the Borel sum and its corresponding ambiguity will be part of the numerical studies of the perturbative series throughout this thesis.

Let us now recall that the CIPT approach is based on the perturbative series for the Adler function given by

$$\hat{D}(s) = \sum_{n=1}^{\infty}c_{n,1}\left(\frac{\alpha_s(-s)\beta_0}{4\pi}\right)^n, \tag{3.31}$$

with real-valued coefficients $c_{n,1}$ and in general complex-valued powers of the strong coupling. The FOPT approach arises from expanding the series Eq. (3.31) in powers of $\alpha_s(s_0)$, such that the complex phases appear only in powers of $\ln(-s/s_0)$ within the coefficients of the power series in

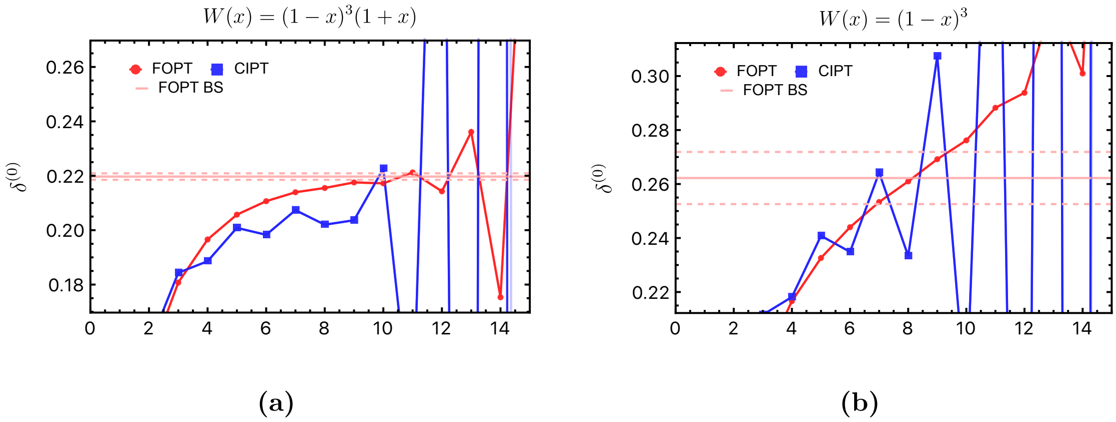

Fig. 3.3: Behaviour of the perturbative series using the CIPT and FOPT expansion methods in the large-β_0 approximation. Fig. 3.3a shows the behaviour for FOPT and CIPT for the kinematic moment. Fig. 3.3b illustrates the runaway behaviour of the perturbative series, in both FOPT and CIPT, for a moment that enhances the $u = 2$ renormalon.

$\alpha_s(s_0)$. The numerical results for FOPT and CIPT are given in Fig. 3.3, where the perturbative expansions are plotted as a function of order in perturbation theory. The light red horizontal line represents the Borel sum in each case. The space between the dashed red horizontal lines is the corresponding ambiguity. The FOPT series are shown in red in both panels and the CIPT expansion is given in blue. For the case of the kinematic moment, Fig. 3.3a, the discrepancy between FOPT and CIPT is clearly visible between orders five and nine. Note that the discrepancy between the two expansions is larger than the ambiguity of the Borel sum. The CIPT series approaches a result at intermediate orders significantly below the value of the FOPT series, and later runs into the asymptotic regime and diverges. The FOPT series on the other hand slowly approaches the Borel sum, before it starts diverging at orders 11 and higher. Note that the weight function arising from the kinematics of the decay is one prominent example of a moment suppressing the GC contribution. The reason for this suppression is the absence of an x^2 term in the polynomial weight function $W(x)$ on the level of the Adler function. As the GC is $1/s^2$ suppressed (see e.g. Eq. (4.13)), the fact that the absence of such an x^2 term causes the GC contribution to be suppressed can be seen from

$$\frac{1}{2\pi i}\oint_{|s|=s_0}\frac{\mathrm{d}s}{s}\left(-\frac{s}{s_0}\right)^k\frac{1}{s^2} = \begin{cases} 0\,, & \text{for } k\neq 2 \\ \frac{1}{s_0^2} & \text{for } k=2 \end{cases}\,. \tag{3.32}$$

Hence the GC can only contribute through its one-loop correction, which yields only a tiny effect for polynomials without an x^2 term. From now on we call moments suppressing the GC, e.g. moments which do not contain an x^2 term, *GC suppressing (GCS)* moments and moments enhancing the GC *GC enhancing (CGE)* moments.

In Fig. 3.3b we show results for the GCE moment $W(x) = (1-x)^3$, which is a *doubly-pinched* moment sensitive to the gluon condensate through its x^2 term. Here 'doubly-pinched' refers to the fact that the corresponding weight function on the level of the spectral function vanishes quadratically at $x = 1$. This wording will be used throughout the thesis and is also common the literature. We clearly observe the run-away behaviour discussed in Ref. [24] and associated with the gluon condensate renormalon singularity. Neither of the two series show any sign of stabilization before they run into the asymptotic regime. Note that the gluon condensate renormalon can be made responsible for this asymptotic behaviour since it is the IR singularity which is located closest to the pole and hence has the most severe effect on the behaviour of the perturbative series. The space between the dashed lines in both figures denotes the ambiguity corresponding to the PV prescription of the Borel integral.

We continue by discussing the analogous perturbative series in full QCD, where we have an additional model dependence, starting from the 6th order term (7-loop coefficient) onwards, due to missing higher order information on the perturbative coefficients.

3.2.2 Fixed-Order and Contour-Improved Perturbation Theory in full QCD

Let us now consider the perturbation series in full QCD. In this analysis it is necessary to construct a physically motivated model for the Adler function series. Since the first four coefficients of the perturbative series of the Adler function are known and there exists an estimate for the six-loop coefficient, a condition on the model should of course be that it reproduces these first four known coefficients plus the estimate for $c_{5,1}$. Furthermore, we know that the large order behaviour of the series is governed by effects arising from the UV renormalons, in particular we observe a sign-alternating divergence. The lower order terms seem untouched by this UV behaviour, which means that likely the normalizations of the UV renormalons are small. Hence it should suffice to include only the $u = -1$ UV renormalon, reflecting the leading UV renormalon divergence in the exactly known Borel function of the large-β_0 approximation given in Eq. (3.26). Note that the leading UV renormalon in Eq. (3.26) corresponds to a double pole singularity. This means that we have to choose the anomalous dimension corresponding to the $u = -1$ singularity such that in the large-β_0 limit we again obtain this double pole structure.

The fact that the lower order terms seem untouched by this UV behaviour of course means that the lower and intermediate orders are governed by IR renormalons, which yields the addition of two IR renormalon singularities to our model, namely the $u = 2$ and the $u = 3$ renormalon. This combination intends to merge the large-order behaviour, i.e. the sign-alternating UV divergence, with the lower-order IR dominated behaviour. Note further the following fact: Since the five-loop running of the QCD coupling is considered in the contour integration which relates the Adler function to the hadronic τ decay rate, the renormalon singularities in the Borel model, originally being single and double poles in the large-β_0 approximation, become cuts in the treatment in full QCD.

Taking all of the above into account, the ansatz for the Borel model in full QCD therefore takes the form

$$B[\hat{D}(s)]_{\rm mr}(u) = b^{(0)} + b^{(1)}u + \frac{N_{4,0}\left[1 + \bar{a}(-s)\bar{c}^{(1)}_{4,0}\right]}{(2-u)^{\gamma_4}} + \frac{N_{6,0}}{(3-u)^{\gamma_6}} + \frac{N_{-2}}{(1+u)^{\gamma_{(-2)}}}, \tag{3.33}$$

where the precise values for all parameters in Eq. (3.33) are found in appendix B. The last three terms in Eq. (3.33) encode the information for the three leading renormalon singularities in the large-β_0 Borel function, where we include the known $\mathcal{O}(\alpha_s)$ correction to the Wilson coefficient of the GC in our model. We also need to emphasize that the construction of the Borel model given in Eq. (3.33) is based in the C-scheme for the strong coupling, introduced in appendix A, which is denoted by the barred quantities in the Borel model.

We now carry out the analogous investigation as in the large-β_0 approximation given in Fig. 3.3. The corresponding results in full QCD, based on the MRM given by Eq. (3.33) (or rather Eq. (B.1)) are shown in Fig. 3.4. As it was the case in the large-β_0 approximation for the kinematic moment we observe a clearly visible discrepancy for the perturbative series stemming from the two different expansion approaches already at orders four and five. This discrepancy remains up to higher orders until the series run into their asymptotic regime at orders ten and onwards. This is depicted in Fig. 3.4a. The runaway behaviour for Fig. 3.4b, associated to the gluon condensate renormalon singularity, is also again clearly visible.

After this brief review of the well-known results from the past we now want to introduce as a last discussion topic the so-called asymptotic separation, which was thoroughly examined in two recent publications [5, 16]. For our purposes it is sufficient to only briefly summarize the findings of Refs. [5, 16] without dwelling too much on the technical details therein.

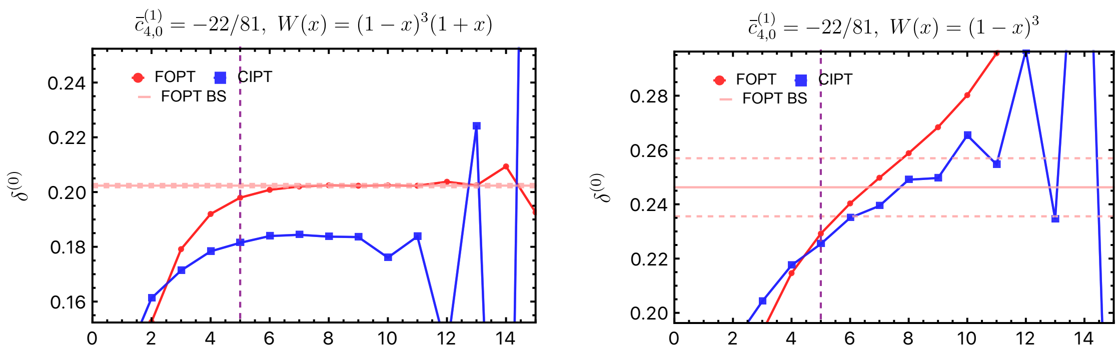

(a) **(b)**

Fig. 3.4: Behaviour of the perturbative series as for Fig. 3.3 in full QCD considering the MRM in Eq. (3.33). Fig. 3.4a shows the behaviour for FOPT and CIPT for the kinematic moment. Fig. 3.4b illustrates the runaway behaviour of the perturbative series, in both FOPT and CIPT, for a moment that enhances the $u = 2$ renormalon. The purple vertical line indicates the model dependence starting from order 6.

3.3 The Asymptotic Separation

In all studies prior to Ref. [5] it was always assumed that the Borel sums of the series for CIPT and FOPT are identical and of the form

$$\delta^{(0),\mathrm{FOPT}}_{\mathrm{Borel}}(s_0) = \mathrm{PV}\int\limits_0^\infty \mathrm{d}u\ \frac{1}{2\pi i}\oint\limits_{|x|=1}\frac{\mathrm{d}x}{x}W(x)B[\hat{D}](u)e^{-\frac{4\pi u}{\beta_0\alpha_s(-xs_0)}}, \tag{3.34}$$

where PV denotes the principal value prescription for the u-integration. In Refs. [5, 16] it was shown that the Borel representation given in Eq. (3.34) is not an accurate description for the CIPT expansion. The reasoning behind this assumption is as follows: For the FOPT expansion, given on the level of the perturbative Adler function by

$$\hat{D}(s) = \sum_{n=1}^{\infty}\left(\frac{\alpha_s(s_0)}{\pi}\right)^n\sum_{k=1}^{\infty}k\ c_{n,k}\ln^{k-1}(-x), \tag{3.35}$$

there exists a clear expansion parameter, namely $\alpha_s(s_0)/\pi$. The corresponding FOPT Borel representation is in this case given by Eq. (3.34). For the case of the CIPT expansion the situation is different in as far as there is no obvious expansion parameter contained in the standard CIPT series representation after performing the contour integration, which can be easily seen from

$$\delta^{(0)}_{\mathrm{CI}}(s_0) = \frac{1}{2\pi i}\sum_{n=1}^{\infty}c_{n,1}\oint\limits_{|x|=1}\frac{\mathrm{d}x}{x}W(x)\left(\frac{\alpha_s(-xs_0)}{\pi}\right)^n. \tag{3.36}$$

The problem is that the coupling in this approach depends on the integration variable and is subsequently gone after performing the contour integration. The problem of not having a clear expansion parameter in the CIPT series can, however, be cured by introducing the following modified CIPT series representation [5]

$$\delta^{(0)}_{\mathrm{CI}}(s_0) = \frac{1}{2\pi i}\sum_{n=1}^{\infty}\left(\frac{\alpha_s(s_0)}{\pi}\right)^n c_{n,1}\oint\limits_{|x|=1}\frac{\mathrm{d}x}{x}W(x)\left(\frac{\alpha_s(-xs_0)}{\alpha_s(s_0)}\right)^n, \tag{3.37}$$

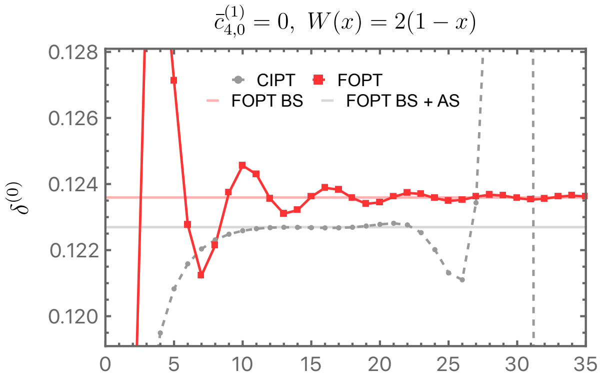

Fig. 3.5: Asymptotic separation arising in the toy model where only the $u = 2$ renormalon singularity is considered. $\bar{c}^{(1)}_{4,0} = 0$ indicates that we consider a vanishing $\mathcal{O}(\alpha_s)$ corrections of the Wilson coefficient of the gluon condensate. Further we take $s_0 = m_\tau^2 = (1.77686\text{ GeV})^2$ together with $\alpha_s(m_\tau^2) = 0.315$.

where the expansion variable is now clearly given by the same parameter as in Eq. (3.35), namely $\alpha_s(s_0)/\pi$. Eq. (3.37) gives rise to a modified CIPT Borel representation

$$\delta^{(0),\mathrm{CIPT}}_{\mathrm{Borel}}(s_0) = \int_0^\infty \mathrm{d}\bar{u}\, \frac{1}{2\pi i} \oint_{\mathcal{C}_x} \frac{\mathrm{d}x}{x} W(x) \left(\frac{\alpha_s(-xs_0)}{\alpha_s(s_0)}\right) B[\hat{D}] \left(\frac{\alpha_s(-xs_0)}{\alpha_s(s_0)}\bar{u}\right) e^{-\frac{4\pi\bar{u}}{\beta_0\alpha_s(s_0)}}, \tag{3.38}$$

where $\mathcal{C}_x$ indicates that the contour needs to be deformed away from $|x| = 1$ to account for the modified singularity structure arising from the introduction of the new Borel variable $\bar{u}$. The actual computation of Eq. (3.38) will not further be discussed in this thesis, see Ref. [5] for details. An important point worth mentioning is the fact that the CIPT Borel representation in Eq. (3.38) has different analytic properties than the FOPT Borel representation given in Eq. (3.34). Apart from the fact that these different analytic properties lead to the aforementioned modified singularity structure, they also have important physical implications. In particular, Hoang and Regner [5] demonstrated, that the CIPT Borel representation has a cut on the negative real x-axis. Due to the fact that the physical Adler function is analytic everywhere along the negative real x-axis, Hoang and Regner concluded that this property of the CIPT Borel representation implies an unphysical behaviour. In other words: The CIPT Borel representatinon is not physically sensible, in contrast to the FOPT Borel representation which obeys the correct analytic properties.

Being confronted with the fact that the two series have different Borel representations when introducing an expansion parameter for CIPT led the authors in a subsequent step to quantify the discrepancy between the two Borel representations corresponding to the CIPT and FOPT expansions. It is precisely this discrepancy that is referred to in Refs. [5, 16] as the asymptotic separation, which is defined in the following way

$$\Delta(s_0) \equiv \delta^{(0),\mathrm{CIPT}}_{\mathrm{Borel}}(s_0) - \delta^{(0),\mathrm{FOPT}}_{\mathrm{Borel}}(s_0). \tag{3.39}$$

A brief numerical analysis (in full QCD) of the asymptotic separation using a very simplistic toy model for the Adler function is now shown in Fig. 3.5. The toy model only contains the gluon condensate renormalon contribution for $N_{4,0} = 1$, where $N_{4,0}$ denotes the residue of the $u = 2$ singularity contained in the Borel model in Eq. (3.33). Furthermore the $\mathcal{O}(\alpha_s)$ Wilson coefficient of the GC is set to zero. The Borel function of the complex-valued parton-level Adler function for this toy model reads

$$B[\hat{D}_{\mathrm{toy}}(s)](u) = \frac{1}{(2-u)^{1+4\hat{b}_1}}, \tag{3.40}$$

where

$$\hat{b}_1 = \frac{\beta_1}{2\beta_0^2}$$

and $\beta_0 = 11 - 2\,n_f/3$ as well as $\beta_1 = 102 - 38\,n_f/3$. In addition, in the context of this toy analysis, the perturbative Adler function reads

$$\hat{D}_{\rm toy}(s) \;=\; \sum_{\ell=1}^{\infty} r_\ell^{(4,0)}\,\bar{a}^\ell(-s)\,. \tag{3.41}$$

where the perturbative coefficients $r_\ell^{(4,0)}$ containing the information on the GC renormalon are given in Eq. (4.19) and $\bar{a}$ denotes the fact that the coupling is considered in the C-scheme discussed in appendix A. The latter is, however, not important for the current discussion, as we consistently expand all numerical results back into the $\overline{\rm MS}$ scheme for the strong coupling.

The important phenomenological implications of this toy model are manifold. First we note that its series constitutes an important contribution of the true Adler function series coefficients, if the gluon condensate renormalon norm $N_{4,0}$ of the Adler function in full QCD is sizeable. Another important aspect is that we consider in this particular case a model where the gluon condensate correction in the OPE vanishes in the contour, due to the absence of $\mathcal{O}(\alpha_s)$ correction term in the Wilson coefficient. This means that the corresponding perturbative series should be convergent. We see, however, in Fig. 3.5 that only the FOPT series converges to the 'true' value, namely the FOPT Borel sum of Eq. (3.34). CIPT exhibits a stable behaviour, approaching the CIPT Borel sum between orders 10 and 20 before diverging at higher orders. This shows two things: First one can record the fact that the asymptotic separation precisely describes the difference in CIPT and FOPT in terms of approaching an asymptotic value, at least at intermediate orders. The second important point concerns the compatibility of CIPT with the standard form of the OPE discussed in section 2.3. Due to the fact that the standard OPE correction vanishes in the contour integration when considering the toy model in Eq. (3.40), we should expect a convergent behaviour of the corresponding perturbative series, which is *not* the case for the CIPT series in Fig. 3.5. Therefore, we can conclude that CIPT is *not* compatible with the standard OPE and the corresponding OPE corrections are of *non-standard* form. This will become relevant in the next chapter where we discuss how we can reconcile the two approaches and re-implement a physical meaning into the CIPT series, which, at this point, is not existent due to the described circumstances.

As we just saw, there exists a discrepancy between FOPT and CIPT which is systematic, and not a problem that can be related to missing higher orders. This systematic discrepancy manifests itself in the asymptotic separation. To motivate the introduction of our new scheme in the following chapter, we want to point out that Hoang and Regner showed that the asymptotic separation in full QCD is numerically dominated by the GC renormalon [5]. This implies that if one would remove the GC renormalon contribution from the perturbative series, the discrepancy between CIPT and FOPT observed at intermediate orders in the full QCD studies may be remedied.

Chapter 4

Renormalon Subtracted Perturbation Theory

In order to motivate the novel approach that is called the *renormalon-free gluon condensate* (RF GC) - scheme, which is introduced in this chapter, we remind the reader of a few important aspects of the usual approach to compute the perturbative and higher dimensional OPE contributions to the theoretical moments $\delta_W^{(0)}(s_0)$ shown in Eq. (3.13). For brevity we call this approach that was used in the past the '$\overline{\text{MS}}$-scheme for the OPE'. As we discussed already in previous chapters the higher dimensional OPE contributions consist of a product of perturbative and non-perturbative contributions, where the non-perturbative contributions also cancel order-by-order the asymptotic behaviour of the leading perturbative contribution of the OPE. Due to this intrinsic cancellation in the $\overline{\text{MS}}$-scheme for the OPE the higher dimensional matrix elements containing the non-perturbative information become order-dependent, particularly at higher orders.

To circumvent this order-by-order cancellation one can switch to an alternative scheme where an infrared cutoff is implemented. In this approach, the IR renormalon contributions which cause the divergent behaviour of the perturbative series are cut off, suggesting that the original series might inhabit improved convergence properties w.r.t. the common $\overline{\text{MS}}$-scheme. Furthermore, since the modified perturbative series should not contain any diverging behaviour stemming from one particular IR renormalon, the order dependence of the corresponding higher dimensional matrix element is influenced as well. As it is common for IR cutoff schemes, we will consider only one IR renormalon which should be the most important one concerning the improvement of the asymptotic behaviour of the perturbative series. Motivated by the exactly known Borel function in the large-β_0 approximation given by Eq. (3.26) we take the gluon condensate renormalon to be the most relevant in full QCD in analogous fashion.

Before we set up the RF GC scheme, we still need a bit of notation. Along with a brief introduction to the C-scheme, which is convenient for the setup of our new formalism in full QCD, this constitutes the content of the following (brief) section. A more general introduction to the C-scheme along the lines of [8] can be found in appendix A.

4.1 Notational and Formal Setup

4.1.1 Strong coupling in the C-scheme

Due to the fact that in the usual $\overline{\text{MS}}$-scheme we are not able to write down closed expressions for the formulae we intend to introduce we consider a different scheme where this is achievable, the so-called C-scheme [8]. Note that the C-scheme corresponds to a class of schemes, depending on the value of C. For our purposes, we will always consider the value $C = 0$. Therefore, whenever we talk about the C-scheme for the remainder of the thesis we always implicitly mean C-scheme for $C = 0$. The reason why we are able to write down closed and exact all-order expression in this choice of scheme is that the β-function has a closed form. Recalling that the β-function coefficients

β_n are independent, the RGE in the $\overline{\rm MS}$-scheme amounts to

$$\frac{d\alpha_s(Q^2)}{d\ln Q} \;=\; \beta(\alpha_s(Q^2)) \;\equiv\; -2\,\alpha_s(Q^2)\sum_{n=0}^{\infty}\beta_n\Big(\frac{\alpha_s(Q^2)}{4\pi}\Big)^{n+1}. \tag{4.1}$$

The corresponding evolution equation in the C-scheme takes the form

$$\frac{d\bar{\alpha}_s(Q^2)}{d\ln Q} \;=\; \bar{\beta}(\bar{\alpha}_s(Q^2)) \;\equiv\; -2\,\bar{\alpha}_s(Q^2)\,\frac{\beta_0\,\bar{\alpha}_s(Q^2)}{4\pi - \frac{\beta_1}{\beta_0}\bar{\alpha}_s(Q^2)}\,, \tag{4.2}$$

where now only β_0 and β_1 appear in the evolution equation and hence the higher order β-function coefficients β_n (for $n \geq 2$) are products of those two scheme invariant quantities. Setting the two couplings in the respective schemes into relation one obtains (for the full expression, where $C \neq 0$ see appendix A)

$$\frac{\pi}{\bar{\alpha}_s(Q^2)} + \frac{\beta_1}{4\beta_0}\ln\big(\bar{\alpha}_s(Q^2)\big) \;=\; \frac{\pi}{\alpha_s(Q^2)} + \frac{\beta_1}{4\beta_0}\ln\big(\alpha_s(Q^2)\big) + \frac{\beta_0}{2}\int\limits_0^{\alpha_s(Q^2)} d\tilde{\alpha}\,\left[\frac{1}{\beta(\tilde{\alpha})} + \frac{2\pi}{\beta_0\tilde{\alpha}^2} - \frac{\beta_1}{2\beta_0^2\tilde{\alpha}}\right]. \tag{4.3}$$

Here and in the following barred quantities denote that the C-scheme is considered. Unbarred quantities, as used in the previous chapters, refer to the $\overline{\rm MS}$-scheme. Note that setting $C = 0$ implies the relation $\Lambda_{\rm QCD}^{\overline{\rm MS}} = \Lambda_{\rm QCD}^{C=0}$.

In order to get a perturbative relation for the couplings in the two schemes one has to solve Eq. (4.3) iteratively. In doing so we take the truncated 5-loop $\overline{\rm MS}$ β-function to be exact. For the $n_f = 3$ flavor scheme the numerical result for the first 15 orders, which are the relevant orders for most of the discussion that follows, amounts to

$$\begin{aligned}\frac{\bar{\alpha}_s}{\alpha_s} &= 1 - 0.132789\ \alpha_s^2 - 0.247879\ \alpha_s^3 - 0.103368\ \alpha_s^4 + 0.137953\ \alpha_s^5 + 0.146252\ \alpha_s^6\\ &\quad + 0.0729472\ \alpha_s^7 - 0.081650\ \alpha_s^8 - 0.122995\ \alpha_s^9 - 0.042241\ \alpha_s^{10} + 0.050279\ \alpha_s^{11}\\ &\quad + 0.091138\ \alpha_s^{12} + 0.033505\ \alpha_s^{13} - 0.038225\ \alpha_s^{14} + \ldots.\end{aligned} \tag{4.4}$$

The value for the C-scheme coupling $\bar{\alpha}_s$ at a reference scale μ^2, given a particular value of the $\overline{\rm MS}$-coupling α_s at the same reference scale μ^2, is obtained by solving Eq. (4.3) numerically.

In order to construct a physically motivated Borel model based in the C-scheme we need to transfer the known perturbative coefficients of the Adler function into this choice of scheme. For the first two coefficients nothing changes, e.g. $\bar{c}_{1,1} = c_{1,1}$ and $\bar{c}_{2,1} = c_{2,1}$. The remaining two known coefficients as well as the six-loop coefficient are, however, different from their $\overline{\rm MS}$-value and given by

$$\begin{aligned}\bar{c}_{3,1} &= \frac{262955}{1296} - \frac{779}{4}\zeta_3 + \frac{75}{2}\zeta_5 \;=\; 7.682\,,\\ \bar{c}_{4,1} &= \frac{357259199}{93312} - \frac{1713103}{432}\zeta_3 + \frac{4185}{8}\zeta_3^2 + \frac{34165}{96}\zeta_5 - \frac{1995}{16}\zeta_7 \;=\; 61.060\,,\\ \bar{c}_{5,1} &= c_{5,1} + \frac{73019059337}{80621568} - \frac{273360539}{373248}\zeta_3 - \frac{445}{8}\zeta_3^2 + \frac{2522915}{20736}\zeta_5 - \frac{89}{1536}\pi^4\\ &= c_{5,1} + 65.477 = 345 \pm 140.\end{aligned} \tag{4.5}$$

To facilitate the following presentation we further introduce the abbreviations

$$\begin{aligned}\bar{a}(-s) \;&\equiv\; \frac{\beta_0\,\bar{\alpha}_s(-s)}{4\pi}\,,\\ \bar{a}_Q \;&\equiv\; \frac{\beta_0\,\bar{\alpha}_s(Q^2)}{4\pi}\,,\\ \bar{c}_n \;&\equiv\; \frac{4^n\,\bar{c}_{n,1}}{\beta_0^n}\,,\end{aligned} \tag{4.6}$$

for the C-scheme coupling and coefficients. Note that they should not be confused with the abbreviations used in the previous chapters for the $\overline{\text{MS}}$ coupling. Note that although all of our expressions derived in the following sections will be based in the C-scheme for the strong coupling, for all numerical studies we convert back to the common $\overline{\text{MS}}$ scheme for the strong coupling. Again, this choice of scheme is purely motivated by obtaining closed expressions due to the simple form of the β-function in Eq. (4.2) and makes no difference for all practical purposes. We continue with revisiting the standard OPE corrections discussed in section 2.3, where the focus will specifically lie on the description for the gluon condensate.

4.1.2 Revisiting the Standard OPE Corrections

As we already eluded to in the introduction of this chapter, each term in the OPE compensates for a certain IR contribution in the perturbative series of the Adler function. Recall that the OPE contributions containing the IR sensitivity are low-energy operators, consisting of products of light-quark and gluon field operators. Assuming no operator mixing, a d dimensional contribution to the Adler function's OPE is given by (here D^{OPE} signifies that we consider higher-dimensional OPE contributions of the Adler function, as opposed to $\hat{D}$, already introduced earlier, which denotes the perturbative contribution)

$$\delta D^{\text{OPE}}_{d,\gamma}(-Q^2) \;=\; \frac{1}{Q^d}\,(\bar{a}_Q)^{-\alpha}\left[1+\bar{c}^{(1)}_{d,\gamma}\,\bar{a}_Q+\ldots\right]\langle\bar{\mathcal{O}}_{d,\gamma}\rangle\,. \tag{4.7}$$

Here $\alpha = -2\gamma^{(1)}/\beta_0$, where $\gamma^{(1)}$ is the LL anomalous dimension of the corresponding operator. $\bar{c}^{(1)}_{d,\gamma}$ is the one-loop correction of the Wilson coefficient of the operator in consideration. We remind the reader that the barred quantity indicates that this correction is given in the C-scheme. Note that the general form of Eq. (4.7) corresponds to the final result we obtained in section 2.3, e.g. compare to Eq. (2.37). The corresponding expression in the Borel function of the perturbative Adler function $\hat{D}(-Q^2)$ is given by

$$B_{d,\gamma}(u) \;=\; \left[1+\bar{c}^{(1)}_{d,\gamma}\,\bar{a}_Q+\ldots\right]\frac{N_{d,\gamma}}{(\frac{d}{2}-u)^{1+d\hat{b}_1+\alpha}}\,. \tag{4.8}$$

Eq. (4.7) and Eq. (4.8) represent the contributions which inhabit the same IR sensitivity and whose IR contributions cancel between each other. The contribution to the perturbative coefficients of $\hat{D}(-Q^2)$ arising from Eq. (4.8) is given by

$$\delta\hat{D}_{b,\gamma}(-Q^2) \;=\; N_{d,\gamma}\left[1+\bar{c}^{(1)}_{d,\gamma}\,\bar{a}_Q+\ldots\right]\sum_{\ell=1}^{\infty} r^{(d,\alpha)}_{\ell}\,\bar{a}^{\ell}_Q\,, \tag{4.9}$$

where $r^{(d,\alpha)}_{\ell}$ represent the perturbative coefficients originating from the renormalon singularity in Eq. (4.8). In particular, those coefficients are given by

$$r^{(d,\alpha)}_{\ell} = \left(\frac{2}{d}\right)^{\ell+d\hat{b}_1+\alpha}\frac{\Gamma(\ell+d\,\hat{b}_1+\alpha)}{\Gamma(1+d\,\hat{b}_1+\alpha)}\,. \tag{4.10}$$

Before discussing the gluon condensate contribution to the Adler function's OPE in detail a few comments are in order: It is clear that the (unknown) full Borel function of the Adler function in QCD is the sum of contributions of the form shown in Eq. (4.8). Recall that the model we considered in section 3.2.2 to yield a good approximation for the unknown higher order coefficients of the perturbative series consisted of three functions of the type of Eq. (4.8) providing the information on the $u = 2, 3$ and $u = -1$ renormalon singularity. What is important to point out in this context is that the normalization of these renormalon singularities in the Borel model dictate how relevant the IR/UV contribution of the renormalon in consideration is for the perturbative series at lower and intermediate orders. Getting a reliable value for the normalization of the GC renormalon is therefore a question of utmost importance and will be discussed extensively in section 5.1.

We now turn our attention to the leading OPE correction of the (massless) Adler function consisting of a single term, namely the well-known gluon condensate. Its renormalization group invariant form in the $\overline{\rm MS}$ scheme for the GC amounts to [26]

$$\langle \bar{\mathcal{O}}_{4,0} \rangle \;=\; \frac{2\pi^2}{3}\,\langle \Omega | \tilde{\beta}(\alpha_s)\, G^{\mu\nu} G_{\mu\nu} | \Omega \rangle \;\equiv\; \frac{2\pi^2}{3}\,\langle \bar{G}^2 \rangle\,, \tag{4.11}$$

where

$$\tilde{\beta}(\alpha_s) \;\equiv\; -\frac{2\,\beta(\alpha_s)}{\beta_0\,\alpha_s} \;=\; \left(\frac{\alpha_s}{\pi}\right) + \frac{\beta_1}{4\beta_0}\left(\frac{\alpha_s}{\pi}\right)^2 + \ldots\,. \tag{4.12}$$

The one-loop correction to the Wilson coefficient of the GC is known [27]. Taking this correction into account one can write down the $D = 4$ OPE contribution in the $\overline{\rm MS}$ scheme as

$$\delta D^{\rm OPE}_{4,0}(-Q^2) \;=\; \frac{1}{Q^4}\frac{2\pi^2}{3}\left[1 + \bar{c}^{(1)}_{4,0}\,\bar{a}_Q\right]\langle \bar{G}^2 \rangle\,, \tag{4.13}$$

with

$$\bar{c}^{(1)}_{4,0} = \frac{4}{\beta_0}\left(\frac{C_A}{2} - \frac{C_F}{4} - \frac{\beta_1}{4\beta_0}\right). \tag{4.14}$$

Here $C_A = 3$, $C_F = 4/3$ and for $n_f = 3$ we have $\bar{c}^{(1)}_{4,0} = -22/81$. The corresponding contribution in the Borel function reads

$$B_{4,0}(u) \;=\; \left[1 + \bar{c}^{(1)}_{4,0}\,\bar{a}_Q\right]\frac{N_{4,0}}{(2-u)^{1+4\hat{b}_1}}\,. \tag{4.15}$$

Recall that the above expression is given in the C-scheme for the strong coupling. Hence when converting to the $\overline{\rm MS}$ scheme for α_s for our numerical studies we obtain higher order terms generated by the one-loop correction of the Wilson coefficient. In the following, we will keep all these resulting higher order contributions.

Another important aspect in the numerical studies is the choice of moments. In section 3.2 we already took note of the fact that the perturbative series for moments suppressing the GC renormalon have a different qualitative behaviour compared to the series of moments which enhance the GC contribution. The GC manifests itself in the divergent runaway-behaviour of the series observed in the latter case. In section 3.2.2 we saw that the GC correction to the Adler function's OPE for the complex-valued scale s

$$\delta D^{\rm OPE}_{4,0}(s) \;=\; \frac{1}{s^2}\frac{2\pi^2}{3}\left[1 + \bar{c}^{(1)}_{4,0}\,\bar{a}(-s)\right]\langle \bar{G}^2 \rangle \tag{4.16}$$

vanishes in the contour (if one neglects the one-loop correction) for GCS moments due to Eq. (3.32).

The final remark of this section concerns the applicability of GCE and GCS moments in strong coupling determinations. As we already pointed out on multiple occasions, GCS moments inhabit a significantly better convergence behaviour compared to GCE moments due to the absence of the x^2 term provoking the runaway behaviour of the perturbative series. This behaviour is already impacting the perturbative coefficient at the six-loop level [24], which is a problem in phenomenological analysis of α_s and suggests that the norm of the GC renormalon in the Adler function is sizeable, in the sense that the perturbative corrections are sensitive to it. For this reason most of the previous extractions of the strong coupling are based exclusively [7, 28, 29] (or mostly [6]) on GCS moments.

4.2 The Renormalon-Free Gluon Condensate Scheme

We now start with the discussion on our renormalon-free GC scheme, which is based on a perturbative redefinition of the GC itself. In this context, we make use of the fact that the associated IR renormalon is universal, which ensures that the scheme choice for our subtraction set up in the following is universal among different observables other than the GC. The introduction of the RF GC scheme will be done in two steps: First we derive a GC which is renormalon-free and scale-dependent and in a second step we get rid of the scale dependence to obtain a subtraction scheme which can be considered to be minimal (in which sense will be eluded to in the following).

4.2.1 Setting up the Scheme

In order to obtain a renormalon-free scale-dependent GC we seek to make the order-dependent compensating contributions of the GC mentioned above Eq. (4.9) explicit. Furthermore, for reasons of transparency and simplicity, we want to keep the form of the original GC OPE correction shown in Eq. (4.13). Based on those considerations we write down the relation between the newly defined renormalon-free, order-independent (but scale-dependent) GC, denoted in the following by $\langle G^2\rangle(R^2)$ and the original order-dependent GC in the $\overline{\text{MS}}$ scheme, denoted in the following by $\langle\bar{G}^2\rangle^{(n)}$

$$\langle\bar{G}^2\rangle^{(n)} \;\equiv\; \langle G^2\rangle(R^2) \;-\; R^4 \sum_{\ell=1}^{n} N_g\, r_\ell^{(4,0)}\, \bar{a}_R^\ell\,, \tag{4.17}$$

where n indicates the order-dependence. Note that in the above equation N_g represents the universal GC renormalon norm. This norm is related to the norm of the GC renormalon in the Borel function of the Adler function, $N_{4,0}$, via the relation

$$N_g \;=\; \frac{3}{2\pi^2}\, N_{4,0}. \tag{4.18}$$

The perturbative coefficients $r_\ell^{(4,0)}$ containing the information on the IR renormalon singularity of the GC are given by

$$r_\ell^{(4,0)} = \left(\frac{1}{2}\right)^{\ell+4\hat{b}_1} \frac{\Gamma(\ell+4\hat{b}_1)}{\Gamma(1+4\hat{b}_1)} \tag{4.19}$$

and are identical to those given in Eq. (4.10). Let us now discuss the scale-dependence that occurs in $\langle G^2\rangle(R^2)$. The quadratic scale R^2 introduced in Eq. (4.17) is considered to be an IR factorization scale, where one may consider the hierarchy w.r.t. the relevant dynamical scale of the Adler function $R^2 < Q^2$. Although R could in principle take on any value, for the purpose of this thesis we will always consider this IR factorization scale to be real-valued, since the observable of interest in our case is the Euclidean Adler function.

On general terms, one can record the fact that the intention of the renormalon-free GC scheme is to re-order the information on the IR renormalon contained in the GC and the corresponding contribution in the Borel function of the Adler function shown in Eq. (4.13) such that through a reshuffling of the series given on the RHS of Eq. (4.17) the two IR renormalon contributions explicitly cancel within the perturbation series. It is clear that from the way we set up the scheme, that the subtracted perturbation series depends on the norm N_g of the GC renormalon in the Borel function of the Adler function. The expression for the subtraction series is then given by

$$\delta\hat{D}_{4,0}(-Q^2,R^2) \;\;=\;\; -\left[1+\bar{c}_{4,0}^{(1)}\,\bar{a}_Q\right]\int_0^\infty \mathrm{d}u\, \left[\frac{R^4}{Q^4}\frac{N_{4,0}}{(2-u)^{1+4\hat{b}_1}}\right]_{\text{Taylor}} e^{-\frac{u}{\bar{a}_R}}\,. \tag{4.20}$$

A very important point concerning Eq. (4.20) is the fact that $\delta\hat{D}_{4,0}(-Q^2,R^2)$ yields a series in $\bar{a}_R$ and therefore, in order to cancel the renormalon singularity contained in the original unsubtracted series, one has to re-expand the series at a common overall renormalization scale and in addition truncate at the same order.

In order to convince ourselves that the subtraction we set up actually works, let us look at the Borel sum for the GC renormalon contribution when the renormalon-free GC $\langle G^2\rangle(R^2)$ is used:

$$\Delta\hat{D}_{4,0}(-Q^2,R^2) \;\;=\;\; \left[1+\bar{c}_{4,0}^{(1)}\,\bar{a}_Q\right] N_{4,0}\int_0^\infty \mathrm{d}u\, \left[\frac{e^{-\frac{u}{\bar{a}_Q}}}{(2-u)^{1+4\hat{b}_1}} - \frac{R^4}{Q^4}\frac{e^{-\frac{u}{\bar{a}_R}}}{(2-u)^{1+4\hat{b}_1}}\right]. \tag{4.21}$$

Eq. (4.21) contains both the orignal series and the subtraction series and it is easy to prove that the ambiguities arising from the cuts of the individual contributions cancel according to the definition of the Borel sum ambiguity given below Eq. (3.30). This in turn means that the subtracted series, e.g. the sum of the original series and the subtraction series, is convergent.

In addition to proving that the integral on the RHS of Eq. (4.21) is ambiguity-free, we can consider an alternative way of showing that the subtraction series fulfils its duty of cancelling the renormalon singularity in the original series. This alternative proof starts from the equality

$$
\begin{aligned}
\frac{\mathrm{d}}{\mathrm{d}\ln R^2}\,\Delta\hat{D}_{4,0}(-Q^2,R^2) &= -\left[1+\bar{c}^{(1)}_{4,0}\,\bar{a}_Q\right]N_{4,0}\int_0^\infty\!\mathrm{d}u\,\frac{\mathrm{d}}{\mathrm{d}\ln R^2}\left[\frac{R^4}{Q^4}\frac{e^{-\frac{u}{\bar{a}_R}}}{(2-u)^{1+4\hat{b}_1}}\right]\\
&= -\left[1+\bar{c}^{(1)}_{4,0}\,\bar{a}_Q\right]N_{4,0}\,\frac{R^4}{Q^4}\,\frac{\bar{a}_R}{1-2\hat{b}_1\bar{a}_R}\,2^{-4\hat{b}_1}
\end{aligned}
\tag{4.22}
$$

and the fact that $\Delta\hat{D}_{4,0}(-Q^2,Q^2)=0$. The derivative of the subtracted series w.r.t. the IR factorization scale R yields a convergent series (within its radius of convergence of course), assuming α_s stays in the perturbative regime. Hence we can now write down an exact all-order expression for the subtracted series $\Delta\hat{D}_{4,0}(-Q^2,R^2)$ by taking the integral of the RHS of Eq. (4.22)

$$
\Delta\hat{D}_{4,0}(-Q^2,R^2) = \left[1+\bar{c}^{(1)}_{4,0}\,\bar{a}_Q\right]\frac{N_{4,0}}{Q^4\,2^{4\hat{b}_1}}\int_{\ln(R^2)}^{\ln(Q^2)}\mathrm{d}\ln\!\left(\tilde{R}^2\right)\,\frac{\tilde{R}^4\,\bar{a}_{\tilde{R}}}{1-2\hat{b}_1\bar{a}_{\tilde{R}}}\,. \tag{4.23}
$$

If one would stick to the GC $\langle G^2\rangle(R^2)$, its R-dependence would be controlled by an R-evolution equation [30] of the form

$$
\frac{\mathrm{d}}{\mathrm{d}\ln R^2}\,\langle G^2\rangle(R^2) = \frac{N_g}{2^{4\hat{b}_1}}\,\frac{R^4\,\bar{a}_R}{1-2\hat{b}_1\bar{a}_R} = -\frac{N_g}{2^{1+4\hat{b}_1}}\,R^4\,\frac{\bar{\beta}(\bar{\alpha}_s(R^2))}{\bar{\alpha}_s(R^2))}\,, \tag{4.24}
$$

which of course relies on the particular form of the subtraction series. It is due to this reason that Eq. (4.24) possesses a scale-dependence, which is not very convenient in practice.

The next step is therefore to get rid of this IR cutoff scale dependence in the RF GC since for practical purposes it is not very convenient. To achieve scale-invariance in our renormalon-free GC condensate we need a function that obeys the same R-evolution equation and a particularly appealing choice is the Borel sum of the subtraction series, since this function clearly obeys the desired evolution equation. The Borel sum of the subtraction series given in Eq. (4.17) reads

$$
\begin{aligned}
\bar{c}_0(R^2) &\equiv R^4\ \mathrm{PV}\int_0^\infty\frac{\mathrm{d}u\ e^{-\frac{u}{\bar{a}_R}}}{(2-u)^{1+4\hat{b}_1}} \qquad (4.25)\\
&= \begin{cases} -\frac{R^4\,e^{-\frac{2}{\bar{a}_R}}}{(-\bar{a}_R)^{4\hat{b}_1}}\,\Gamma\!\left(-4\hat{b}_1,-\frac{2}{\bar{a}_R}\right)-\mathrm{sig}[\mathrm{Im}[a_R]]\,\frac{i\pi\,R^4\,e^{-\frac{2}{\bar{a}_R}}}{\Gamma(1+4\hat{b}_1)\,\bar{a}_R^{4\hat{b}_1}} & \text{for } \mathrm{Im}[R^2]\neq 0\\ -\frac{R^4\,e^{-\frac{2}{\bar{a}_R}}}{(\bar{a}_R)^{4\hat{b}_1}}\,\mathrm{Re}\left[e^{4\pi\hat{b}_1 i}\,\Gamma\!\left(-4\hat{b}_1,-\frac{2}{\bar{a}_R}\right)\right] & \text{for } \mathrm{Im}[R^2]=0\end{cases}\,.
\end{aligned}
$$

Note that although the result for the case of R^2 being complex is quoted, we will exclusively consider R^2 attaining real values. As a short remark, one can observe that the expression for the complex-valued strong coupling, in the limit of $\mathrm{Im}[\bar{a}_R]\to 0$ agrees with the real-valued result. Due to the fact that we only discuss the case of real-valued R^2 the subtraction series in Eq. (4.17) is real-valued as well, leading to a strong suppression for the case of GCS moments. This is analogous to the discussion we had in the previous section, where we considered the GC OPE contributions without the one-loop correction and convinced ourselves that they vanish for GCS moments.

The definition for the Borel sum we have introduced in Eq. (4.25) is not unique due to presence of the cut along the positive real axis. In this context we again adopted the common principle value prescription. An important point is that the choice of the Borel sum of the subtraction series is defining the scheme of our *scale-invariant* renormalon-free GC, which we call RF GC, $\langle G^2\rangle^{\mathrm{RF}}$. The final definition of $\langle G^2\rangle^{\mathrm{RF}}$ is given by

$$
\langle G^2\rangle(R^2) \equiv \langle G^2\rangle^{\mathrm{RF}}+N_g\,\bar{c}_0(R^2)\,. \tag{4.26}
$$

Before we discuss how the RF GC scheme applies to spectral function moments, let us mention some important points of the derivation of the scale-invariant RF GC: First, neither the subtraction series nor the choice for $\bar{c}_0$ are in principle unique. Here we have made the choice to use the Borel sum of Eq. (4.25). Because the subtracted series, which does not inhabit the GC renormalon singularity anymore, will approach the original FOPT Borel sum of Eq. (3.34) our scheme can be considered minimal. One practical aspect of this is that the GCS spectral function moments have similar values for the original and subtracted series at intermediate orders, independent of the value for R.

4.2.2 Spectral Function Moments in the New Scheme

After having obtained a conceptual overview of how to apply the RF GC scheme to the real-valued Euclidean Adler function, we now look at the impact of our newly defined scheme on spectral function moments. We start by pointing out that the function $\bar{c}_0(R^2)$ achies that the Borel sum of the subtracted series agrees with the Borel sum of the unsubtracted Adler function. It is treated as a *tree-level contribution*, which should not be expanded. This means that conceptually it is also part of the general tree-level contribution to the theoretical moments shown in Eq. (3.13). Collecting the pieces we elaborated on in the previous sections, the perturbative series for the Adler function in the RF GC scheme, denoted in the following by $\hat{D}^{\rm RF}(s,R^2)$, reads

$$\begin{aligned}
\hat{D}^{\rm RF}(s,R^2) \;&=\; \frac{1}{s^2}\Big[1+\bar{c}^{(1)}_{4,0}\bar{a}(-s)\Big]\,N_{4,0}\,\bar{c}_0(R^2) \,+\, \int_0^\infty \mathrm{d}u\,\Big[B[\hat{D}(s)](u)\Big]_{\rm Taylor}\,e^{-\frac{u}{\bar{a}(-s)}} \\
&\quad -\Big[1+\bar{c}^{(1)}_{4,0}\,\bar{a}(-s)\Big]\,N_{4,0}\,\frac{R^4}{s^2}\int_0^\infty \mathrm{d}u\,\bigg[\frac{1}{(2-u)^{1+4\hat{b}_1}}\bigg]_{\rm Taylor}\,e^{-\frac{u}{\bar{a}_R}} \\
&=\; \frac{1}{s^2}\Big[1+\bar{c}^{(1)}_{4,0}\bar{a}(-s)\Big]\,N_{4,0}\,\bar{c}_0(R^2) \,+\, \sum_{\ell=1}^{\infty}\bar{c}_\ell\,\bar{a}^\ell(-s) \\
&\quad -\Big[1+\bar{c}^{(1)}_{4,0}\,\bar{a}(-s)\Big]\,N_{4,0}\,\frac{R^4}{s^2}\sum_{\ell=1}^{\infty}\Big(\frac{1}{2}\Big)^{\ell+4\hat{b}_1}\frac{\Gamma(\ell+4\hat{b}_1)}{\Gamma(1+4\hat{b}_1)}\,\bar{a}_R^\ell\,.
\end{aligned} \tag{4.27}$$

In Eq. (4.27) $B[\hat{D}(s)](u)$ represents the Borel function of the original Adler function in the $\overline{\rm MS}$ GC scheme w.r.t. an expansion in powers of $\bar{\alpha}_s(-s)$. The GC OPE contribution for the case of the RF GC scheme amounts to

$$\delta D^{\rm OPE,RF}_{4,0}(s) \;=\; \frac{1}{s^2}\frac{2\pi^2}{3}\Big[1+\bar{c}^{(1)}_{4,0}\,\bar{a}(-s)\Big]\,\langle G^2\rangle^{\rm RF}\,. \tag{4.28}$$

Taking Eq. (4.27) it is now possible to prove the claim that the Borel sum of the Adler function in the RF GC scheme is unchanged, compared to the Borel sum of the original unsubtracted Adler function. This statement also holds, irrespective of the value for the norm of the gluon condensate. In the following we define the Borel function of the Adler function in the RF GC scheme $\hat{D}^{\rm RF}(s,R^2)$ w.r.t. an expansion in powers of $\bar{\alpha}_s(-s)$ as $B[\hat{D}^{\rm RF}(s)](u)$. We subsequently obtain the identity

$$\begin{aligned}
&\frac{1}{s^2}\Big[1+\bar{c}^{(1)}_{4,0}\bar{a}(-s)\Big]\,N_{4,0}\,\bar{c}_0(R^2) \,+\, {\rm PV}\int_0^\infty \mathrm{d}u\,\Big[B[\hat{D}^{\rm RF}(s)](u)\Big]\,e^{-\frac{u}{\bar{a}(-s)}} \\
&\;=\; \frac{1}{s^2}\Big[1+\bar{c}^{(1)}_{4,0}\bar{a}(-s)\Big]\,N_{4,0}\,\bar{c}_0(R^2) \,+\, {\rm PV}\int_0^\infty \mathrm{d}u\,\Big[B[\hat{D}(s)](u)\Big]\,e^{-\frac{u}{\bar{a}(-s)}} \\
&\quad -\Big[1+\bar{c}^{(1)}_{4,0}\,\bar{a}(-s)\Big]\,N_{4,0}\,\frac{R^4}{s^2}\,{\rm PV}\int_0^\infty \mathrm{d}u\,\bigg[\frac{1}{(2-u)^{1+4\hat{b}_1}}\bigg]\,e^{-\frac{u}{\bar{a}_R}} \\
&\;=\; {\rm PV}\int_0^\infty \mathrm{d}u\,\Big[B[\hat{D}(s)](u)\Big]\,e^{-\frac{u}{\bar{a}(-s)}}\,.
\end{aligned} \tag{4.29}$$

In the first equality we used the fact that Borel sums based on the principal value prescription is renormalization-scale invariant. The second equality then follows from Eq. (4.25). Furthermore, due to the fact that the Borel sum is also renormalization-scheme independent, we can deduce that the Borel sum of the Adler function in the RF GC scheme is unchanged compared to the Borel sum of the Adler function based in the original $\overline{\text{MS}}$ GC scheme.

As a closing remark to this brief section we want to emphasize an important point regarding the dependence of the subtracted series on the IR factorization scale R. As we now know, the Borel sums of the subtracted and unsubtracted Adler function are equivalent. Further, recall that $\langle G^2\rangle^{\text{RF}}$ is a scale-invariant quantity. This shows that the dependence of the subtracted series on the IR factorization scale vanishes in the limit of large orders. The truncated series of course still have a residual dependence on the scale R. The different values one can realistically consider for the IR factorization scale are quite limited. Since R represents an IR factorization scale, it is natural to consider $R^2 < s_0$. Furthermore, due to the fact that we obtain logarithms of R^2/s_0 when re-expanding the perturbative series in $\bar{a}_R$ at a common renormalization scale, the case of R^2 being much smaller than s_0, e.g. $R^2 \ll s_0$, should be avoided. In practice, those strong hierarchies will, however, never arise. This already shows that the freedom in choosing R^2 is quite limited. The condition that we should stay in the realm of perturbation theory with the choice of the IR factorization scale, together with the fact that s_0 is bounded from above by the square of the τ mass, further limits the freedom of choice in R^2. Nevertheless, variations of R constitute a new perturbative uncertainty of the subtracted Adler function $\hat{D}^{\text{RF}}$ and we will have to include it in our strong coupling determinations in the last section of this thesis.

4.3 Toy Model Analysis

From the last paragraph in section 3.3 (see also Refs. [5, 16]) we know that the GC renormalon, being the most dominant IR singularity, in the sense that it is the IR singularity closest to the origin in the Borel plane, has the most impact on the asymptotic separation. Therefore removing the GC renormalon from the perturbative series in FOPT and CIPT should yield compatible results, at least at intermediate orders in full QCD (or large-β_0), where the UV renormalon is not yet dominant.

To illustrate this we consider again the toy model from section 3.3. The perturbative series for the case of the original Adler function is (using the notation introduced in the previous sections) given by

$$\hat{D}_{\text{toy}}(s) \;=\; \sum_{\ell=1}^{\infty} r_\ell^{(4,0)}\, \bar{a}^\ell(-s)\,. \tag{4.30}$$

The analogous expression for the series in the RF GC scheme reads

$$\hat{D}^{\text{RF}}_{\text{toy}}(s,R^2) \;=\; \frac{\bar{c}_0(R^2)}{s^2} + \sum_{\ell=1}^{\infty} r_\ell^{(4,0)}\, \bar{a}^\ell(-s) - \frac{R^4}{s^2}\sum_{\ell=1}^{\infty} r_\ell^{(4,0)}\, \bar{a}_R^\ell\,. \tag{4.31}$$

Although this model has no explicit phenomenological relevance, the conclusions one can draw from it are manifold, as was pointed out in section 3.3. The most important aspect of this analysis is that the impact of the GC renormalon on the asymptotic separation can be seen very clearly.

On the level of the spectral function moments we consider for the perturbative contributions in the original $\overline{\text{MS}}$ GC scheme and the RF GC scheme

$$\delta_W^{(0)}(s_0) \;=\; \frac{1}{2\pi i}\oint_{|s|=s_0}\frac{\mathrm{d}s}{s}\,W(\tfrac{s}{s_0})\,\hat{D}_{\text{toy}}(s), \tag{4.32}$$

$$\delta_W^{(0)}(s_0,R^2) \;=\; \frac{1}{2\pi i}\oint_{|s|=s_0}\frac{\mathrm{d}s}{s}\,W(\tfrac{s}{s_0})\,\hat{D}^{\text{RF}}_{\text{toy}}(s,R^2), \tag{4.33}$$

respectively. The weight functions for the numerical analysis are of the form $W_m(x) = 2(1-x^m)$, where $m \in \{1,3,4,5\}$, and they originate from the monomial weight functions $w_{m-1} = x^{m-1}$ on the level of the spectral function. All weights functions are chosen such that they belong to the family of GCS moments. An important feature of the model we are considering, which was already present in section 3.3, is the fact that the one-loop correction of the Wilson coefficient of the GC is set to zero. This implies directly that the scheme compensating term $\bar{c}_0(R^2)/s^2$ gives no contribution to $\delta_W^{(0)}(s_0, R^2)$.

Let us briefly recall the most important points that were discussed in the analysis of the asymptotic separation in the context of this particular toy model: Assuming the standard approach to the OPE and the established relation of higher dimensional condensates to renormalons in the perturbative series, we took note of the fact that perturbative expansions, which intend to be consistent with this standard approach to the OPE, have to be convergent. To be precise: A perturbative expansion for spectral function moments consistent with the standard treatment of the OPE in the original unsubtracted approach to the Adler function has to be convergent. This implies that the subtraction series related to this perturbative expansion has to vanish, or at least converge to zero. Consequently, a perturbative series (in the context of this toy model) which does not satisfy these two conditions cannot be compatible with the standard treatment of the OPE. As we already saw in section 3.3, FOPT satisfies the condition of providing a convergent expansion, whereas CIPT does not. What we want to show in the following is that CIPT also fails to satisfy the condition that the subtraction series related to the original perturbative expansion does not fulfil the consistency requirement and one can therefore conclude, now with even stronger arguments than in section 3.3, that CIPT is not compatible with the standard OPE.

First, however, we briefly discuss the subtraction series corresponding to the FOPT expansion. Considering the IR factorization scale R to be constant in the contour integration, e.g. real-valued, the subtraction series is not just convergent to zero but zero for every order by construction. We therefore have

$$\frac{1}{2\pi i}\oint_{|s|=s_0}\frac{\mathrm{d}s}{s}\,W_{m\neq 2}(\tfrac{s}{s_0})\left[-\frac{R^4}{s^2}\sum_{\ell=1}^{n} r_\ell^{(4,0)}\,\bar{a}_R^\ell\right]^{\text{FOPT}} = 0 \tag{4.34}$$

for any $n \in \mathbb{N}$. The reason for this simple equality is that the FOPT expansion is based on a real-valued expansion parameter $\alpha_s(s_0)$. Hence, when computing the subtraction series and re-expanding the series in $\alpha_s(R^2)$ in powers of $\alpha_s(s_0)$, one solely obtains logarithms with real-valued arguments that vanish due to the contour integral. Subsequently, the subtraction series vanishes due to Eq. (3.32).

Let us now have a look at the numerical results for the original unsubtracted perturbative expansions $\delta_W^{(0)}(s_0)$ and their corresponding subtracted series $\delta_W^{(0)}(s_0, R^2)$ as a function of order in perturbation theory n. The parameters are chosen identical to section 3.3, e.g. $\alpha_s(m_\tau^2) = 0.315$ and $s_0 = m_\tau^2$. Now we have in addition to the original parameters the IR factorization scale involved in the subtracted series, which in this toy analysis is chosen to be $R = 0.8m_\tau$.

First we focus on the results for FOPT, which are shown in red in the column on the LHS of Fig. 4.1. We see of course that the unsubtracted and subtracted results agree (both indiciated by the red dots) and further record an oscillatory behaviour which gets damped at higher orders in perturbation theory. Eventually, we observe a convergence to the corresponding Borel sums indicated by the red horizontal line. Note that the FOPT series possesses a finite radius of convergence, presumably a tick smaller than $\alpha_s(m_\tau^2) = 0.315$ [3]. Formally, the Borel sum integral shown in Fig. 4.1 is given by

$$\delta_{W_m,\text{Borel}}^{(0),\text{FOPT}}(s_0) = \text{PV}\int_0^\infty \mathrm{d}u\,\frac{1}{2\pi i}\oint_{|s|=s_0}\frac{\mathrm{d}s}{s}\,W_m(\tfrac{s}{s_0})\,\frac{e^{-\frac{u}{\bar{a}(-s)}}}{(2-u)^{1+4\hat{b}_1}}\,. \tag{4.35}$$

An important point worth emphasizing is the fact that the Borel sum does not possess an ambiguity. Recall that this is due to the fact that we only consider GCS moments in this toy model study and take the one-loop correction of the Wilson coefficient of the GC to be zero. In summary we can conclude that FOPT satisfies the consistency conditions it has to obey in order to be compatible with the standard approach to the OPE.

Let us now take a look at the results for CIPT, starting with the unsubtracted series represented by the gray dots on the LHS in Fig. 4.1. Although we already discussed this case in section 3.3,

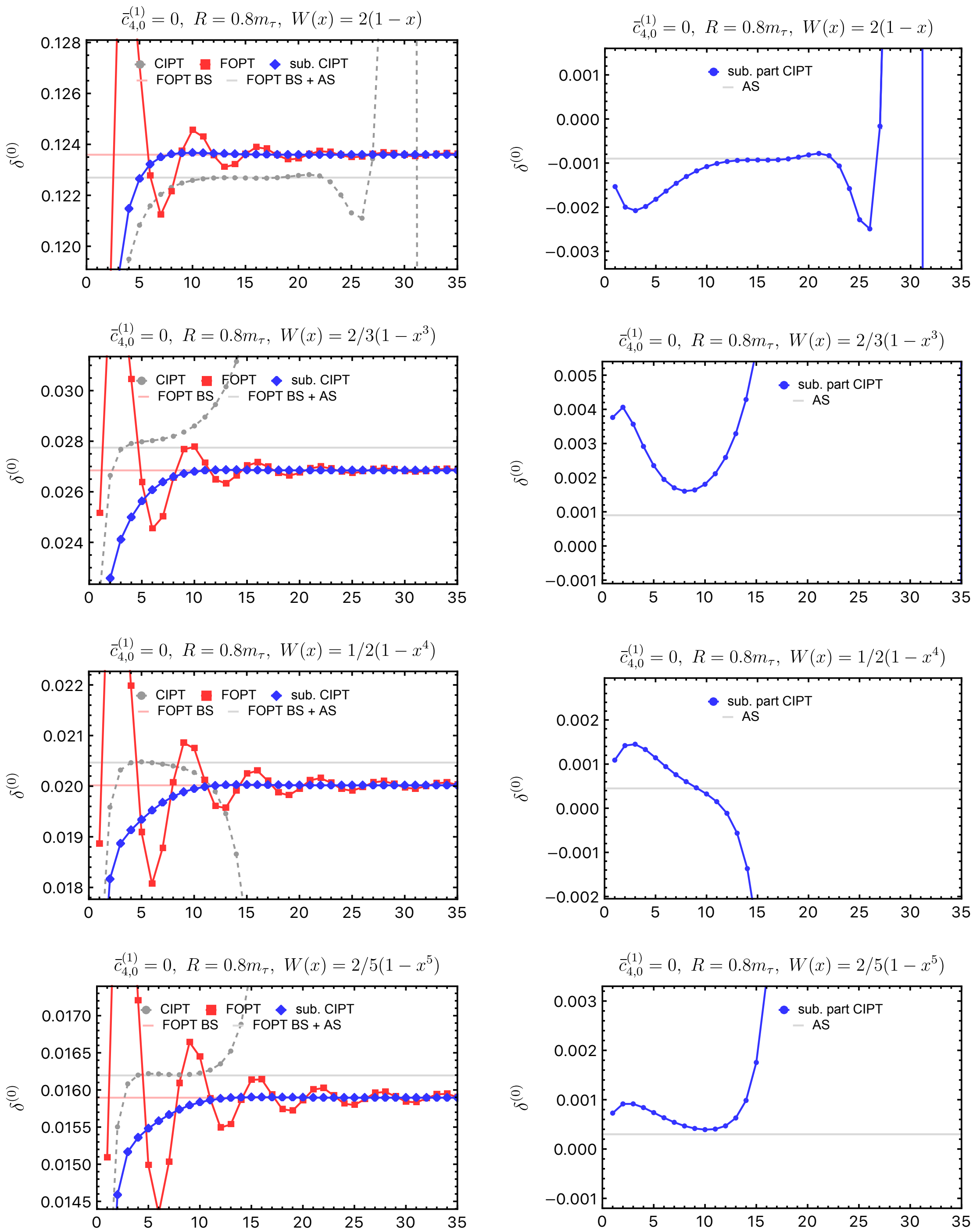

Fig. 4.1: Left panels: FOPT and CIPT expansions for $W(x) = 2(1-x^m)/m$ with $m = 1, 3, 4, 5$ and $\alpha_s(m_\tau^2) = 0.315$ ($\bar{\alpha}_s(m_\tau^2) = 0.30827$) in the $\overline{\text{MS}}$ GC scheme and the RF GC scheme. Right panels: The subtraction contribution for the subtracted CIPT expansion in the corresponding left panels.

it is worthwhile to recall the most important findings: We observe that none of the series are converging, therefore contradicting the first consistency condition. Furthermore we see that the unsubtracted CIPT series approaches a value at intermediate orders which differs from the FOPT Borel sum, but agrees with the sum of the Borel sum integral and the asymptotic separation [5], shown as the gray horizontal line. This leads us to the conclusion that, in the common $\overline{\text{MS}}$ GC scheme, the renormalon in the CIPT expansion is still present after having performed the contour integration, which was already suggested by Refs. [5, 16] and Refs. [4, 24].

Next we examine the results for the subtracted CIPT series. They are given by the blue dots on the LHS of Fig. 4.1. In contrast to the unsubtracted series, the expansion for CIPT in the RF GC scheme is now approaching the same Borel sum as the (un)subtracted FOPT series and no discrepancy at intermediate orders is visible. One also observes that the subtracted CIPT series converges to the Borel sum faster than the (un)subtracted FOPT series and further does not inhabit the oscillatory behaviour. The fact that the subtracted CIPT series differs from the unsubtracted expansion implies that the subtraction series gives a non-vanishing contribution, therefore contradicting the consistency condition on the subtraction series. The CIPT subtraction series is given by the blue dots on the RHS of Fig. 4.1. Formally this series reads

$$\frac{1}{2\pi i}\oint_{|s|=s_0}\frac{\mathrm{d}s}{s}\,W_{m\neq 2}(\tfrac{s}{s_0})\left[-\frac{R^4}{s^2}\sum_{\ell=1}^{\infty} r_\ell^{(4,0)}\,\bar{a}_R^\ell\right]^{\text{CIPT}} \neq 0 \text{ and divergent}\,. \tag{4.36}$$

An interesting aspect of the series shown in the right panels of Fig. 4.1, i.e. the subtraction series corresponding to the unsubtracted CIPT expansion, is that they approach the asymptotic separation (indicated by the horizontal gray line). To understand this behaviour we consider a schematic relation, where for simplicity we denote $\delta^{\text{or}}_{\text{CI/FO}}$ as the perturbative series for CIPT/FOPT in the original $\overline{\text{MS}}$ GC scheme and take $\delta^{\text{or}}_{\text{CI}}$ as the subtraction series corresponding to the CIPT expansion. We observe the relation

$$\delta^{\text{or}}_{\text{CI}} - \delta^{\text{sub}}_{\text{CI}} = \delta^{\text{or}}_{\text{FO}} \quad\Rightarrow\quad \delta^{\text{sub}}_{\text{CI}} = \delta^{\text{or}}_{\text{CI}} - \delta^{\text{or}}_{\text{FO}} = \Delta. \tag{4.37}$$

Since the subtraction series for CIPT gives precisely the contribution which compensates for the difference in the original CIPT and FOPT series, it becomes clear that the subtraction series for CIPT has to approach the asymptotic separation. This is what we observe in the right panels in Fig. 4.1.

We now draw the following conclusions from the carried out toy analysis: The asymptotic value that the unsubtracted CIPT series approaches at intermediate orders, e.g. the sum of the Borel sum integral and the asymptotic separation, should not be considered as the true value of the series. Rather one can view this asymptotic value as a manifestation of the inconsistency of CIPT, and one needs to apply the RF GC scheme in order to obtain a CIPT series which approaches the actual true value.

Another very important conclusion is that strong coupling determinations based on the original CIPT approach in combination with higher order OPE corrections in the common $\overline{\text{MS}}$ GC scheme are physically inconsistent. On this note, we record the fact that the assignment of the usual Borel sum

$$\delta^{(0),\text{FOPT}}_{W,\text{Borel}}(s_0) = \text{PV}\int_0^\infty \mathrm{d}u\,\frac{1}{2\pi i}\oint_{|s|=s_0}\frac{\mathrm{d}s}{s}\,W(\tfrac{s}{s_0})\;B[\hat{D}(s)](u)e^{-\frac{u}{\bar{a}(-s)}}\,, \tag{4.38}$$

where $B[\hat{D}(s)](u)$ is again considered to be the Borel function of the Euclidean Adler function, is consistent with the standard $\overline{\text{MS}}$ scheme of the OPE.

After this toy model analysis it is clear that, assuming the norm of the GC to be sizeable and as a consequence the Adler function perturbation series having a sizeable contribution from the $u = 2$ renormalon, the apparent discrepancy between both series at intermediate orders may be strongly suppressed when switching to the RF GC scheme. In addition, one is able to include at least the GC OPE correction in phenomenological analysis in a physically meaningful way in FOPT *and* CIPT. This is not the case in the $\overline{\text{MS}}$ GC scheme due to the inconsistency of CIPT w.r.t. the standard treatment of the OPE.

4.4 Application in the large-β_0 approximation

In order to get a more realistic illustration of the RF GC scheme we now consider the application in the large-β_0 approximation where the exact form of the Borel function of the Adler function is known [25], see section 3.2.1. As there are infinitely many other IR and UV renormalons present in the analysis of the large-β_0 results we obtain a more concrete idea about the impact of the

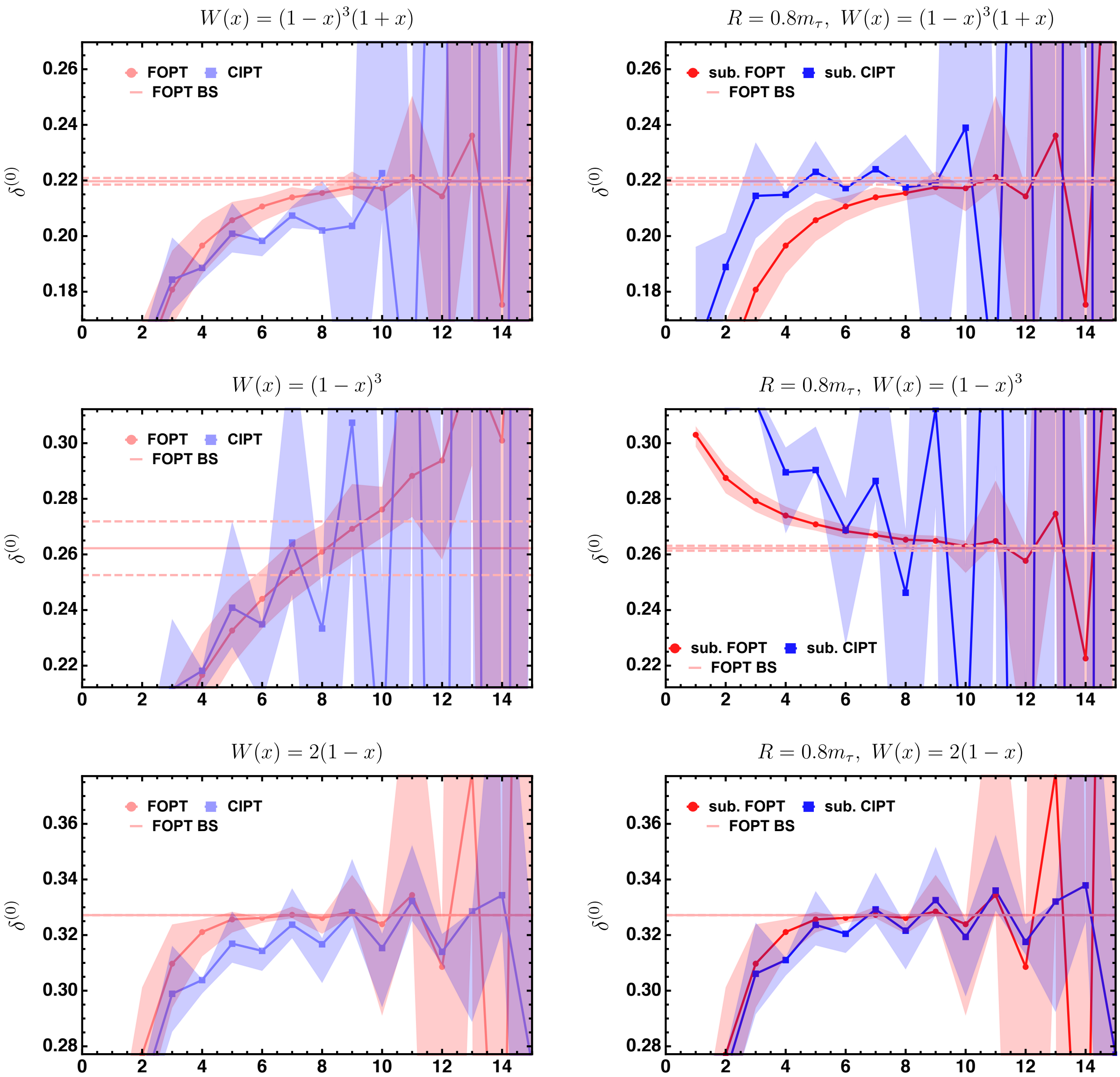

Fig. 4.2: Left panels: FOPT and CIPT expansions in the usual $\overline{\text{MS}}$ scheme for the OPE as a function of order in the large-β_0 approximation for different weight functions $W(x)$ and $\alpha_s(m_\tau^2) = 0.315$. Errors arising from renormalization scale variations are depicted by the colored bands. Right panels: Corresponding series for FOPT and CIPT expansions in the RF GC scheme.

subtraction of the GC on the perturbative series for full QCD. Note that some of the results presented in the following were included in Ref. [31].

Due to the fact that the Borel function is known, we have an explicit value for the normalization of the GC renormalon pole, which is given by $N_{4,0} = \frac{2\pi^2}{3} N_g = 8e^{10/3}/9 \approx 24.92$. Recall that the normalization is needed for the implementation of the RF GC scheme. How to obtain a value for this quantity in full QCD will be discussed extensively in section 5.1. In addition, since the RGE for the strong coupling is already exact at $\mathcal{O}(\alpha_s^2)$ (i.e. $\beta_{n>0} = 0$), the C-scheme and the $\overline{\text{MS}}$ scheme for α_s are identical. Furthermore, as can be seen from Eq. (3.26), the GC renormalon singularity is only a simple pole. This is because the coefficient $\hat{b}_1$ vanishes. Another simplification compared to full QCD is that the higher order corrections to the Wilson coefficients of all higher dimensional terms in the OPE vanish, implying for the case of the GC $\bar{c}_{4,1}^{(1)} = 0$ [16], which also simplifies the subtraction term.

Before talking about the individual series depicted in Fig. 4.2 let us collect a bit of general information: In all plots we compare FOPT expansions, denoted by the red colors in different opacities, to CIPT expansions shown in blue colors of different opacities. We picked three different moments with phenomenological relevance, as will be eluded to in the following, to illustrate the impact of the GC renormalon being subtracted from the perturbative series. The left panels consistently display the unsubtracted series, whereas the right panels show the corresponding subracted series. The connected dots, shown in both the unsubtracted and subtracted cases, indicate the results where the renormalization scale agrees with $-s$ and s_0, respectively. The shaded bands arise from the scale variation described below. The red horizontal lines are again the Borel sums corresponding to the individual moments and the space between the dashed red horizontal lines reflects the ambiguity of the PV prescription of the Borel sum integral.

The general parameters we chose for this analysis are given by $s_0 = m_\tau^2$ and $\alpha_s(m_\tau^2) = 0.315$. The IR factorization scale is chosen to be $R = 0.8m_\tau$ for the case of the subtracted series and we consistently implemented a scale variation arising from $\alpha_s(-\xi s)$ and $\alpha_s(\xi s_0)$, respectively, for $1/2 \leq \xi \leq 2$ for both the unsubtracted as well as the subtracted perturbative expansions. We choose to include this variation as a proxy for the uncertainty which would arise in phenomenological studies. Lastly, we record the fact that all plots on the left correspond to the CIPT and FOPT expansions in the $\overline{\text{MS}}$ GC scheme and all plots on the right correspond to CIPT and FOPT in the RF GC scheme.

Now that the underlying conditions are set, we want to discuss the individual results in detail, starting with the upper two panels showing the results for the kinematic moment. As we know by now, this is a member of the family of GCS moments. The discrepancy between the unsubtracted CIPT and FOPT expansions is clearly visible. If we turn our attention to the perturbative series in the RF GC scheme, we see immediately that the subtracted CIPT series approaches the same Borel sum as the FOPT series. Recall that in large-β_0 the subtracted FOPT series for GCS moments is identical to the unsubtracted expansion, since the contribution of the subtraction would only come through the one-loop correction of the Wilson coefficient of the GC, which is zero in this case. For GCE moments this is not the case. The reason being that the corresponding contributions do not vanish after doing the contour integration. Another interesting aspect of the subtracted CIPT series is that it approaches the Borel sum much faster than the (un)subtracted FOPT expansion, which is in analogy to the observation we made in the toy model study in section 4.3. What one can conclude from this study is that the GC renormalon gives the largest contribution to the discrepancy observed in the original series and that the discrepancy arising from higher dimensional condensates can basically be neglected for all practical purposes, which corroborates the proposition at the end of section 3.3.

The two panels in the middle of Fig. 4.2 show the same GCE moment we already considered in sections 3.2.1 and 3.2.2. In the past these type of moments were not part of most phenomenological analyses due to their bad perturbative behaviour. The unsubtracted FOPT and CIPT expansions shown in Fig. 4.2 exhibit precisely this unpleasant character, where the contribution arising from the GC renormalon leads to an immediate divergent run-away behaviour [24]. This observation was already made in sections 3.2.1 and 3.2.2. An additional observation which is connected to the non-suppressed GC renormalon contribution is the size of the ambiguity of the Borel sum integral being significantly larger compared to the ambiguity for the Borel sum of the kinematic moment. If we now again consider the related series in the RF GC scheme we observe that the subtracted CIPT series as well as the subtracted FOPT series both approach the Borel sum. In addition, the ambiguity related to the Borel sum integral reduced to a basically negligible size.

Finally, we want to discuss the lowest two panels shown in Fig. 4.2, which depict the results for the perturbative expansions considering the moment that was used in strong coupling determinations by Refs. [7, 28, 29]. This moment has the property that the contamination from higher dimensional terms in the OPE in fits of the strong coupling is negligible. Note, however, that due to the double poles appearing in the full Borel function of the Adler function in the large-β_0 approximation the corresponding higher dimensional IR renormalon effects are not completely removed. Looking at the perturbative series, first in the unsubtracted case, we observe again a similar discrepancy between the FOPT and CIPT expansions as we did for the case of the kinematic moment. The FOPT series again approaches the Borel sum given in Eq. (3.34), whereas the

CIPT expansion is systematically below at intermediate orders. For the RF GC scheme we obtain once more a vanishing discrepancy and both expansions now approach the FOPT Borel sum.

Based on the studies of these three moments we record the fact that in the RF GC scheme the discrepancy, which originally existed between the FOPT and CIPT expansions for GCS moments, is strongly suppressed to almost negligible size. Both series approach the 'true' Borel sum, which is given by the FOPT Borel sum in Eq. (3.34), in the RF GC scheme. This of course implies that strong coupling determinations using those moments should now yield results which are in much better agreement compared to the analyses where the unsubtracted series were considered. We will have a thorugh discussion on precisely this aspect in section 5.2. For GCE moments we observe a much better perturbative behaviour as the subtraction removes the run-away behaviour originating from the CG renormalon. As we already mentioned, in the past these moments were excluded from phenomenological studies but in the RF GC scheme they might become relevant for future strong coupling extractions.

In the next section, which will also conclude the discussion on the impact of the RF GC scheme on the perturbative expansions, we will have a look at the results in full QCD, using the MRM introduced at the beginning of section 3.2.2.

4.5 Renormalon Subtracted Perturbation Theory in full QCD

The studies in full QCD discussed in this section are based on the Borel model given by Eq. (B.1) in appendix B. Recall that the first four coefficients are known and reproduced by the model (see Eqs. (3.19) and (3.20) for the $\overline{\text{MS}}$ scheme and Eq. (4.5) for the case of the C-scheme). In the construction we also included the estimate for the six-loop coefficient given in Eq. (3.20) and Eq. (4.5) for the case of the $\overline{\text{MS}}$ scheme for α_s and the C-scheme for the strong coupling, respectively. Starting from $n = 6$ (n being the order in perturbation theory) the results for the unsubtracted series shown in the left panels of Fig. 4.3 are therefore model-dependent (this is indicated by the purple vertical line). An important point worth emphasizing is that, in contrast to the results for the unsubtracted series, the terms for the subtracted series (right panels) are model dependent starting from the first order since the value for the GC renormalon norm predicted by the model is part of the subtraction series. We nevertheless decided to include the vertical line in the plots showing the results in the RF GC scheme to re-emphasize the model dependence of the original series. Due to the fact that the parameter settings are identical to the large-β_0 approximation in the previous section we refer to the introduction of section 4.4 for the considered values and directly shift to discussing the results.

Starting with the upper two panels of Fig. 4.3, showing the impact of the RF GC scheme for the kinematic moment, we observe already for the first five terms in the unsubtracted series the appearance of the discrepancy between FOPT and CIPT, which is also reflected in the experimental analysis discussed in chapter 5. Looking at orders beyond $n = 5$, which are now predictions by the model, we see again that the unsubtracted FOPT series approaches the 'true' Borel sum, whereas the CIPT series lies systematically below before exhibiting the divergent behaviour for orders $n \gtrsim 9$. In the RF GC scheme the discrepancy is now reduced, as it was the case in the large-β_0 approximation. What is important at this point, is that the effect of the subtraction of the GC renormalon is already visible at orders five and less. Note that FOPT only receives tiny corrections through the one-loop correction of the Wilson coefficient of the GC in the subtraction term, whereas CIPT changes visibly. Taking into account the predictions by the model, we record the fact that the main qualitative features of the previous section are again observed for the case of full QCD.

The second line of panels in Fig. 4.3 show the GCE moment from the previous section, where both the CIPT and FOPT series inhabit the runaway behaviour originating from the GC renormalon in the $\overline{\text{MS}}$ GC scheme (left panel). Already at order five the bad perturbative behaviour is clearly visible, which was the reason why many past studies of α_s determinations did not include these types of moments. The error arising from scale variation is also much larger for the unsubtracted series compared to the kinematic moment shown in the first line of panels in Fig. 4.3.

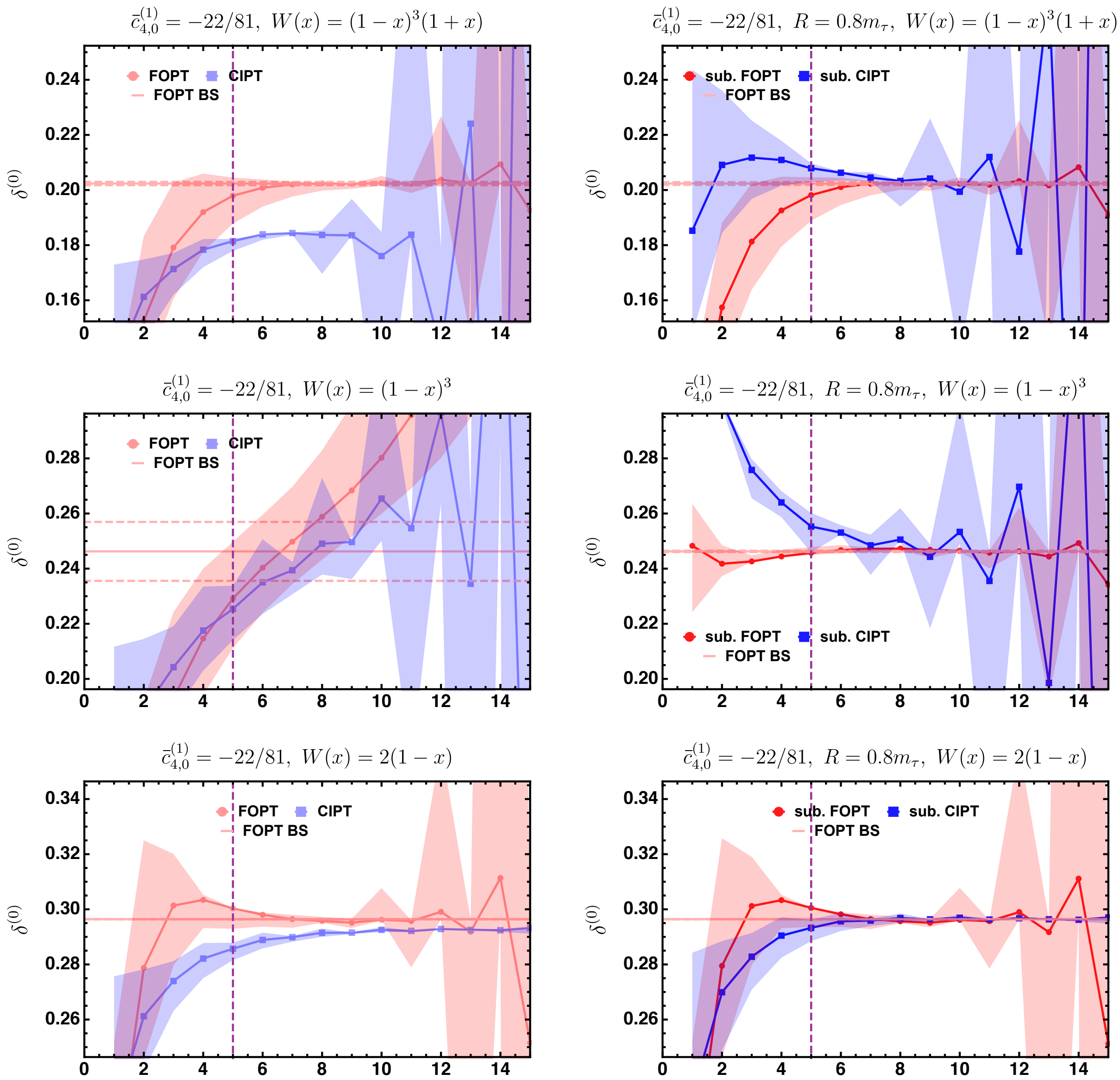

Fig. 4.3: Left panels: FOPT and CIPT expansions in the usual $\overline{\mathrm{MS}}$ scheme for the OPE as a function of order in full QCD for different weight functions $W(x)$ and $\alpha_s(m_\tau^2) = 0.315$. Errors arising from renormalization scale variations are depicted by the colored bands. Right panels: Corresponding series for FOPT and CIPT expansions in the RF GC scheme.

Switching to the RF GC scheme (right panel) we observe two things: First we see that the runaway behaviour is strongly tamed, and the two series now approach the 'true' value of the Borel sum, at least when one takes into account the higher orders predicted by the model. But crucially even at order five the two subtracted series become compatible with the Borel sum value within errors from renormalization scale variation. For the FOPT series, the improvement is quite dramatic as the subtracted series stabilizes around the Borel sum value for practically all orders up to $n = 10$, where the UV renormalon effect sets in. Note that the rather small renormalization scale variation error at lower orders arises due to phase cancellations of scale variation effects in α_s. Therefore, for this case renormalization scale variation alone does not provide an adequate error estimate in α_s extractions and one has to use alternative methods, such as R variation, to obtain a reliable theory error. As a last comment, we observe that the Borel sum ambiguity shrinks to almost negligible size. These results suggest what we already hinted upon previously, namely that the type of moments which enhance the GC contribution may become eligible for future strong coupling

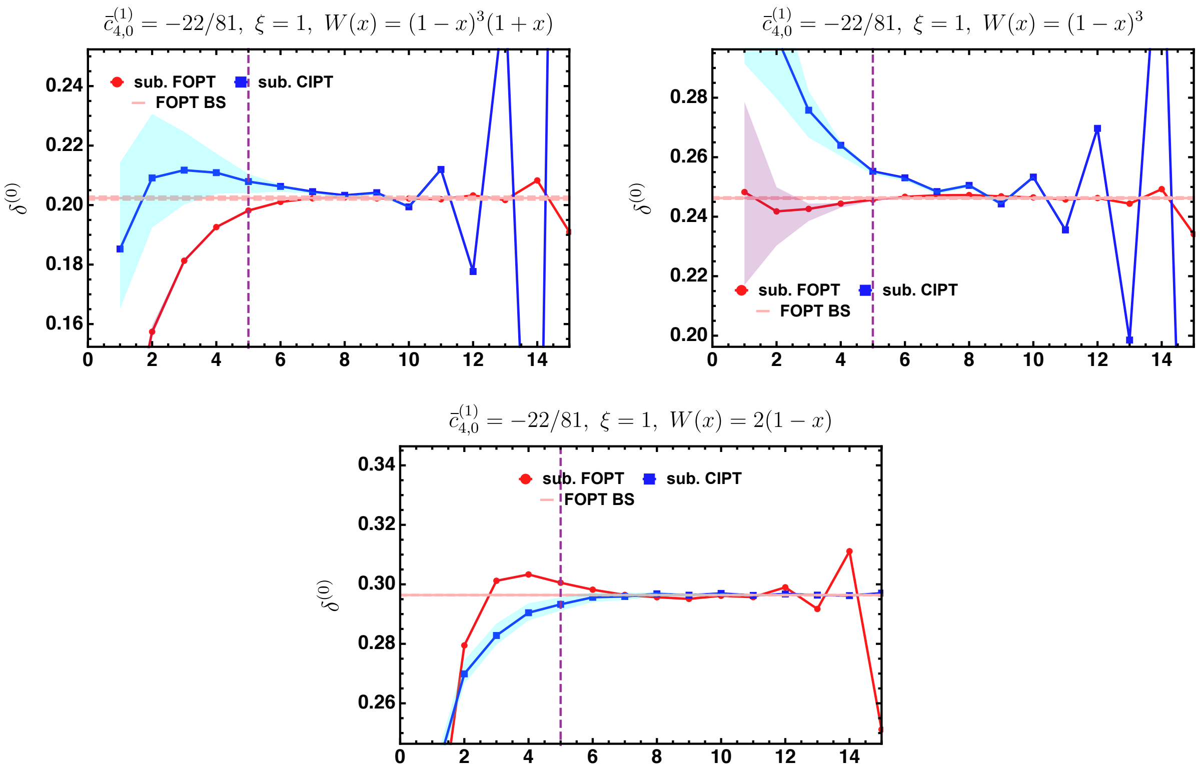

Fig. 4.4: FOPT and CIPT expansions in the RF GC scheme. In this case the renormalization scale is set to $\xi = 1$ and the IR subtraction scale is varied in the range $0.7\, m_\tau \leq R \leq 0.9\, m_\tau$ for the weight functions of the previous studies and we again take $\alpha_s(m_\tau^2) = 0.315$.

determinations, where in addition one obtains information on the GC itself.

In the lowest two panels of Fig. 4.3 we consider the moment used in the DV approach of extracting the strong coupling from τ hadronic spectral function moments [7, 28, 29, 32]. The discrepancy at intermediate orders and in particular at order five is again visible in the $\overline{\text{MS}}$ GC scheme (left panel). When switching to the RF GC scheme (right panel) the improvement of this discrepancy, at order $n = 5$ and beyond, is also present. As it was the case for the kinematic moment, seeing this improvement already at order five should subsequently lead to results for CIPT and FOPT that are in better agreement in phenomenological studies based on this choice of moment.

Finally, we still need to discuss the dependence on the IR subtraction scale R of the RF GC scheme. In particular, we are interested in the impact on the subtracted CIPT and FOPT series when choosing different values of R. As we mentioned before, these variations of the IR factorization scale should constitute an additional uncertainty estimate in the theory predictions of phenomenological analysis when considering the RF GC scheme. In addition, this variation can be considered as a diagnostic tool to test the reliability of the subtracted FOPT and CIPT series.

The results for this IR factorization scale variation are now shown in Fig. 4.4. The moments and parameter settings are identical to Fig. 4.2 and Fig. 4.3. The connected red and blue dots are precisely the results depicted in Fig. 4.3, e.g. the subtracted FOPT and CIPT series, respectively, with the default value $R = 0.8 m_\tau$. The error bands in Fig. 4.4 arise from varying the factorization scale between $0.7 m_\tau \leq R \leq 0.9 m_\tau$. For the GCS moments we see that the scale variation has little impact on the subtracted FOPT series, which is what we expected, as the subtraction only contributes through the one-loop correction of the Wilson coefficient. For the subtracted CIPT series, on the other hand, the variation in R has a visible impact on the GCS moment series. We observe that the R-dependence decreases with order in perturbation theory, which is what one expects. Recall that in the large-order limit, the R dependence formally vanishes. For the

GCE moment, shown in the top right panel of Fig. 4.4, both series have a visible dependence on the choice of R. In this case, the R variation is actually numerically larger than the usual renormalization scale variation for both expansions up to order four, corroborating the fact that renormalization scale variation alone does not provide an adequate estimate of the perturbative error in theory predictions for strong coupling determinations using the RF GC scheme.

Overall, we can record the fact that the conclusions drawn at the end of section 4.4 also hold for the case of full QCD. In particular, we observe that these modifications already take place at order five, implying that these findings may impact the current theoretical predictions for strong coupling determinations from τ hadronic spectral function moments. As already mentioned, a detailed investigation of the application of the RF GC scheme will be presented in section 5.2. However, before one can study the impact of this scheme on the determinations of α_s we need to obtain a reliable estimate for the norm of the GC, as this value is contained in the subtracted perturbative expansion coefficients at all orders. This will be the first question addressed in the following final phenomenological chapter.

Chapter 5

Determination of N_g and Phenomenology

This final chapter brings together everything that we discussed up until now in this thesis and shows how the RF GC scheme introduced in the previous chapter impacts current determinations of the strong coupling. In particular, we are going to apply our new scheme to two studies from the past, which use different approaches to account for non-perturbative corrections, and analyse the results individually. But first we need a reliable estimate for the norm of the GC renormalon N_g since it is conceptually part of the RF GC scheme for all orders in perturbation theory and therefore also for the relevant 6-loop contributions that enter the phenomenological analysis.

5.1 Determination of the norm of the gluon condensate

In the previous section we demonstrated through a thorough analysis the effectiveness of the RF GC scheme, where in full QCD we relied on models for the Borel function of the Adler function. Recall that in our case the precise expression is given by Eq. (B.1). In this section we want to quantify the norm of the GC, N_g, obtaining a reliable estimate for the central value and a corresponding uncertainty. The final result then enters our phenomenological analysis in section 5.2, where the error on N_g represents an additional parametric error. Note that all of the following studies to obtain a value for N_g are based on the $n_f = 3$ active flavor scheme as this is the flavor number relevant for hadronic spectral function moments.

The analysis is carried out in three subsections, where each section contains a different method of obtaining an estimate for the norm of the GC renormalon N_g. Section 5.1.1 contains the straightforward approach of modifying the MRM in various ways and looking at the impact on N_g. In section 5.1.2 we revisit a method introduced by Lee [33], which we call the 'Conformal Mapping Approach', where the strategy used by Ref. [33] will be discussed and modifications thereof are investigated. Lastly, we introduce a novel approach to determine the norm of the GC, which we call the 'Optimal Subtraction Approach'. The idea in this case is to obtain N_g from a minimization procedure relying on the two improvements the RF GC achieves for GCS and GCE spectral function moments. To be precise, we rely on (a) the reduction of the discrepancy between CIPT and FOPT for GCS moments and (b) the improvement of the perurbative convergence of GCE moments. These approaches all yield compatible results and at the end of this section we will quote our final value for N_g plus the corresponding uncertainty from the new optimal subtraction approach.

5.1.1 Renormalon Model Approach

As we now mentioned numerous times, the exact Borel function of the Adler function in full QCD is a priori not known. The general structure of the non-analytic contributions which are related to the IR renormalons can, however, be deduced from the one-to-one association of renormalons to higher-dimensional terms in the OPE for the case of the IR renormalons. For completeness, we note that the structure of the UV renormalons can be deduced from higher-dimensional operator insertions, which are related to short-distance quantum corrections that are being integrated out. This will, however, not be relevant in the following.

Recall that the model we based our studies on in full QCD was motivated by Ref. [4] and of the form

$$B[\hat{D}(s)]_{\rm mr}(u) = b^{(0)} + b^{(1)}u + \frac{2\pi^2}{3}\frac{N_g\left[1-\frac{22}{81}\bar{a}(-s)\right]}{(2-u)^{1+4\hat{b}_1}} + \frac{N_6}{(3-u)^{1+6\hat{b}_1}} + \frac{N_{-2}}{(1+u)^{2-2\hat{b}_1}}, \tag{5.1}$$

where the three renormalon norms and the two polynomial coefficients are obtained by the constraint that the model should reproduce the known perturbative coefficients up to order five in perturbation theory. The exact values for the parameters in Eq. (5.1) can be found in appendix B. The value for the norm of the GC renormalon in Eq. (5.1) is given by $N_g = 0.64$. The idea of the renormalon model approach is straightforward and solely based on modifications of Eq. (5.1), where we look at the impact on N_g that the individual changes of the model provide.

The first thing that one can have a look at is the impact of the uncertainty of the six-loop coefficient. In particular, we take the central value given in Eq. (3.20) and vary it by $\pm 50\%$. As a result one obtains $N_g = 0.64 \pm 0.27$. In relative terms we obtain a symmetric relative error of 43%. Here we of course did not modify the model itself. This will be done in the following and the first modification we consider is the inclusion of the two-loop correction of the Wilson coefficient of the GC. For the purpose of the current analysis, we thus consider a modification of the Borel model of the form

$$B[\hat{D}(s)]_{\rm mr}(u) = b^{(0)} + b^{(1)}u + \frac{2\pi^2}{3}\frac{N_g\left[1-\frac{22}{81}\bar{a}(-s)+\delta\bar{a}^2(-s)\right]}{(2-u)^{1+4\hat{b}_1}} + \frac{N_6}{(3-u)^{1+6\hat{b}_1}} + \frac{N_{-2}}{(1+u)^{2-2\hat{b}_1}}, \tag{5.2}$$

with $-0.5 \leq \delta \leq 0.5$. Since the known one-loop correction of the Wilson coefficient of the GC has an absolute size of ≈ 0.27 and the perturbative coefficients of the Adler function are well behaved (i.e. with the coefficients significantly smaller than 0.5 up to the three-loop level), we find it reasonable to assume that the size of the two-loop correction of the Wilson coefficient of the GC does not exceed 0.5 as well. The norm of the GC in this case yields the result $N_g = 0.64^{+0.11}_{-0.08}$ corresponding to a relative error of $+18\%$ and -13%, which is smaller than the error obtained from taking the uncertainty of the 6-loop approximate.

Further variations of the model are now performed by (a) introducing a one-loop correction of the Wilson coefficient of the $d = 6$ IR renormalon (b) doing the same for the $u = -1$ UV renormalon using the same δ variation as in the previous case. This leads to the results: $N_g = 0.64^{+0.09}_{-0.03}$ and $N_g = 0.64^{+0.01}_{-0.01}$, respectively, which are also relatively small compared to the error obtained from varying the six-loop coefficient.

Finally, we consider two structural changes of the Borel model. We drop the polynomial coefficient $b^{(1)}$ and replace it with (a) an additional $d = 8$ IR renormalon (b) an additional $u = -2$ UV renormalon. These modifications can be justified based on the fact that the polynomial coefficient $b^{(1)}$ in the original model is relatively small, indicating that the structure of the renormalons included already accounts for the corrections at the three-loop level and beyond. The result we obtain for modification (a) reads $N_g = 0.68$, which corresponds to a deviation of the norm of the GC w.r.t. Eq. (5.1) (where $N_g = 0.64$) of 6%. For modification (b) we only obtain a deviation by 0.5% from the Borel model value.

Summarizing the findings of this study we conclude that the largest uncertainty in determining the norm of the GC arises from the error that the 6-loop coefficient inhabits. The carried out analysis does, however, by no means exhaust the available possibilities of modifying the Borel model. We subsequently only consider the outcome as a guideline for our studies in the following sections and continue with the conformal mapping approach.

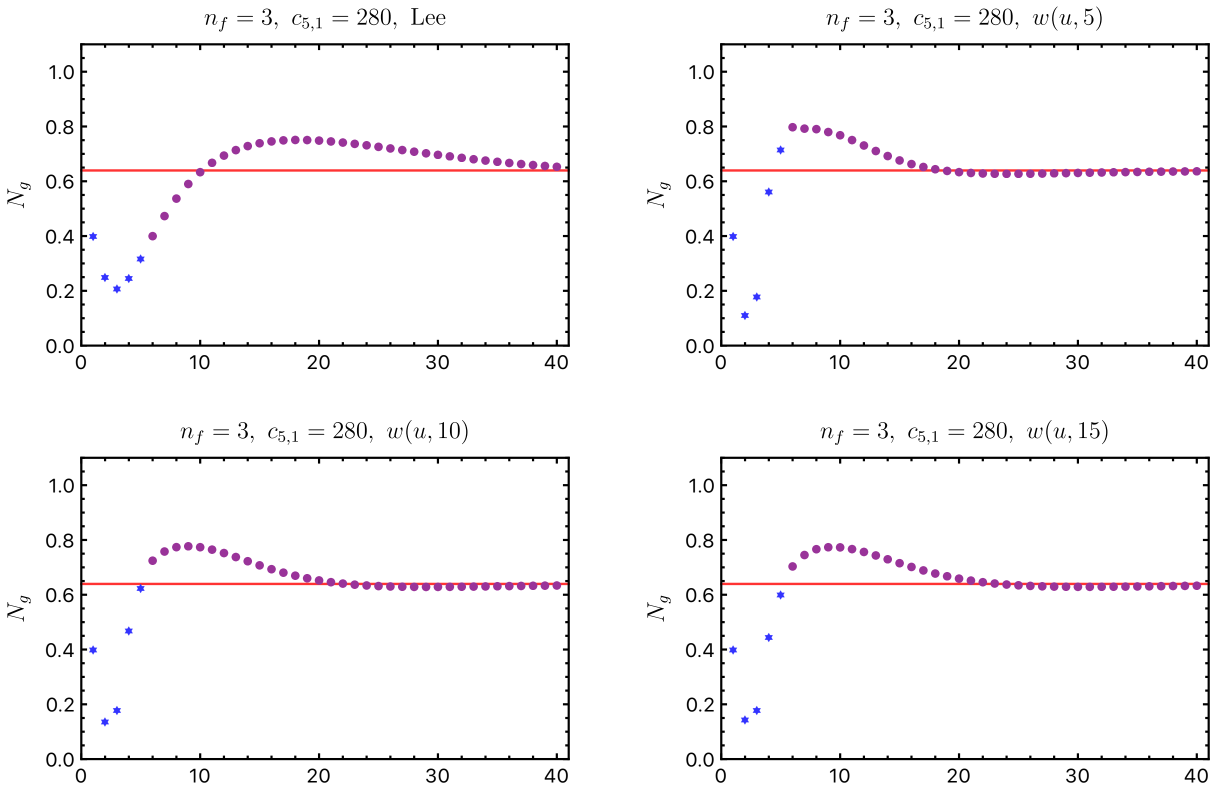

Fig. 5.1: Conformal mappings for the $n_f = 3$ flavor scheme in full QCD. The values for the norm of the GC are given as a function of order in perturbation theory. The orders beyond $n = 5$ are model dependent and based on Eq. (B.1). The known perturbative coefficients are indicated by a blue star. The upper left panel shows the Taylor series using the conformal map introduced by Lee. The remaining three panels depict the Taylor series based on Eq. (5.5) and show the outcome using different values of the parameter p.

5.1.2 Conformal Mapping Approach

The conformal mapping approach [33] is based on the fact that the function

$$\tilde{B}(u) \equiv \frac{3(2-u)^{1+4\hat{b}_1}}{2\pi^2} B[\hat{D}(s)](u) \tag{5.3}$$

is analytic in the neighbourhood of the point $u = 2$, even though other renormalons contained in $B[\hat{D}(s)](u)$ at $u = 3, 4, -1, -2, \ldots$ are still present. The idea is now to apply a conformal transformation, denoted by $z = f(u)$, to $\tilde{B}(u)$, such that $f(0) = 0$ and the point $z_2 = f(2)$ is moved inside the radius of convergence of the Taylor series of the function $\tilde{B}(f^{-1}(z))$ around $z = 0$. The radius of convergence in this case is given by the point contained in the set of mapped branch points, e.g. $\{f(3), f(4), \ldots, f(-1), f(-2), \ldots\}$, which is closest to the origin. Having applied such a conformal transformation it is then possible to obtain N_g from the Taylor series of $\tilde{B}(f^{-1}(z))$ in powers of z evaluated at $z = z_2$. In order to use the conformal mapping approach to obtain a value for the norm of the GC the only thing needed is the form of the most singular term contained in the GC renormalon contribution to the Borel function of the Adler function, which is simply given by $1/(2-u)^{1+4\hat{b}_1}$. It is clear by construction that this conformal mapping approach is dependent on the choice of the conformal transformation function $f(u)$. In the following we will consider different conformal transformations and analyse the obtained results in detail.

The first conformal map that we use is taken from an analysis carried out by Lee [33–35]

$$z = \frac{u}{1+u}, \tag{5.4}$$

	$w(u,5)$	$w(u,10)$	$w(u,15)$
order 4	0.57	0.47	0.45
order 5	0.72 ± 0.24	0.63 ± 0.17	0.60 ± 0.15

Table 5.1: Results for the norm of the GC obtained from the conformal mapping approach using the class of transformations arising from Eq. (5.5) for different values of p and different orders in perturbation theory.

where his intention was the same as ours, i.e. to get a value for the norm of the GC. The point z_2 is now moved to $z_2 = 2/3$, which is close to but still inside the convergence radius of $r_c = 0.75$. Since the Borel model given by Eq. (B.1) is considered to be a reasonable approximation of the full Borel function of the Adler function in full QCD, we seek to take Eq. (5.4) to the test and check at which order in perturbation theory the resulting Taylor series converges to the value of N_g predicted by the model. The result is given by the upper left panel of Fig. 5.1. We see that the series only converges to the model value for N_g for orders $n \gtrsim 40$. On the other hand, for orders $n \lesssim 5$, which are the known orders, the series undershoots the model value significantly. This unsatisfying behaviour motivates us to consider alternative conformal transformation functions.

It turns out that a class of conformal transformations which is much better suited for our purposes, introduced by Refs. [36–38] in this and other contexts, reads

$$w(u,p) = \frac{\sqrt{1+u} - \sqrt{1-\frac{u}{p}}}{\sqrt{1+u} + \sqrt{1-\frac{u}{p}}}\,, \tag{5.5}$$

where the parameter p can be chosen freely. Setting $p = (5, 10, 15)$ yields $z_2 = (0.38, 0.32, 0.30)$ with the corresponding convergence radius $r_c = (0.52, 0.41, 0.38)$, where we again see that the points are now located within the radius of convergence. The numerical outcome for the resulting Taylor series are depicted in the upper right and lower two panels of Fig. 5.1. For the conformal transformations belonging to the class arising from Eq. (5.5) we see an improved convergence behaviour compared to the results obtained from using the conformal transformation given by Eq. (5.4). The Taylor series for all values of p already approach the model value for N_g for $n \gtrsim 20$. What is more important, is that at the $\mathcal{O}(\alpha_s^4)$ and $\mathcal{O}(\alpha_s^5)$ level the values for the norm of the GC are already within 30% and 10% of the model value, respectively. In addition, the results for $n > 5$ do not exceed a deviation from the model value of 20%.

As a first step of determining a final value for N_g we extract the value obtained from the conformal mapping approach based on Eq. (5.5) at $\mathcal{O}(\alpha_s^4)$ and $\mathcal{O}(\alpha_s^5)$. For the latter we include the error accompanying the six-loop coefficient given in Eq. (3.20). The numerical results are given in Tab. 5.1 for $p = (5, 10, 15)$. Overall, the results are in good agreement with the outcome in the previous section, where we considered modifications of the MRM given in Eq. (5.1). This supports the supposition that N_g is sizeable. To further back up these findings we consider a last method to obtain a value for the norm of the GC, which we call the 'optimal subtraction approach'.

5.1.3 Optimal Subtraction Approach

The last method we discuss to obtain a value for N_g relies on the improvements that the RF GC yields for the perturbative series compared to the original $\overline{\text{MS}}$ GC scheme. To facilitate the current discussion, we write the FOPT (FO) and CIPT (CI) spectral function moments for a given weight function at order m in perturbation theory as

$$\delta^{(0),\text{FO/CI}}_{W,m}(N_g, s_0, \alpha_s(s_0)) \;=\; \sum_{n=0}^{m} r^{\text{FO/CI}}_{W,n}(N_g, R^2, \xi, s_0, \alpha_s(s_0))\,, \tag{5.6}$$

where we remind the reader that the resulting series is based on an expansion in the $\overline{\text{MS}}$ strong coupling α_s. Further we recall that the perturbative coefficients $r^{\text{FO/CI}}_{W,n}$ for $n = 1, 2, 3, 4$ are based on known results and the coefficient $r_{W,5}^{\mathrm{FO/CI}}$ encodes the information from the six-loop estimate given in Eq. (3.20). In general, the perturbative series terms $r_{W,n}^{\mathrm{FO/CI}}$ depend on the IR factorization scale R as well as on the renormalization scaling parameter ξ. However, in the large order limit the dependence on these parameters vanishes, therefore we suppressed them as arguments of the function $\delta_{W,m}^{(0),\mathrm{FO/CI}}$. In practice one always truncates the series at a certain order in perturbation theory. Hence, the residual dependence on R and ξ remains. As a final comment on the perturbative series shown in Eq. (5.6) we note that the 'tree-level' term arising in the RF GC scheme, i.e. the term proportional to $N_g\,\bar{c}_0(R^2)$ contained in $r_{W,0}^{\mathrm{FO/CI}}$, does not depend on the renormalization scaling parameter.

The optimal subtraction approach is based on a χ^2-type function, where the improvements from the RF GC scheme provide a quantitative measure. In particular, the χ^2-function is constructed from a set of GCS and GCE spectral function moments and consists of two additive parts

$$\chi^2_m(N_g) = \chi^2_{m,\mathrm{GCS}}(N_g) + \chi^2_{m,\mathrm{GCE}}(N_g)\,. \tag{5.7}$$

Note that in Eq.(5.7) we suppressed all arguments from Eq. (5.6), except for N_g, to make our expressions more compact. Let us now take a closer look at the individual contributions to Eq. (5.7). The first term represents a measure for the improvement w.r.t. the discrepancy of the CIPT and FOPT expansion at order m in perturbation theory for a set of GCS moments, see section 4.5. The precise expression amounts to

$$\chi^2_{m,\mathrm{GCS}}(N_g) = \sum_{i=1}^{5}\Big(\,\delta^{(0),\mathrm{CI}}_{W_i,m}(N_g) - \delta^{(0),\mathrm{FO}}_{W_i,m}(N_g)\Big)^2\,. \tag{5.8}$$

Conceptually, Eq. (5.8) approaches a minimum if the discrepancy between the CIPT and FOPT expansions becomes small for each GCS weight function at the same time. The second term in Eq. (5.7) gives a measure for the improvement of the convergence of the series for GCE moments and is given by

$$\chi^2_{m,\mathrm{GCE}}(N_g) = \sum_{i=6}^{10}\Big(\,r^{\mathrm{FO}}_{W_i,m}(N_g) - r^{\mathrm{FO}}_{W_i,m-1}(N_g)\Big)^2\,. \tag{5.9}$$

In this case a minimum is approached if the series is well behaved and does not exhibit the 'classic' runaway behaviour connected to GCE moments in the past, see again section 4.5. We point out that in the numerical analysis which follows we only account for FOPT series terms in the contribution to χ^2_m arising from $\chi^2_{m,\mathrm{GCE}}$. This is, due to the fact that the CIPT expansion exhibits a more pronounced sign-alternating behaviour compared to the FOPT series. This could potentially lead to artificial enhancements or suppressions for N_g at certain orders m in perturbation theory, which we want to avoid.

The GCS moments which we consider for our analysis in the optimal subtraction approach are based on the following set of weight functions (on the level of the Adler function):

$$\begin{aligned}
W_1(x) &= 1-2x+2x^3-x^4 = (1-x)^3(1+x)\,,\\
W_2(x) &= \frac{6}{5}-2x+2x^4-\frac{6x^5}{5} = \frac{2}{5}(1-x)^3(3+4x+3x^2)\,,\\
W_3(x) &= \frac{4}{3}-2x+2x^5-\frac{4x^6}{3} = \frac{2}{3}(1-x)^3(1+x)(2+x+2x^2)\,,\\
W_4(x) &= \frac{10}{7}-2x+2x^6-\frac{10x^7}{7} = \frac{2}{7}(1-x)^3(5+8x+9x^2+8x^3+5x^4)\,,\\
W_5(x) &= \frac{3}{2}-2x+2x^7-\frac{3x^8}{2} = \frac{1}{2}(1-x)^3(1+x)(3+2x+4x^2+2x^3+3x^4)\,.
\end{aligned} \tag{5.10}$$

Recall that W_1 in this notation correspond to the kinematic weight function, which we already considered at numerous stages throughout this thesis. All of the weight functions considered for

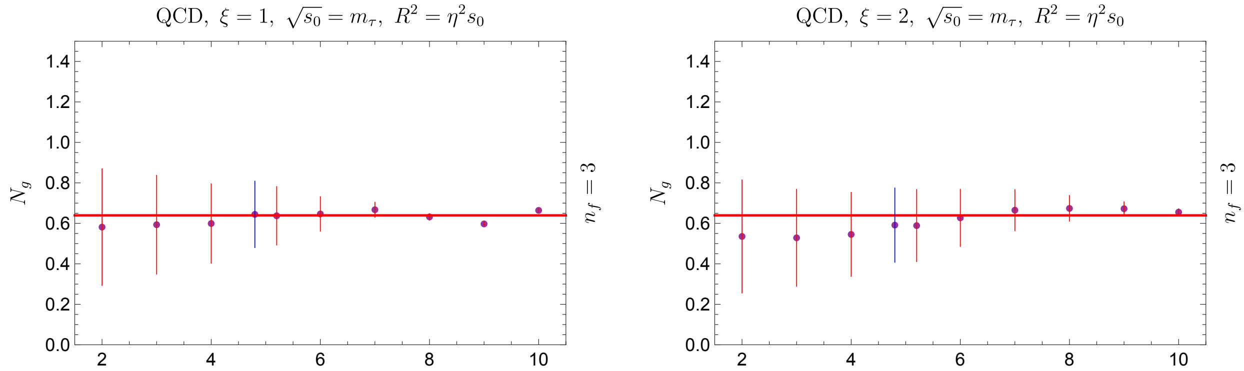

Fig. 5.2: Results for the determination of the norm of the GC in the $n_f = 3$ flavor scheme obtained from the optimal subtraction approach. The red error bars arise from variations of the IR factorization scale in the range $0.7m_\tau \leq R \leq m_\tau$ ($0.7 \leq \eta \leq 1$ in the headings of each plot). The purple dots represent the average of the maximal and minimal results at each order in perturbation theory. The additional blue error bar at order $m = 5$ corresponds to the case where we included, in addition to the R variation the error arising from the Padé approximate. In the left panel we show the results for $s_0 = m_\tau^2$ and $\xi = 1$. The right panel corresponds to the case where $s_0 = m_\tau^2$ and $\xi = 2$.

the analysis are linearly independent and doubly pinched. Furthermore, the GCS moments used for our determination of N_g have also been employed in recent strong coupling determinations by Ref. [6]. For the GCE moments the representative weight functions for our study are given by:

$$\begin{aligned}
W_6(x) &= (1-x)^3 = 1 - 3x + 3x^2 - x^3\,,\\
W_7(x) &= (1-x)^3\left(1+\frac{5x}{6}\right) = 1 - \frac{13x}{6} + \frac{x^2}{2} + \frac{3x^3}{2} - \frac{5x^4}{6}\,,\\
W_8(x) &= (1-x)^3\,(1-2x) = 1 - 3x + x^2 + 5x^3 - 6x^4 + 2x^5\,,\\
W_9(x) &= (1-x)^3\left(1 - x^2 + \frac{x^3}{3}\right) = 1 - 3x + 2x^2 + \frac{7x^3}{3} - 4x^4 + 2x^5 - \frac{x^6}{3}\,,\\
W_{10}(x) &= (1-x)^2\left(1+\frac{x^4}{4}\right) = 1 - 2x + x^2 + \frac{x^4}{4} - \frac{x^5}{2} + \frac{x^6}{4}\,.
\end{aligned} \tag{5.11}$$

They are again all linearly independent and doubly pinched, except for W_{10} which is only singly pinched.

Since the setting for the IR factorization scale R is relevant for the outcome of the series in the RF GC scheme, at least when considering truncations at some order m, we include variations of R between $0.7\sqrt{s_0} \leq R \leq \sqrt{s_0}$ in our method to obtain a value for N_g through the optimal subtraction approach. This leads to an uncertainty in our results for the norm of the GC which we take care of as follows: We adopt half of the range of N_g values that we get from the R variation as the uncertainty. The central value we obtain through averaging the maximum and minimum values of N_g.

The outcome of this third approach to obtain a value for the norm of the GC is now shown in Fig. 5.2, where the results for the renormalization scaling parameter settings are shown separately for $\xi = 1$ (left panel) and $\xi = 2$ (right panel). We observe for both cases that the results for N_g converge to the value predicted by the model in Eq. (5.1) ($N_g = 0.64$) at higher orders, which shows that our approach works in principle. Furthermore, for the case of $\xi = 2$, we see a slightly more stable behaviour of the results. This is related to the fact that the sign-alternating effects are suppressed in this case w.r.t. the GC renormalon. It is, however, clear that the UV renormalon will dominate the series eventually at larger orders. This means that for orders beyond the ones we show in Fig. 5.2 this method will eventually stop working, as the sign-alternating effects from

	$\sqrt{s_0} = m_\tau$	$\sqrt{s_0} = 3$ GeV
$m = 4$ ($\xi = 1$)	0.60 ± 0.20	0.51 ± 0.17
$m = 4$ ($\xi = 2$)	0.54 ± 0.21	0.55 ± 0.11
$m = 5$ ($\xi = 1$)	0.64 ± 0.16	0.50 ± 0.19
$m = 5$ ($\xi = 2$)	0.59 ± 0.18	0.52 ± 0.15

Table 5.2: Results for the norm of the GC using the optimal subtraction approach in the $n_f = 3$ flavor scheme. We show the outcome for orders $m = 4$ and 5. The uncertainties at the five-loop level arise from varying the IR factorization scale between $0.7\sqrt{s_0} \leq R \leq \sqrt{s_0}$. For the results at six-loop level we added the error from the Padé approximate to the error we get by varying R. The central values are obtained by averaging the maximum and minimum of the results for N_g at each order in perturbation theory.

the UV renormalon start to dominate the series. Nevertheless, for orders $m < 10$ we see that the optimal subtraction approach actually works very well. Recall that we can again only reliably consider the predictions for N_g for orders up to α_s^5, as the corrections are only known/estimated up to this level, see Eq. (3.19) and Eq. (3.20).

Note that for the results at $m = 5$ we included, in addition to the error related to IR factorization scale variation, the error connected to the six-loop coefficient, see Eq. (3.20). This is indicated by the blue horizontal line in both panels.

The actual results we obtain from this method for N_g are now given in Tab. 5.2. We quote the results at orders $m = 4, 5$ for the energy scales $\sqrt{s_0} = m_\tau$ and $\sqrt{s_0} = 3$ GeV and the renormalization scaling parameter settings $\xi = 1, 2$. The way we obtain a final result from this approach to determine the norm of the GC is that we take the envelope of all the results at $m = 4$. This then yields our final value

$$N_g = 0.57 \pm 0.23\,. \tag{5.12}$$

The uncertainty we obtain is about 40%. This makes Eq. (5.12) fully compatible with the results that we obtained from the previous two approaches. Note that due to the fact that we took as a basis for Eq. (5.12) the five-loop results, the value for N_g we obtain in the optimal subtraction approach is independent of the error connected to the six-loop coefficient. In conclusion, we believe Eq. (5.12) represents a reasonable estimate of the norm of the GC. Hence, we adopt this value together with the uncertainty as our final result which will enter the final phenomenological analysis.

5.2 Strong coupling determinations from experiment

We now want to demonstrate the improvements the RF GC scheme has on realistic strong coupling extractions from τ hadronic spectral function moments. In order to do so, we perform our analysis as follows: In the recent literature there are two major approaches of determining α_s from τ decays, which apply the different treatments of the nonperturbative corrections. We now consider as two representative studies 1) the work from Pich and Rodriguez-Sanchez [6] (to whom we will refer to as PRS) 2) the collaborative effort from Boito, Maltman Peris, Rodrigues, and Schaaf [7]. They differ from each other in as far as PRS employ a truncated version of the standard OPE corrections to account for non-perturbative effect (see also Refs. [39–42]), whereas Boito et al. include DV corrections in addition to higher-dimensional OPE corrections (see also Refs. [28,29,32]). For each of those analysis we first employ the $\overline{\text{MS}}$ GC scheme for the CIPT and FOPT expansions, where we intend to reproduce their results. Then we conduct the same analysis in the framework of the RF GC scheme, using our final result for N_g given in Eq. (5.12).

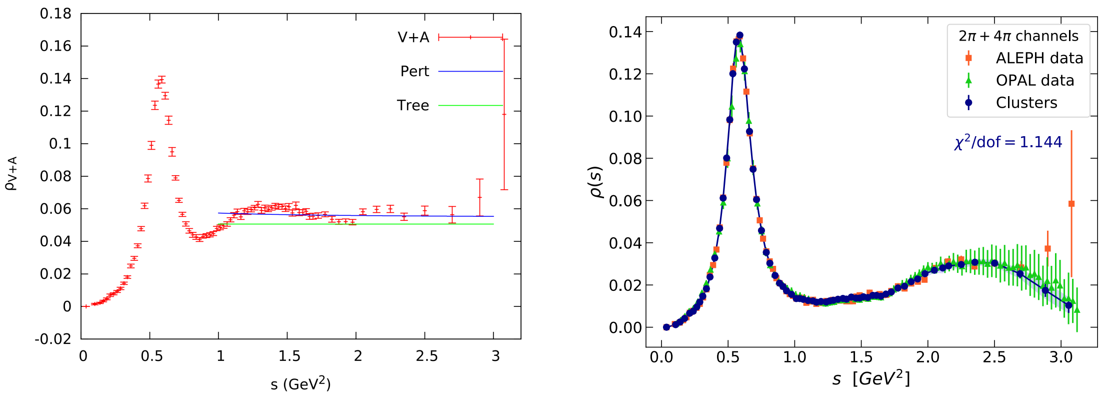

Fig. 5.3: Experimental spectral functions from the ALEPH collaboration for the $V + A$ channel (left panel) and the new vector-isovector spectral function from Ref. [7] for the V channel (right panel).

5.2.1 Experimental data in α_s extractions from τ decays

Before we go into the details of how the fits for the strong coupling work in these two approaches, we need to comment on the situation regarding the experimental data. The LEP experiments ALEPH [41–44] and OPAL [29,45] have produced data for the spectral function from the analysis of hadronic τ decays for the decay channels V, A, $V+A$ and $V-A$, where in our analysis the only relevant channels will be V and $V+A$. In the already mentioned work by Boito et al. [7,28,29,32] the data produced at $e^+e^- \to$ hadrons experiments was combined with the ALEPH and OPAL results to produce a new vector-isovector spectral function.

In order to illustrate the qualitative differences of the two different experimental data sets used for the strong coupling determinations we display the individual spectral functions in Fig. 5.3. The first immediate observation is that both spectra exhibit the characteristic resonance structures at lower values of s_0, representing the $\rho(2\pi)$ and $a_1(3\pi)$ peaks. As the hadronic invariant mass increases we see a flattening of the spectral distribution, where Ref. [6] states that the flattening is 'especially good in the most inclusive channel' $V + A$ (left panel). For the 'ALEPH spectral function', however, the experimental uncertainties are rather large for larger values of s, where the short-distance QCD methods become more precise [6]. When we compare this to the spectral function obtained by Ref. [7], we observe that the experimental uncertainties are significantly smaller near the high-energy region.

Nowadays, state-of-the-art α_s extractions from τ decays are based on either the 2013 update of the ALEPH spectral function [6,28,42,46,47] (for the case of the $V + A$ channel shown in the left panel of Fig. 5.3), or on the purely data based vector-isovector spectral function (right panel of Fig 5.3). As the work by Ref. [6] is based on the $V + A$ spectral function from the 2013 update from the ALEPH collaboration and the strong coupling determinations by Ref. [7] are based on their vector-isovector spectral function, we follow the approaches of the respective studies in order to precisely mimic the analysis of Refs. [6,7]. As already mentioned, in a first step we intend to reproduce their results. The second step is then to implement our newly defined RF GC scheme accounting for the result for the norm of the GC in Eq. (5.12) to study the impact our scheme has in a thorough phenomenological analysis.

5.2.2 Truncated OPE Analysis: Multiple Moments at fixed s_0

We start by carrying out the analysis conducted in section 5.3 of Ref. [6]. In the literature the approach they follow is referred to as the 'truncated OPE' (tOPE) strategy. What is done in this approach is the following: One picks a number of linearly independent weight functions, where the upper boundary of the FESR is always set to the highest possible value $s_0 = m_\tau^2$. All of the moments used in this analysis are at least doubly-pinched w.r.t. their representation on the level of the spectral function. Since pinching suppresses the effects stemming from duality violations, the corresponding contributions are then argued to be negligible and are subsequently dropped.

To allow for an actual fit, the number of moments entering the analysis has to be greater than the number of fit-parameters included. Due to the fact that the objective of having a set of linearly independent moments is achieved by adding additional powers of x to the polynomial weight function, the OPE terms beyond a certain dimension have to be truncated. The justification for the truncation of the OPE is based on the argument that the contributions which are not included in the fit are hierarchical and small.

At this point we want to briefly comment on the higher-dimensional OPE contributions entering the fit in this (and all other) approaches of determining the strong coupling. The general form of these corrections for the Adler function are given by

$$D^{\rm OPE}_{V/A}(s) \,=\, \frac{C_{4,0}(\alpha_s(-s))}{s^2}\langle\bar{\mathcal{O}}_{4,0}\rangle + \sum_{d=6}^{\infty}\frac{1}{(-s)^{d/2}}\sum_i C^{V/A}_{d,i}(\alpha_s(-s))\langle\bar{\mathcal{O}}_{d,\gamma_i}\rangle_{V/A}, \tag{5.13}$$

where the $C_{d,i}$ are the Wilson coefficients of the corresponding operators. The sum in i arises since there are several different condensates of the same dimensionality in the OPE starting from $d=6$ onwards. In the massless limit, the GC is the only contribution at dimension four. In actual phenomenological analysis, due to lack of knowledge, one usually considers an in some sense 'effective' analogue to Eq. (5.13) [6, 7, 28, 29, 41, 42, 48] on which we elaborate in the following. In the approximation used in actual fits, the Wilson coefficients are neglected and the anomalous dimension of all matrix elements are neglected as well. The Wilson coefficients in Eq. (5.13) subsequently basically reduce to constants. Note that sometimes the OPE is written down in terms of the correlator $\Pi^{(1+0)}_{V/A}$. Taking the 'standard' approximation of the OPE terms into account, where we now collectively denote the effective condensates together with the Wilson coefficients as $\mathcal{C}_d$, the expression for the OPE of the correlator reads

$$\Pi^{\rm OPE}_{V/A} \,=\, \frac{1}{12}\frac{\langle\bar{G}^2\rangle}{s^2} + \sum_{d=6}^{\infty}\frac{\mathcal{C}^{V/A}_d}{(-s)^{d/2}}\,. \tag{5.14}$$

Considering our definition of the Adler function in Eq. (3.11) the corresponding expression which then enters the fit amounts to

$$D^{\rm OPE}_{V/A} \,=\, \frac{2\pi^2}{3}\frac{\langle\bar{G}^2\rangle}{s^2} + 2\pi^2\sum_{d=6}^{\infty} d\,\frac{\mathcal{C}^{V/A}_d}{(-s)^{d/2}}\,. \tag{5.15}$$

Let us now return to the discussion on the setup of the analysis carried out in Ref. [6]. In the form of Eq. (5.15) a monomial x^m in the polynomial weigh function $W(x)$ exclusively picks up an OPE correction with dimension $d=2m$. The number of independent moments PRS chose as their basis in the fit is five and the polynomial weight functions they considered are shown in Eq. (5.10). This means that there are four parameters available which one can determine. In addition to α_s, Ref. [6] included the first three OPE condensates $\mathcal{C}_6$, $\mathcal{C}_8$ and $\mathcal{C}_{10}$.

The outcome for the fits based on the FOPT and CIPT expansions in the orignal $\overline{\rm MS}$ GC scheme are given in the upper half of Tab. 5.3. The results for $\alpha_s(m_\tau^2)$ read

$$\begin{aligned}\alpha_s(m_\tau^2)^{\rm CIPT} &= 0.3366 \pm 0.0070\\ \alpha_s(m_\tau^2)^{\rm FOPT} &= 0.3169 \pm 0.0065\end{aligned}\qquad (\text{tOPE, }\overline{\rm MS}\text{ GC, ALEPH }V+A). \tag{5.16}$$

In order to obtain the above results we took the six-loop estimate given in Eq. (3.20), where the corresponding error σ_5 is part of the overall error. The other contributions to the total error are the experimental uncertainty $\sigma_{\rm exp}$, as well as the error arising from scale variation σ_μ. For σ_μ we took the same prescription w.r.t. the variation of the scaling parameter ξ as in the previous sections, see e.g. section 4.4. The final value for the total error is then obtained by adding the individual errors in quadrature.

If we look at the results for α_s, we observe that there is a discrepancy between the FOPT and CIPT results of 0.0197, which is almost three times larger then the total uncertainties of the individual outcomes. This is of course well known and has been prior to our work the status quo.

	central value	σ_{exp}	σ_μ	σ_R	σ_{N_g}	σ_5	σ_{tot}
CIPT, $\chi^2/\text{dof} = 0.82$, p-value $= 0.37$							
$\alpha_s(m_\tau)$	0.3366	0.0042	0.0051	–	–	0.0024	0.0070
$\mathcal{C}_6 \times 10^3$	0.95	0.38	0.44	–	–	0.012	0.58
$\mathcal{C}_8 \times 10^3$	-1.07	0.46	0.22	–	–	0.055	0.51
$\mathcal{C}_{10} \times 10^3$	0.22	0.28	0.49	–	–	0.0052	0.56
FOPT, $\chi^2/\text{dof} = 1.23$, p-value $= 0.27$							
$\alpha_s(m_\tau)$	0.3169	0.0031	0.0056	–	–	0.0014	0.0065
$\mathcal{C}_6 \times 10^3$	1.37	0.43	1.22	–	–	0.076	1.29
$\mathcal{C}_8 \times 10^3$	-0.95	0.45	1.02	–	–	0.069	1.12
$\mathcal{C}_{10} \times 10^3$	0.43	0.30	0.58	–	–	0.041	0.66
RF GC scheme, CIPT, $\chi^2/\text{dof} = 2.14$, p-value $= 0.14$							
$\alpha_s(m_\tau)$	0.3197	0.0035	0.0047	0.0054	0.0058	0.0017	0.010
$\mathcal{C}_6 \times 10^3$	4.96	0.63	0.40	0.70	1.13	0.14	1.53
$\mathcal{C}_8 \times 10^3$	-3.40	0.54	0.42	0.37	0.76	0.017	1.09
$\mathcal{C}_{10} \times 10^3$	1.50	0.33	0.22	0.33	0.41	0.020	0.65
RF GC scheme, FOPT, $\chi^2/\text{dof} = 1.21$, p-value $= 0.27$							
$\alpha_s(m_\tau)$	0.3169	0.0031	0.0059	0	0	0.0014	0.0068
$\mathcal{C}_6 \times 10^3$	1.39	0.43	0.96	0.11	0.0048	0.075	1.06
$\mathcal{C}_8 \times 10^3$	-0.80	0.45	0.99	0.14	0.059	0.065	1.10
$\mathcal{C}_{10} \times 10^3$	0.40	0.30	0.57	0.039	0.014	0.040	0.65

Table 5.3: Fitted parameters using the $V + A$ spectral function from the ALEPH collaboration in analogy to Ref. [6] for CIPT and FOPT. The first two sections show the results in the $\overline{\text{MS}}$ GC scheme. The last two sections the corresponding results in the RF GC scheme, where for the central values we used $N_g = 0.57$ and $R = 0.8m_\tau$. The uncertainties are denoted in the following way: σ_{exp} is the experimental uncertainty, σ_μ the error from scale variation, σ_R corresponds to the uncertainty from IR factorization scale variation and σ_{c_5} is the error inherent to the six-loop coefficient. The two zeros in the first line of the last section denote that the uncertainty is smaller than 10^{-5}. The effective condensates $\mathcal{C}_k$ are given in units of GeV^k.

The results for the fit parameters in the RF GC scheme are now given in the lower half of Tab. 5.3. The CIPT and FOPT predictions for the strong coupling read

$$\begin{aligned} \alpha_s(m_\tau^2)^{\text{CIPT}} &= 0.3197 \pm 0.0100 \\ \alpha_s(m_\tau^2)^{\text{FOPT}} &= 0.3169 \pm 0.0068 \end{aligned} \qquad \text{(tOPE, RF GC, ALEPH } V+A\text{)}. \tag{5.17}$$

The central values are obtained from using the central value of $N_g = 0.57$ and $R = 0.8m_\tau$ as the IR factorization scale. For the analysis in the RF GC we have two additional sources of uncertainty. The first one σ_R arises from varying the IR factorization scale between $0.7m_\tau \leq R \leq m_\tau$ and the second error σ_{N_g} comes from varying the norm of the GC within the uncertainty bounds determined in the previous section. For FOPT the results are almost equivalent to the outcome in the $\overline{\text{MS}}$ GC scheme, which is expected as the subtraction has little impact for the GCS moments used in this analysis. It is, however, an interesting observation that even the fit results for the condensates barely change. In CIPT the situation is different, as the subtraction has a large impact even for the case of GCS moments. For α_s we see that the discrepancy between the two resummation approaches has shrunk to 0.0028, which is smaller than the individual total uncertainties. A rather surprising fact is that the additional uncertainties in the RF GC scheme due to N_g and R have only a minor impact on the total uncertainties of the individual parameters. The total uncertainty for the strong coupling only receives a contribution of 0.003, growing from 0.007 to 0.01. Needless to say, that this growth in the total uncertainty of α_s is more than compensated by the significant reduction of the discrepancy between CIPT and FOPT. Note that in contrast to the FOPT results, for CIPT the central values of the OPE condensates in the RF GC scheme change w.r.t. the $\overline{\text{MS}}$ GC scheme.

As the asymptotic separation is removed in the RF GC scheme it is now adequate to determine a combined FOPT-CIPT result for the strong coupling, which we do in the following way: We take the average of the FOPT and CIPT central values as the combined central value. The corresponding uncertainty we get by using the prescription advocated in Ref. [6]. We take the smaller of the two uncertainties and add in quadrature half of the difference of the FOPT and CIPT central values. This yields

$$\alpha_s(m_\tau^2) \,=\, 0.3183 \pm 0.0069 \qquad (\text{tOPE, RF GC, ALEPH } V+A). \tag{5.18}$$

All of the results for the strong coupling quoted in this section are visualized in Fig. 5.4. There we clearly see the impact the RF GC scheme has on the outcome of α_s when we compare the original results (left panel) to the results in our new scheme (right panel). Furthermore, we also give a visual account of the average in Eq. (5.18) as the additional black vertical line in the right panel.

5.2.3 Single Weight Function Analysis with Multiple s_0 values

The analysis from Ref. [7] followed the other major approach for treating the non-perturbative effects in the recent literature, the so-called 'DV-model strategy' method. The main aim of this method is to avoid truncations of the OPE by using weight functions which suppress these higher-dimensional contributions to the theoretical moments. For the approximation in Eq. (5.15) the OPE corrections actually vanish in the DV approach. The weight functions which are used in this context are unpinched (or at most singly-pinched), since the pinching would imply higher powers of x in the polynomial weight function. The consequence of considering weight functions which do no inhabit the pinching property is that DV effects get enhanced. As a result, one has to include them in the fit.

We now have to comment on the DV component of the spectral function $\rho^{\text{DV}}_{V/A}$, as this is important for the current discussion. The most important aspect of $\rho^{\text{DV}}_{V/A}$ is that it can't be obtained from first principles. Nevertheless, for sufficiently large s, considering general assumptions of the QCD spectrum, one can parametrize the DV component of the spectral function. Based on analyticity properties of the correlator, and in similar spirit to the 'derivation' of the FESR, one can write down the DV contributions to the theoretical moments as [49]

$$\delta^{(\text{DV})}_{w,V/A} = -8\pi^2 \int_{s_0}^{\infty} \frac{\mathrm{d}s}{s_0} w(\tfrac{s}{s_0}) \rho^{(\text{DV})}_{V/A}(s). \tag{5.19}$$

Note that the integral from s_0 to infinity appears since the approximation for the DV effects is only valid away from the resonance peaks at sufficiently large values for s. For the phenomenological analysis in this section (and following the ansatz of Ref. [7]) the DV component of the spectral function given in Eq. (5.19) is parametrized as

$$\rho^{(\text{DV})}_{V/A}(s) = e^{-\delta_{V/A} - \gamma_{V/A} s} \sin\left(a_{V/A} + b_{V/A} s\right). \tag{5.20}$$

This parametrization subsequently introduces four new parameters per channel which have to be included in the fit: $\delta_{V/A}$, $\gamma_{V/A}$, $a_{V/A}$, and $b_{V/A}$. The dependence on the channel arises from the relation of DV effects to residual resonance effects.

After this short interlude on the DV component of the spectral function, we return to the discussion on the concrete setup of the analysis, which is given as follows: In order to keep the contamination from higher-dimensional OPE effects to an absolute minimum, one only considers a single weight function in the DV strategy, which is given by $w(x) = 1$, see e.g. sections 4.4 and 4.5. The necessary degrees of freedom are then obtained from using different values for the upper bound of the FESR, e.g. s_0 is varied from the highest possible value m_τ^2 down to a certain threshold energy s_{min}. We emphasize that strong coupling extractions using the DV strategy are of

	central value	σ_{exp}	σ_μ	σ_R	σ_{N_g}	σ_5	σ_{total}
CIPT, $\chi^2/\text{dof} = 12.97/15$, p-value $= 0.60$							
$\alpha_s(m_\tau)$	0.3256	0.0089	0.0033	–	–	0.0021	0.0097
δ_V	3.33	0.28	0.021	–	–	0.0055	0.28
γ_V	0.66	0.18	0.010	–	–	0.0029	0.18
a_V	−1.27	0.49	0.0026	–	–	0.0011	0.49
b_V	3.76	0.26	0.0023	–	–	0.0001	0.26
FOPT, $\chi^2/\text{dof} = 12.55/15$, p-value $= 0.64$							
$\alpha_s(m_\tau)$	0.3083	0.0066	0.0014	–	–	0.0025	0.0072
δ_V	3.51	0.28	0.054	–	–	0.027	0.29
γ_V	0.57	0.17	0.029	–	–	0.013	0.18
a_V	−1.26	0.48	0.022	–	–	0.0002	0.48
b_V	3.77	0.26	0.0063	–	–	0.0020	0.26
RF GC scheme, CIPT, $\chi^2/\text{dof} = 12.70/15$, p-value $= 0.63$							
$\alpha_s(m_\tau)$	0.3159	0.0080	0.0033	0.0015	0.0035	0.0017	0.0096
δ_V	3.44	0.28	0.028	0.055	0.041	0.0024	0.29
γ_V	0.61	0.17	0.013	0.027	0.020	0.0012	0.18
a_V	−1.26	0.49	0.0037	0.0023	0.0023	0.0007	0.49
b_V	3.77	0.26	0.0031	0.0054	0.0023	0.0001	0.26
RF GC scheme, FOPT, $\chi^2/\text{dof} = 12.53/15$, p-value $= 0.64$							
$\alpha_s(m_\tau)$	0.3081	0.0065	0.0015	0	0.0001	0.0025	0.0072
δ_V	3.52	0.28	0.053	0.0037	0.0038	0.026	0.29
γ_V	0.57	0.17	0.029	0.0016	0.0018	0.013	0.18
a_V	−1.26	0.48	0.024	0.0018	0.0008	0.0003	0.48
b_V	3.77	0.26	0.0076	0.0010	0.0006	0.0019	0.26

Table 5.4: Fitted parameters using the improved vector-isovector spectral function from Ref. [7] for CIPT and FOPT. The first two sections show the results in the $\overline{\text{MS}}$ GC scheme. The last two sections the corresponding results in the RF GC scheme, where for the central values we used $N_g = 0.57$ and $R = 0.8\sqrt{s_0}$. The uncertainties are denoted in the following way: σ_{exp} is the experimental uncertainty, σ_μ the error from scale variation, σ_R corresponds to the uncertainty from IR factorization scale variation and σ_{c_5} is the error inherent to the six-loop coefficient. The zero in the first line of the last section again denotes that the uncertainty is smaller than 10^{-5}. The DV parameters b_V and γ_V scale in units of GeV^{-2}. The other two DV parameters are dimensionless.

course reliant on the assumption that the DV component of the spectral function is parametrized in an adequate way.

In Ref. [7] a variety of results are presented including variations in the number of s_0's and the addition of one higher-dimensional condensate among others. For the main result we consider 20 values of s_0, with $s_{\text{min}} = 1.55$ GeV^2 (see the entries in the last four lines of table 1 in Ref. [7]). Recall that in the approximation of Eq. (5.15) this implies that the higher-dimensional OPE terms yield no contribution. In this setup, Ref. [7] then extracted five parameters, namely the strong coupling and the four DV parameters δ_V, γ_V, a_V, and b_V.

The outcome in the original $\overline{\text{MS}}$ GC scheme is shown in the upper half of Tab. 5.4. The 6-loop coefficient was included in the same manner as it was the case in the tOPE analysis. The FOPT and CIPT results for the strong coupling read

$$\begin{aligned} \alpha_s(m_\tau^2)^{\text{CIPT}} &= 0.3256 \pm 0.0097 \\ \alpha_s(m_\tau^2)^{\text{FOPT}} &= 0.3083 \pm 0.0072 \end{aligned} \qquad (\text{DV, } \overline{\text{MS}} \text{ GC, new } V \text{ spec. func.}). \qquad (5.21)$$

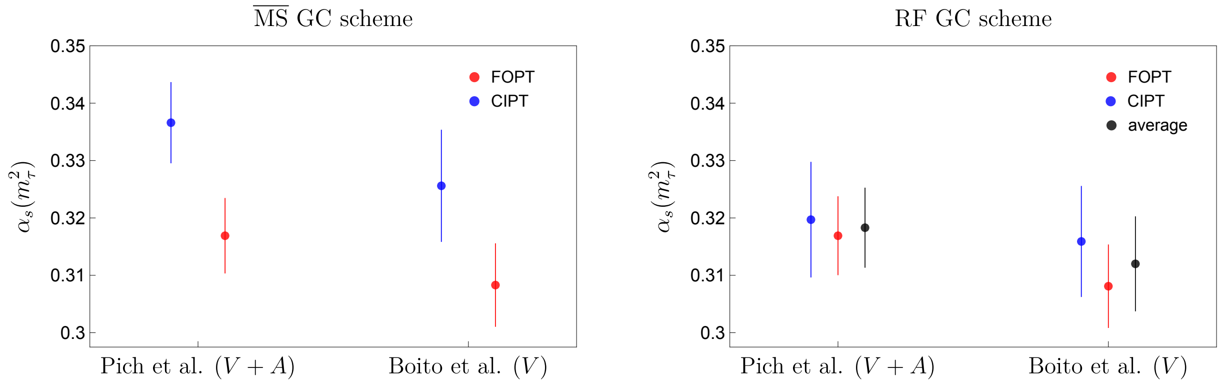

Fig. 5.4: Results for the strong coupling in the $\overline{\text{MS}}$ GC scheme (left panel) and in the RF GC scheme (right panel). The left set of FOPT and CIPT predictions in each plot show the outcome from the analysis where the tOPE strategy from Ref. [6] was employed. Correspondingly, the right set of results depicts the strong coupling results using the DV strategy from Ref. [7]. The additional black vertical lines in the right panel indicate the averaged results for α_s for each extraction method.

The error inherent to the six-loop coefficient, see Eq. (3.20), was included in the exact same way as in the tOPE analysis. For the uncertainty arising from renormalization scale variation we performed a similar, but not completely identical procedure compared to the truncated OPE analysis. The difference arises from the fact that one has to impose a lower bound on the ξ variation, as non-perturbative scales need to be avoided for choices $s_0 < m_\tau^2$. Hence, for the case of $\xi \geq 1$ we perform the same variation as in the tOPE analysis. To also consider smaller values of ξ we take as a global lower bound $s_{\text{min}} = 1.55$ GeV^2 for all values of s_0. This is still acceptable regarding the avoidance of the region where perturbative QCD breaks down.

If we look at the results for α_s in Eq. (5.21) we observe again that the discrepancy, which in this analysis amounts to 0.017, is larger than the individual total uncertainties by (roughly) a factor of two. Note that the total uncertainty is obtained in analogous fashion to the tOPE analysis. A well known fact is that σ_μ is much smaller than the experimental error. What is interesting is that the DV parameters turn out very similar for FOPT and CIPT. They are actually compatible within errors.

Let us consider the same study in the RF GC scheme. The outcome is shown in the lower half of Tab. 5.4. The central values are again obtained in the same manner as in the tOPE analysis, i.e. using $N_g = 0.57$ and $R = 0.8\sqrt{s_0}$. The results for the strong coupling now read

$$\begin{aligned} \alpha_s(m_\tau^2)^{\text{CIPT}} &= 0.3159 \pm 0.0096 \\ \alpha_s(m_\tau^2)^{\text{FOPT}} &= 0.3081 \pm 0.0072 \end{aligned} \qquad \text{(DV, RF GC, new } V \text{ spec. func.).} \tag{5.22}$$

σ_5 and σ_μ are obtained in analogy to the $\overline{\text{MS}}$ GC scheme analysis and σ_{N_g} arises from the error given in Eq. (5.12). The IR facorization scale variation is again not completely identical to the tOPE analysis. In analogy to the restrictions imposed on the renormalization scale variation, we also do not want to run into the non-perturbative regime when varying R. What is done to prevent such a scenario, is that we impose an absolute lower bound in the following way: We take $R = \eta\sqrt{s_0}$ and consider the variation range $0.7 \leq \eta \leq 1$. If $\eta\sqrt{s_0} \leq 0.7 m_\tau$ we set $R = 0.7 m_\tau$ as the lower bound.

The central values for the case of FOPT are again basically unchanged and the corresponding uncertainties arising form σ_R and σ_{N_g} are also tiny. In CIPT we observe a significant change in the RF GC scheme compared to the $\overline{\text{MS}}$ GC scheme. The discrepancy between the two strong coupling results has shrunk to 0.008, which may be larger than the discrepancy that we obtained in the tOPE analysis given in Eq. (5.17) in the RF GC scheme but it is still less than 50% of the original difference.

There exist, however, some differences between the outcomes of the two extraction approaches. For instance, if we look at the total error on the strong coupling we see that in the tOPE analysis it has slightly increased, whereas in the DV analysis we even observe a small decrease due to the smaller experimental uncertainty related to the strong coupling result in the RF GC scheme. Another interesting observation is that, while in the tOPE analysis the condensate values changed notably, the DV parameters in the current method do not feel such a big impact from switching to the RF GC scheme.

The results for the strong coupling in the $\overline{\mathrm{MS}}$ GC scheme (left panel) and the RF GC scheme (right panel) are again visualized in Fig. 5.4. We again include an average of the FOPT and CIPT results for α_s, where the numerical outcome reads

$$\alpha_s(m_\tau^2) \,=\, 0.3120 \pm 0.0082 \qquad \text{(DV mod., RF GC, new } V \text{ spec. func.)}. \tag{5.23}$$

Note that even though we have carried out our studies for the case of 20 values of s_0, the observations concerning the improvement in the RF GC scheme are unaltered even if we chose to perform the same type of fits with a different number of s_0 values. Finally, we want to highlight the fact that it might be tempting to average Eq. (5.18) and Eq. (5.23) to get a combined final result with a corresponding uncertainty. This should, however, not be done at this point as the results are based on different data sets and it may be better to carry out the tOPE and the DV analysis for the same data set to average the final results from the two approaches in the RF GC scheme in a meaningful way. But this is beyond the scope of this thesis.

Chapter 6

Summary

Strong coupling extractions from inclusive τ decays represent one of the most precise determinations of this fundamental parameter of QCD. In these strong coupling determinations, weighted integrals over the experimental spectral function are tested against theory predictions. To relate experiment and theory so-called finite-energy sum rules (FESR) are used.

The theory predictions can be dissected into various contributions, where the perturbative QCD corrections constitute one important part. For these QCD corrections one has to adopt a prescription for setting the renormalization scale. The two most widely used prescriptions are called fixed-order (FOPT) and contour-improved (CIPT) perturbation theory. One of the dominant sources of theoretical uncertainty in state-of-the-art strong coupling determinations from tau decays is that FOPT and CIPT predictions for α_s give incompatible results. In particular, strong coupling results based on CIPT are consistently higher than those based on FOPT. This observation is independent of the treatment of the non-perturbative corrections that enter the phenomenological analysis.

In a recent article [5], Hoang and Regner showed that CIPT and FOPT have a different infrared (IR) sensitivity, which implies that their non-perturbative corrections differ. Furthermore, they showed that CIPT is inconsistent with the standard treatment of the operator product expansion (OPE) in the presence of IR renormalons in the theoretical correlation function. In the following, they introduced the so-called asymptotic separation, which is defined as the discrepancy of CIPT to FOPT at asymptotically large orders. An important observation, which they additionally made, is that the asymptotic separation is dominated by the effect of the gluon condensate (GC) renormalon. This observation is what we took as the starting point for our work: Starting from the proposition that CIPT can be (largely) cured if the GC renormalon is removed, we introduced a novel IR-subtracted scheme for the GC.

In the original approach to the OPE, one considers the sum of perturbative contributions and higher-dimensional, non-perturbative matrix elements, where the renormalon singularities (contained in the perturbative coefficients and in the non-perturbative matrix elements) intrinsically cancel in the framework of the OPE. To introduce our novel IR-subtracted scheme for the GC, we subsequently started from precisely this proposition, namely that the higher-dimensional OPE contributions do not only provide non-perturbative corrections, but also compensate for the asymptotic behaviour of the QCD corrections. Therefore, we made the order-dependent compensating contribution explicit through a perturbative redefinition of the GC. This renormalon-free GC is by construction dependent on the scale R, which conceptually relates to an IR factorization scale. Furthermore, the universal norm of the GC renormalon N_g appears in the definition of the renormalon-free GC. The idea is then to re-shuffle the perturbative series, containing the information on the GC renormalon, back into the QCD corrections, such that the GC renormalon cancels in the perturbative contribution. The dependence on the IR factorization scale R is, however, not very convenient. We therefore took the additional step to get rid of this R-dependence through the addition of a function which obeys the same R-evolution equation as does the subtraction series containing the information on the GC renormalon.

In the following we took the RF GC scheme to the test, where we first studied the FOPT and

CIPT expansions in the original approach to the OPE ('$\overline{\text{MS}}$' GC scheme) and then compared the outcome to the FOPT and CIPT expansions in the RF GC scheme. We saw in a (model-dependent) study in full QCD that the discrepancy between the FOPT and CIPT expansions was actually removed at higher orders, corroborating the findings of Hoang and Regner [5]. In addition, we took note of the fact that, already at the six-loop level, the discrepancy between the two series was strongly reduced.

As the norm of the GC renormalon N_g was conceptually part of the construction of the perturbative series in the RF GC scheme, we then performed a study where we intended to obtain a reliable estimate for this parameter. In particular, we introduced a novel method, which we called the optimal subtraction approach, to obtain a value for N_g together with a conservative error estimate. The final result we obtained, e.g. the prediction from the optimal subtraction approach based on the known $\mathcal{O}(\alpha_s^4)$-corrections, was then part of the phenomenological analysis in the final investigation of this thesis.

In the last section we analysed the impact of the RF GC scheme on state-of-the-art strong coupling determinations. We repeated, in detail, two strong coupling extractions from the recent literature [6, 7], which treat the non-perturbative corrections differently. Irrespective of this different treatment of non-perturbative corrections, we found that α_s extractions based on CIPT and FOPT in the RF GC scheme lead to results which are in much better agreement, than those which are obtained using the original $\overline{\text{MS}}$ GC scheme. Note that in the RF GC scheme one has two additional sources of uncertainty, namely the error arising from IR factorization scale variation as well as the error connected to the final result for the norm of the GC N_g. These additional errors, however, only have a minor impact on the overall error connected to the strong coupling.

Appendix A

The C-scheme

A problem related to the strong coupling is the dependence of it on its renormalization procedure. One considers the QCD coupling to be in that sense an unphysical observable. There exists, however, a definition of the strong coupling constant in which its running is scheme independent and parameterized by only one parameter. The derivation of this so-called C-scheme will be discussed in this section. Here we follow the lines of Ref. [8].

We know the scale running of the QCD coupling to be described by the β-function

$$-\mu\frac{\mathrm{d}a_\mu}{\mathrm{d}\mu} = \beta(a_\mu) = \beta_0 a_\mu^2 + \beta_1 a_\mu^3 + \dots \tag{A.1}$$

where $a_\mu = \alpha_s(\mu)/\pi$ and the β-function coefficients are given by

$$\begin{aligned}
\beta_0 &= 11 - \frac{2}{3}\,n_f, \\
\beta_1 &= 102 - \frac{38}{3}\,n_f, \\
\beta_2 &= \frac{2857}{2} - \frac{5033}{18}\,n_f + \frac{325}{54}\,n_f^2, \\
\beta_3 &= \frac{149753}{6} + 3564\,\zeta_3 - \left(\frac{1078361}{162} + \frac{6508}{27}\,\zeta_3\right) n_f + \left(\frac{50065}{162} + \frac{6472}{81}\,\zeta_3\right) n_f^2 + \frac{1093}{729}\,n_f^3, \\
\beta_4 &= \frac{8157455}{16} + \frac{621885}{2}\,\zeta_3 - \frac{88209}{2}\,\zeta_4 - 288090\,\zeta_5 \\
&\quad + \left(-\frac{336460813}{1944} - \frac{4811164}{81}\,\zeta_3 + \frac{33935}{6}\,\zeta_4 + \frac{1358995}{27}\,\zeta_5\right) n_f \\
&\quad + \left(\frac{25960913}{1944} + \frac{698531}{81}\,\zeta_3 - \frac{10526}{9}\,\zeta_4 - \frac{381760}{81}\,\zeta_5\right) n_f^2 \\
&\quad + \left(-\frac{630559}{5832} - \frac{48722}{243}\,\zeta_3 + \frac{1618}{27}\,\zeta_4 + \frac{460}{9}\,\zeta_5\right) n_f^3 \\
&\quad + \left(\frac{1205}{2916} - \frac{152}{81}\,\zeta_3\right) n_f^4.
\end{aligned} \tag{A.2}$$

Integrating Eq. (A.1) at first order

$$\int_{a_{\mu_1}}^{a_{\mu_2}} \frac{da_\mu}{\beta_0 a_\mu^2} = -\int_{\mu_1}^{\mu_2} \frac{d\mu}{\mu}$$

yields

$$a_{\mu_2} = \frac{a_{\mu_1}}{1 - a_{\mu_1}\beta_0 \ln\left(\frac{\mu_1}{\mu_2}\right)} \tag{A.3}$$

as the solution, which represents the one-loop running of the coupling in QCD. We further know that the coupling diverges if the denominator goes to zero

$$1 - a_{\mu_1}\beta_0 \ln\left(\frac{\mu_1}{\Lambda'}\right) \overset{!}{=} 0,$$

which implies for Λ'

$$\Lambda' = \mu_1 e^{-1/(a_{\mu_1}\beta_0)}. \tag{A.4}$$

An important observation of Eq. (A.4) is that Λ' is not dependent on the scale μ_1

$$\begin{aligned}
\frac{\mathrm{d}\Lambda'}{\mathrm{d}\mu_1} &= e^{-1/(a_{\mu_1}\beta_0)} - \frac{\mu_1}{\beta_0} e^{-1/(a_{\mu_1}\beta_0)} \frac{\mathrm{d}a_{\mu_1}^{-1}}{\mathrm{d}\mu_1} \\
&= e^{-1/(a_{\mu_1}\beta_0)} - \frac{\mu_1}{\beta_0} e^{-1/(a_{\mu_1}\beta_0)} \left(\frac{\beta_0}{\mu_1}\right) \\
&= 0.
\end{aligned}$$

The scale invariance of Λ' motivates a different definition of the coupling

$$\frac{1}{\bar{a}_{\mu_1}} + \frac{\beta_1}{\beta_0} \ln \bar{a}_{\mu_1} - \frac{\beta_0}{2} C \equiv \beta_0 \ln \frac{\mu_1}{\Lambda}. \tag{A.5}$$

Note that we use the notation $\bar{a}_{\mu_i} = \alpha_s(\mu_i)/\pi$ to denote the strong coupling in the C-scheme. In Eq. (A.5) the scale Λ is defined by

$$\Lambda \equiv \mu_1 e^{-1/(a_{\mu_1}\beta_0)} (a_{\mu_1})^{-\frac{\beta_1}{\beta_0^2}} \exp\left\{ \int_0^{a_{\mu_1}} \frac{\mathrm{d}a}{\tilde{\beta}(a)} \right\}, \tag{A.6}$$

with

$$\tilde{\beta}(a) \equiv \frac{1}{\beta(a)} - \frac{1}{\beta_0 a^2} + \frac{\beta_1}{\beta_0^2 a}.$$

Eq. (A.5) can also be written as

$$\frac{1}{\bar{a}_{\mu_1}} + \frac{\beta_1}{\beta_0} \ln \bar{a}_{\mu_1} \equiv \beta_0 \ln \frac{\mu_1}{\Lambda^C},$$

where Λ^C is defined to be

$$\Lambda^C \equiv \Lambda\, e^{-C/2}.$$

Due to the fact that the Landau pole only depends on the parameter C, the renormalization scheme has the same property. In other words, the choice of the renormalization scheme is entailed in the choice of the value for C.

Eq. (A.5) can be solved in two ways: The first way is numerical, e.g. for a given value of the strong coupling in the $\overline{\mathrm{MS}}$ scheme at a reference scale μ we take the β-function on the RHS of Eq. (A.5) up to order 5, which is the last known value in this scheme and solve the equality for an arbitrary value of the parameter C. The second way one can solve Eq. (A.5) is iteratively, which would correspond to a perturbative approach. As we already saw in section 4.1.1, for $C = 0$ (which is the choice we adapt throughout the main body of the thesis) the numerical perturbative relation between the coupling in the C-scheme and in the $\overline{\mathrm{MS}}$-scheme at any common renormalization scale and for $n_f = 3$ dynamic quark flavors reads

$$\begin{aligned}
\frac{\bar{\alpha}_s}{\alpha_s} &= 1 - 0.132789\,\alpha_s^2 - 0.247879\,\alpha_s^3 - 0.103368\,\alpha_s^4 + 0.137953\,\alpha_s^5 + 0.146252\,\alpha_s^6 \\
&\quad + 0.0729472\,\alpha_s^7 - 0.081650\,\alpha_s^8 - 0.122995\,\alpha_s^9 - 0.042241\,\alpha_s^{10} + 0.050279\,\alpha_s^{11} \\
&\quad + 0.091138\,\alpha_s^{12} + 0.033505\,\alpha_s^{13} - 0.038225\,\alpha_s^{14} + \dots.
\end{aligned}$$

Appendix B

Asymptotic separation, Borel Model and Ambiguity Formulae

The exact expression for the Multi-Renormalon Model (MRM) in the C-scheme for the Borel function of the Adler function $\hat{D}(s)$ used to study the higher-order perturbative behaviour in full QCD reads

$$B[\hat{D}(s)]_{\rm mr}(u) = b^{(0)} + b^{(1)}u + \frac{N_{4,0}\left[1+\bar{a}(-s)\bar{c}_{4,0}^{(1)}\right]}{(2-u)^{\gamma_4}} + \frac{N_{6,0}}{(3-u)^{\gamma_6}} + \frac{N_{-2}}{(1+u)^{\gamma_{(-2)}}}, \tag{B.1}$$

where the relevant parameters are given by

$$\begin{aligned} N_{4,0} &= \frac{2\pi^2}{3}N_g = 4.20757\,, & N_{6,0} &= -15.64640\,, & N_{-2} &= -0.02714\,,\\ \gamma_4 &= \frac{209}{81}\,, & \gamma_6 &= \frac{91}{27}\,, & \gamma_{(-2)} &= \frac{98}{81}\,,\\ b^{(0)} &= 0.15381\,, & b^{(1)} &= 0.00790\,, & \bar{c}_{4,0}^{(1)} &= -\frac{22}{81}\,. \end{aligned}$$

$\bar{c}_{4,0}^{(1)}$ corresponds to the $\mathcal{O}(\alpha_s)$ Wilson coefficient correction of the GC, and N_g is the associated renormalon norm of the GC.

The asymptotic separation for a generic IR renormalon term in the Borel function of the Adler function discussed in section 3.3

$$B^{\rm IR}_{\hat{D},d,\gamma}(u) \;=\; \frac{1}{(p-u)^{\gamma}}\,, \tag{B.2}$$

considering the C-scheme and a generic weight function $W(x) = (-x)^m$ (on the level of the Adler function), is given by

$$\begin{aligned} \Delta(m\neq p, p,\gamma,s_0) \;&=\; \delta^{(0),\rm CIPT}_{(-x)^m,\rm Borel}(s_0) - \delta^{(0),\rm FOPT}_{(-x)^m,\rm Borel}(s_0) \\ =\;& \left(\frac{\Lambda^2_{\rm QCD}}{s_0}\right)^m \frac{2^{2m\hat{b}_1}}{\Gamma(\gamma)}\times \\ & \Big\{{\rm Re}\left[(p-m+i0)^{2m\hat{b}_1-\gamma}\Gamma(-2m\hat{b}_1+\gamma,-2(p-m)t_-)\right] - \\ & -2\hat{b}_1{\rm Re}\left[(p-m+i0)^{2m\hat{b}_1-\gamma+1}\Gamma(-2m\hat{b}_1+\gamma-1,-2(p-m)t_-)\right]\Big\}\,, \end{aligned} \tag{B.3}$$

where $\Gamma(a,z)$ is the (upper) incomplete gamma function. In this single case we adopt the t-variable notation introduced in Ref. [5]. Furthermore, the scale $\Lambda_{\rm QCD}$ is defined as

$$\Lambda^2_{\rm QCD} \;\equiv\; Q^2\left(\frac{2\pi}{\beta_0\bar{\alpha}_s(Q^2)}\right)^{2\hat{b}_1}\exp\left(-\frac{4\pi}{\beta_0\bar{\alpha}_s(Q^2)}\right) \;=\; Q^2\,(2\bar{a}_Q)^{-2\hat{b}_1}\exp\left(-\frac{1}{\bar{a}_Q}\right)\,. \tag{B.4}$$

Note that this again corresponds to the C-scheme expression. It is worthwhile to mention the fact that the formula for $\Lambda_{\rm QCD}$ considering the strong coupling in the $\overline{\rm MS}$ scheme cannot be written down in such a closed form due to the higher-order coefficients of the β-function appearing in this case.

The ambiguity of the Borel sum integral, given representatively by Eq. (4.35), is obtained from

$$\begin{aligned}
&\frac{1}{2\pi i}\oint_{|s|=s_0}\frac{{\rm d}s}{s}\Big(-\frac{s}{s_0}\Big)^k\,\frac{i}{2\pi}\int_0^\infty {\rm d}u\left[\frac{e^{-\frac{u}{\bar a(-s)}}}{(2+i0-u)^{1+4\hat b_1}}-\frac{e^{-\frac{u}{\bar a(-s)}}}{(2-i0-u)^{1+4\hat b_1}}\right] \\
&=\frac{1}{2\pi i}\oint_{|s|=s_0}\frac{{\rm d}s}{s}\Big(-\frac{s}{s_0}\Big)^k\,\frac{(\bar a(-s))^{-4\hat b_1}}{\Gamma(1+4\hat b_1)}\,e^{-\frac{2}{\bar a(-s)}} \\
&=\frac{1}{2\pi i}\oint_{|s|=s_0}\frac{{\rm d}s}{s}\Big(-\frac{s}{s_0}\Big)^k\,\frac{1}{s^2}\,\frac{2^{4\hat b_1}\,\Lambda_{\rm QCD}^4}{\Gamma(1+4\hat b_1)}=\begin{cases}0\,, & \text{for } k\neq 2\\ \frac{2^{4\hat b_1}\,\Lambda_{\rm QCD}^4}{s_0^2\,\Gamma(1+4\hat b_1)} & \text{for } k=2\end{cases}\,.
\end{aligned}\tag{B.5}$$

Bibliography

[1] PARTICLE DATA GROUP collaboration, P. A. Zyla et al., *Review of Particle Physics*, *PTEP* **2020** (2020) 083C01.

[2] A. Pivovarov, *Renormalization group analysis of the tau lepton decay within QCD*, *Sov. J. Nucl. Phys.* **54** (1991) 676–678, [hep-ph/0302003].

[3] F. Le Diberder and A. Pich, *The perturbative QCD prediction to R_τ revisited*, *Phys. Lett. B* **286** (1992) 147–152.

[4] M. Beneke and M. Jamin, *α_s and the tau hadronic width: fixed-order, contour-improved and higher-order perturbation theory*, *JHEP* **09** (2008) 044, [0806.3156].

[5] A. H. Hoang and C. Regner, *Borel Representation of τ Hadronic Spectral Function Moments in Contour-Improved Perturbation Theory*, 2008.00578.

[6] A. Pich and A. Rodríguez-Sánchez, *Determination of the QCD coupling from ALEPH τ decay data*, *Phys. Rev. D* **94** (2016) 034027, [1605.06830].

[7] D. Boito, M. Golterman, K. Maltman, S. Peris, M. V. Rodrigues and W. Schaaf, *Strong coupling from an improved τ vector isovector spectral function*, *Phys. Rev. D* **103** (2021) 034028, [2012.10440].

[8] D. Boito, M. Jamin and R. Miravitllas, *Scheme Variations of the QCD Coupling and Hadronic τ Decays*, *Phys. Rev. Lett.* **117** (2016) 152001, [1606.06175].

[9] M. Beneke, *Renormalons*, *Physics Reports* **317** (Aug, 1999) 1–142.

[10] M. Luke, A. V. Manohar and M. J. Savage, *Renormalons in effective field theories*, *Physical Review D* **51** (May, 1995) 4924–4933.

[11] M. Neubert, *Scale setting in qcd and the momentum flow in feynman diagrams*, *Physical Review D* **51** (May, 1995) 5924–5941.

[12] N. Watson, *The gauge-independent qcd effective charge*, *Nuclear Physics B* **494** (Jun, 1997) 388–432.

[13] P. Ball, M. Beneke and V. M. Braun, *Resummation of $(\beta_0\alpha_s)^n$ corrections in QCD: Techniques and applications to the tau hadronic width and the heavy quark pole mass*, *Nucl. Phys. B* **452** (1995) 563–625, [hep-ph/9502300].

[14] D. J. Broadhurst and A. G. Grozin, *Matching qcd and heavy-quark effective theory heavy-light currents at two loops and beyond*, *Physical Review D* **52** (Oct, 1995) 4082–4098.

[15] M. A. Shifman, A. Vainshtein and V. I. Zakharov, *QCD and Resonance Physics. Theoretical Foundations*, *Nucl. Phys. B* **147** (1979) 385–447.

[16] A. H. Hoang and C. Regner, *On the Difference between FOPT and CIPT for Hadronic Tau Decays*, 2105.11222.

[17] R. Zwicky, *A brief Introduction to Dispersion Relations and Analyticity*, in *Quantum Field Theory at the Limits: from Strong Fields to Heavy Quarks*, pp. 93–120, 2017. 1610.06090. DOI.

[18] S. Gorishnii, A. Kataev and S. Larin, *The $O(\alpha_s^3)$-corrections to $\sigma_{tot}(e^+e^- \to hadrons)$ and $\Gamma(\tau^- \to \nu_\tau + hadrons)$ in QCD*, *Phys. Lett. B* **259** (1991) 144–150.

[19] L. R. Surguladze and M. A. Samuel, *Total hadronic cross-section in e^+e^- annihilation at the four loop level of perturbative QCD*, *Phys. Rev. Lett.* **66** (1991) 560–563.

[20] P. Baikov, K. Chetyrkin and J. H. Kuhn, *Order α_s^4 QCD Corrections to Z and tau Decays*, *Phys. Rev. Lett.* **101** (2008) 012002, [0801.1821].

[21] D. Boito, P. Masjuan and F. Oliani, *Higher-order QCD corrections to hadronic τ decays from Padé approximants*, *JHEP* **08** (2018) 075, [1807.01567].

[22] I. Caprini, *Higher-order perturbative coefficients in QCD from series acceleration by conformal mappings*, *Phys. Rev. D* **100** (2019) 056019, [1908.06632].

[23] M. Jamin, *Higher-order behaviour of two-point current correlators*, *Eur. Phys. J. ST* **230** (2021) 2609–2624, [2106.01614].

[24] M. Beneke, D. Boito and M. Jamin, *Perturbative expansion of tau hadronic spectral function moments and α_s extractions*, *JHEP* **01** (2013) 125, [1210.8038].

[25] D. J. Broadhurst, *Large-N expansion of QED: Asymptotic photon propagator and contributions to the muon anomaly, for any number of loops*, *Z. Phys. C* **58** (1993) 339–346.

[26] A. Pich and J. Prades, *Strange quark mass determination from Cabibbo suppressed tau decays*, *JHEP* **10** (1999) 004, [hep-ph/9909244].

[27] L. R. Surguladze and F. V. Tkachov, *Two Loop Effects in QCD Sum Rules for Light Mesons*, *Nucl. Phys. B* **331** (1990) 35.

[28] D. Boito, M. Golterman, K. Maltman, J. Osborne and S. Peris, *Strong coupling from the revised ALEPH data for hadronic τ decays*, *Phys. Rev. D* **91** (2015) 034003, [1410.3528].

[29] D. Boito, M. Golterman, M. Jamin, A. Mahdavi, K. Maltman, J. Osborne et al., *An Updated determination of α_s from τ decays*, *Phys. Rev. D* **85** (2012) 093015, [1203.3146].

[30] A. H. Hoang, A. Jain, I. Scimemi and I. W. Stewart, *R-evolution: Improving perturbative QCD*, *Phys. Rev. D* **82** (2010) 011501, [0908.3189].

[31] M. A. Benitez-Rathgeb, D. Boito, A. H. Hoang and M. Jamin, *Reconciling the FOPT and CIPT Predictions for the Hadronic Tau Decay Rate*, in *16th International Workshop on Tau Lepton Physics* , 11, 2021. 2111.09614.

[32] D. Boito, O. Cata, M. Golterman, M. Jamin, K. Maltman, J. Osborne et al., *A new determination of α_s from hadronic τ decays*, *Phys. Rev. D* **84** (2011) 113006, [1110.1127].

[33] T. Lee, *Estimation of the large order behavior of the Plaquette*, *Phys. Lett. B* **711** (2012) 360–363, [1112.4433].

[34] T. Lee, *Renormalons beyond one loop*, *Phys. Rev. D* **56** (1997) 1091–1100, [hep-th/9611010].

[35] T. Lee, *Normalization constants of large order behavior*, *Phys. Lett. B* **462** (1999) 1–6, [hep-ph/9908225].

[36] I. Caprini and J. Fischer, *Accelerated convergence of perturbative QCD by optimal conformal mapping of the Borel plane*, *Phys. Rev. D* **60** (1999) 054014, [hep-ph/9811367].

[37] G. Cvetic and T. Lee, *Bilocal expansion of Borel amplitude and hadronic tau decay width*, *Phys. Rev. D* **64** (2001) 014030, [hep-ph/0101297].

[38] G. Cvetic, C. Dib, T. Lee and I. Schmidt, *Resummation of the hadronic tau decay width with modified Borel transform method*, *Phys. Rev. D* **64** (2001) 093016, [hep-ph/0106024].

[39] F. Le Diberder and A. Pich, *Testing QCD with tau decays*, *Phys. Lett. B* **289** (1992) 165–175.

[40] M. Davier, A. Hocker and Z. Zhang, *The Physics of Hadronic Tau Decays*, *Rev. Mod. Phys.* **78** (2006) 1043–1109, [hep-ph/0507078].

[41] M. Davier, S. Descotes-Genon, A. Hocker, B. Malaescu and Z. Zhang, *The Determination of alpha(s) from Tau Decays Revisited*, *Eur. Phys. J. C* **56** (2008) 305–322, [0803.0979].

[42] M. Davier, A. Höcker, B. Malaescu, C.-Z. Yuan and Z. Zhang, *Update of the ALEPH non-strange spectral functions from hadronic τ decays*, *Eur. Phys. J. C* **74** (2014) 2803, [1312.1501].

[43] ALEPH collaboration, R. Barate et al., *Measurement of the spectral functions of axial - vector hadronic tau decays and determination of $\alpha_s(m_\tau^2)$*, *Eur. Phys. J. C* **4** (1998) 409–431.

[44] ALEPH collaboration, S. Schael et al., *Branching ratios and spectral functions of tau decays: Final ALEPH measurements and physics implications*, *Phys. Rept.* **421** (2005) 191–284, [hep-ex/0506072].

[45] OPAL collaboration, K. Ackerstaff et al., *Measurement of the strong coupling constant alpha(s) and the vector and axial vector spectral functions in hadronic tau decays*, *Eur. Phys. J. C* **7** (1999) 571–593, [hep-ex/9808019].

[46] C. Ayala, G. Cvetic and D. Teca, *Determination of perturbative QCD coupling from ALEPH τ decay data using pinched Borel–Laplace and Finite Energy Sum Rules*, *Eur. Phys. J. C* **81** (2021) 930, [2105.00356].

[47] C. Ayala, G. Cvetic and D. Teca, *Using improved operator product expansion in Borel-Laplace sum rules with ALEPH τ decay data, and determination of pQCD coupling*, *Eur. Phys. J. C* **82** (2022) 362, [2112.01992].

[48] K. Maltman and T. Yavin, *$\alpha_s(M_Z^2)$ from hadronic tau decays*, *Phys. Rev. D* **78** (2008) 094020, [0807.0650].

[49] O. Cata, M. Golterman and S. Peris, *Unraveling duality violations in hadronic tau decays*, *Phys. Rev. D* **77** (2008) 093006, [0803.0246].

Acknowledgements

First of all I want to thank the entire particle physics group at the University of Vienna for the past two years. As the members of this group know, I like to ask a lot of questions and in general enjoy having extensive conversations, so I thank all of you for your patience, endurance and support during my time here. A special thanks goes to Christoph Regner, who had to endure many hours of me asking him all sorts of technical (and non-technical) questions. I appreciate everything that you did for me, thank you! A further sincere thank you goes to Massimiliano Procura, for always taking the time, even before I was a student at our group, to talk to me and for the advice you gave me along the way.

Furthermore, I want to thank Matthias Jamin and Diogo Boito for the wonderful collaboration during the past two years. I want to express my gratitude especially towards Diogo, who was always available for any type of question or for any advice in general, independent of whether it was about science or life. Thank you both for everything.

Of course this thesis would not have been possible without a supervisor. I had the good fortune to be under the wings of André Hoang, which, as anyone who has ever worked with him knows, was never boring. But in all seriousness, I believe it is fair to say that during the past two years André changed me as a young scientist and more importantly as a person for the better. Therefore, I sincerely want to thank you for everything that you did for me. In particular, for all the professional and life lessons that you gave me and for all the time you invested in me and our project. Thank you!

I also need to thank my family. As I do not come from a particularly wealthy background, I always thought about being able to study physics as a privilege. I never took it for granted that my family constantly supported me and will be forever grateful that they enabled me to do what I love.

Lastly, I want to thank the most important person in my life, my girlfriend Tamara. Due to the fact that I am a rather emotional person, you had to endure quite a lot during the last two years, and in general throughout my studies. I sincerely want to thank you, for always being at my side, giving me advice, supporting me in the frustrating periods and being the best partner for life which I can ever imagine. I would not have been able to do what I did during the past five years if it was not for your constant support. Thank you.